INVESTIGATION OF THE ATMOSPHERIC OZONE FORMATION POTENTIAL OF SELECTED ALKYL BROMIDES

Final Report to
Albemarle Corporation

by
William P. L. Carter, Dongmin Luo, and Irina L. Malkina

November 10, 1997

College of Engineering
Center for Environmental Research and Technology
University of California
Riverside, California 92521

97-AP-RT5B-001-FR

ABSTRACT

Environmental chamber experiments and computer model calculations were conducted to assess the atmospheric ozone formation potentials of 1-propyl and 1-butyl bromides. The experiments consisted of blacklight irradiations, in a dual ~5000-liter chamber, of simulated photochemical smog mixtures with and without propyl or butyl bromide added. They employed two different reactive organic gas surrogate mixtures to represent other organic pollutants in the atmosphere, and used different surrogate/NO_x levels. The results indicated that the alkyl bromides cause accelerated rates of ozone formation once ozone formation begins in the higher NO_x experiments, but have smaller effects on O_3 formation rates in lower NO_x experiments, and cause ozone levels to peak and then decline in the later stages of the runs. A chemical mechanism was developed to represent the atmospheric reactions for these alkyl bromides, and the bromine atom, BrO_x species, and bromine-containing carbonyl products they are predicted to form. This mechanism could simulate the results of the chamber experiments only if it is assumed that there is a rapid reaction between O_3 and HBr, forming HOBr, which photolyzes rapidly to form OH + Br. However, separate measurements in another chamber indicate that this reaction is relatively slow. This indicates that there is some unknown process which is occurring in our chamber experiments which has the same effect as a rapid O_3 + HBr reaction. The calculated ozone impacts of the bromides under atmospheric conditions were found to depend significantly on NO_x conditions and whether the unknown process, represented by the rapid O_3 + HBr reaction, is assumed to occur in the atmosphere as it does in our chamber. Propyl bromide is calculated to be an ozone inhibitor or have very low ozone impact under low to moderate NO_x conditions regardless of whether the rapid O_3 + HBr reaction is included in the model. The magnitude of this inhibition depends on whether the reaction is included. Under higher NO_x, Maximum Incremental Reactivity (MIR) conditions propyl bromide is calculated to have comparable ozone impact (on a mass basis) as ethane if the reaction is not included, but it is calculated to form about three times more ozone than ethane if the O_3 + HBr reaction is included. Butyl bromide calculated to have 1.5 - 2 times more ozone impact than calculated for propyl bromide using the same assumptions about the O_3 + HBr reaction under high NO_x MIR conditions, and correspondingly higher, or less negative, ozone impacts under lower NO_x conditions. It is concluded that these compounds can be reasonably be expected to have low or negative ozone impacts under low NO_x conditions, but that their atmospheric ozone impacts under higher NO_x conditions are uncertain. In the case of propyl bromide, the range of uncertainty is between approximately the reactivity of ethane to approximately one-fourth of the average of the reactivity of all reactive VOC emissions.

ACKNOWLEDGEMENTS

The authors acknowledge Dr. Roger Atkinson for helpful discussions, Dr. Ernesto Tuazon for carrying out the measurements of the ozone and HBr reaction, and Mr. Dennis Fitz for assistance in administering this program. Although this work was funded by Albemarle corporation, the opinions and conclusions expressed in this report are entirely those of the primary author, Dr. William P. L. Carter. Mention of trade names or commercial products do not constitute endorsement or recommendation for use.

TABLE OF CONTENTS

LIST OF TABLES

LIST OF FIGURES

INTRODUCTION

Ozone in photochemical smog is formed from the gas-phase reactions of volatile organic compounds (VOCs) and oxides of nitrogen (NO_x) in sunlight. Although Los Angeles has the worst ozone problem in the United States, other areas of the country also have episodes where ozone exceeds the federal air quality standard of 0.12 ppm. Ozone control strategies in the past have focused primarily on VOC controls, though the importance of NO_x control has become recognized in recent years. VOC and NO_x controls have differing effects on ozone formation. NO_x is required for ozone formation, and if the levels of NO_x are low compared to the levels of reactive VOCs, then changing VOC emissions will have relatively little effect on ozone. Since NO_x is removed from the atmosphere more rapidly than VOCs, ozone in areas far downwind from the primary sources tend to be more NO_x limited, and thus less responsive to VOC controls. VOC controls tend to reduce the rate that O_3 is formed when NO_x is present, so VOC controls are the most beneficial in reducing O_3 in the urban source areas, where NO_x is relatively plentiful, and where O_3 yields are determined primarily by how rapidly it is being formed. Because of this, any comprehensive ozone control strategy must involve reduction of emissions of both NO_x and VOCs.

Many different types of VOC compounds are emitted into the atmosphere, each reacting at different rates and having different mechanisms for their reactions. Because of this, they can differ significantly in their effects on ozone formation, or their "reactivity". Some compounds, such as CFCs, do not react in the lower atmosphere at all, and thus make no contribution to ground-level ozone formation. Others, such as methane, react and contribute to ozone formation, but react so slowly that their practical effect on ozone formation is negligible. Obviously, it does not make sense to regulate such compounds as ozone precursors. In recognition of this, the EPA has exempted certain compounds from such regulations on the basis of having "negligible" effects on ozone formation. Although the EPA has no formal policy on what constitutes "negligible" reactivity, in practice it has used the ozone formation potential of ethane as the standard in this regard. This is because ethane is the most reactive of the compounds that the EPA has exempted to date. Therefore, the ozone formation potential of a compound relative to ethane is of particular interest when assessing whether it might be a likely candidate for exemption from regulation as an ozone precursor.

The ozone formation potential of a compound is influenced by a number of factors. These include how rapidly the compound reacts, the amount ozone directly formed by the intermediates formed in the VOC's reactions, whether the VOC's reactions tend to enhance or inhibit radical levels, the extent to which the VOC's reactions affect NO_x and O_3 removal, and the reactivity characteristics of the VOC's major oxidation products. The relative importance in affecting the net effect of the VOC on ozone formation can vary significantly depending on what other reactants are present, so the ozone impact of

a VOC also depends on environmental conditions. Because it is difficult to experimentally duplicate in the laboratory all the environmental conditions which might affect ozone formation, the only practical way to estimate a VOC's ozone impact under various conditions is to conduct airshed model calculations simulating the effects of emissions of the VOCs. These require a model for the airshed conditions, and a chemical mechanism for the VOCs major atmospheric reactions. However, the results of these predictions are no more valid than the chemical mechanism which is employed. Because of the complexity and uncertainties in these mechanisms for all but the simplest VOCs, no mechanism can be considered reliable for estimating ozone impacts unless its predictive capability has been demonstrated. This can be evaluated by conducting environmental chamber experiments designed to represent varying conditions which affect atmospheric ozone formation.

N-propyl and n-butyl bromides are compounds whose potential uses as solvents and for other purposes are being investigated by Albemarle Corporation. These compounds are sufficiently volatile that their use may result in their being emitted into the atmosphere, where they might react to participate in ozone formation. The appropriateness of regulating these compounds as ozone precursors is of obvious interest in assessing their potential utility and marketability.

There is already some information available concerning the atmospheric reactions of 1-propyl and 1-butyl bromides. On a per-gram basis, the OH radical rate constant for n-propyl bromide is approximately the same as that for ethane, and that for n-butyl bromide is approximately twice as much (Donaghy et al. 1993). However, when considering relative ozone impacts, one must also consider the nature of the reaction mechanism. If these compounds turn have low reactivity products or react in such a way that they inhibit radical levels, they would have a much lower ozone impact than estimated based on their reaction rates, and may even be ozone inhibitors. On the other hand, if they have unusually reactive products or react in such a way as to enhance radical levels, might be much more reactive than ethane. Although mechanisms for these compounds can be estimated, information concerning the atmospheric reactions of bromine-containing organic compounds is highly limited, and predictions of these mechanisms would be highly uncertain.

To obtain data needed to evaluate the appropriateness of regulating these compounds as ozone precursors, Albemarle corporation contracted the College of Engineering Center for Environmental Research and Technology (CE-CERT) to carry out the environmental chamber experiments to measure the ozone impacts of these compounds under various simulated atmospheric conditions, develop and evaluate mechanisms for their atmospheric reactions, and then use the evaluated mechanism to calculate their ozone impacts under a variety of atmospheric conditions, and compare them with those calculated for ethane. The results of this study are documented in this report.

EXPERIMENTAL AND DATA ANALYSIS METHODS

Overall Experimental Approach

The environmental chamber experiments carried out for this study consisted primarily of measurements of "incremental reactivities" of 1-propyl bromide or 1-butyl bromide under various conditions. These involve two types of irradiations of model photochemical smog mixtures. The first is a "base case" experiment where a mixture of reactive organic gases (ROGs) representing those present in polluted atmospheres (the "ROG surrogate") is irradiated in the presence of oxides of nitrogen (NO_x) in air. The second is the "test" experiment which consists of repeating the base case irradiation except that the VOC whose reactivity is being assessed is added. The differences between the results of these experiments provide a measure of the atmospheric impact of the test compound, and the difference relative to the amount added is a measure of its reactivity.

To provide data concerning the reactivities of the bromides under varying atmospheric conditions, three types of base case experiments were carried out:

1. Mini-Surrogate Experiments. This base case employed a simplified ROG surrogate and relatively low ROG/NO_x ratios. Low ROG/NO_x ratios represent "maximum incremental reactivity" (MIR) conditions, which are most sensitive to VOC effects. This is useful because it provides a sensitive test for the model, and also because it is most important that the model correctly predict a VOC's reactivity under conditions where the atmosphere is most sensitive to the VOCs. The ROG mini-surrogate mixture employed consisted of ethene, n-hexane, and m-xylene. This same surrogate was employed in our previous studies (Carter et al, 1993a,b; 1995a.), and was found to provide a more sensitive test of the mechanism than the more complex surrogates which more closely represent atmospheric conditions (Carter et al, 1995a). This high sensitivity to mechanistic differences makes the mini-surrogate experiments most useful for mechanism evaluation.

2. Full Surrogate Experiments. This base case employed a more complex ROG surrogate under somewhat higher, though still relatively low, ROG/NO_x conditions. While less sensitive to the mechanism employed, experiments with a more representative ROG surrogate are needed to evaluate the mechanism under conditions that more closely resembling the atmosphere. The ROG surrogate employed was the same as the 8-component "lumped molecule" surrogate as employed in our previous study (Carter et al., 1995a), and consists of n-butane, n-octane, ethene, propene, trans-2-butene, toluene, m-xylene, and formaldehyde. Calculations have indicated that use of this 8-component mixture will give essentially the same results in incremental reactivity experiments as actual ambient mixtures (Carter et al., 1995a).

3. Full Surrogate, low NO_x Experiments. This base case employing the same 8-component lumped molecule surrogate as the full surrogate experiments described above, except that lower NO_x levels (higher ROG/NO_x ratios) were employed to represent NO_x-limited conditions. Such experiments are necessary to assess the ability of the model to properly simulate reactivities under conditions where NO_x is low. The initial ROG and NO_x reactant concentrations were comparable to those employed in our previous studies (Carter et al. 1995a).

An appropriate set of control and characterization experiments necessary for assuring data quality and characterizing the conditions of the runs for mechanism evaluation were also carried out. These are discussed where relevant in the results or modeling methods sections.

Environmental Chamber

The environmental chamber system employed in this study was the CE-CERT "Dividable Teflon Chamber" (DTC) with a blacklight light source. This consists of two ~5000-liter 2-mil heat-sealed FEP Teflon reaction bags located adjacent to each other and fitted inside an 8'x8'x8' framework, and which uses two diametrically opposed banks of 32 Sylvania 40-W BL black lights as the light source. The lighting system in the DTC was found to provide so much intensity that only half the lights were used for irradiation. The unused black lights were covered with aluminum sheet as well, and were used to bring the chamber up to the temperature it will encounter during the irradiation before the uncovered lights are turned on. The air conditioner for the chamber room was turned on before and during the experiments. Four air blowers which are located in the bottom of the chamber were used to help cool the chamber as well as mix the contents of the chamber. The CE-CERT DTC is very similar to the SAPRC DTC which is described in detail elsewhere (Carter et al, 1995a,b).

The DTC is designed to allow simultaneous irradiations of the base case and the test experiments under the same reaction conditions. Since the chamber is actually two adjacent FEP Teflon reaction bags, two mixtures can be simultaneously irradiated using the same light source and with the same temperature control system. These two reaction bags are referred to as the two "sides" of the chamber (Side A and Side B) in the subsequent discussion. The sides are interconnected with two ports, each with a box fan, which rapidly exchange their contents to assure that base case reactants have equal concentrations in both sides. In addition, a fan is located in each of the reaction bags to rapidly mix the reactants within each chamber. The ports connecting the two reactors can then be closed to allow separate injections on each side, and separate monitoring of each side. This design is optimized for carrying out incremental reactivity experiments such as those for this program.

Experimental Procedures

The reaction bags were flushed with dry air produced by an AADCO air purification system for 14 hours (6pm-8am) on the nights before experiments. The continuous monitors were connected prior to reactant injection and the data system began logging data from the continuous monitoring systems. The

reactants were injected as described below (see also Carter et al, 1993a,, 1995b). The common reactants were injected in both sides simultaneously using a three-way (one inlet and two outlets connected to side A and B respectively) bulb of 2 liters in the injection line and were well mixed before the chamber was divided. The contents of each side were blown into the other using two box fans located between them. Mixing fans were used to mix the reactants in the chamber during the injection period, but these were turned off prior to the irradiation. The sides were then separated by closing the ports which connected them, after turning all the fans off to allow their pressures to equalize. After that, reactants for specific sides (the test compound in the case of reactivity experiments) were injected and mixed. The irradiation began by turning on the lights and proceeded for 6 hours. After the run, the contents of the chamber were emptied by allowing the bag to collapse, and then was flushed with purified air. The contents of the reactors were vented into a fume hood.

The procedures for injecting the various types of reactants were as follows. The NO and NO_2 were prepared for injection using a high vacuum rack. Known pressure of NO, measured with MKS Baratron capacitance manometers, were expanded into Pyrex bulbs with known volumes, which were then filled with nitrogen (for NO) or oxygen (for NO2). The contents of the bulbs were then flushed into the chamber with AADCO air. The other gas reactants were prepared for injection either using a high vacuum rack or a gas-tight syringes whose amounts were calculated. The gas reactants in a gas-tight syringe was usually diluted to 100-ml with nitrogen in a syringe. The volatile liquid reactants (including both alkyl bromides were injected, using a micro syringe, into a 1-liter Pyrex bulb equipped with stopcocks on each end and a port for the injection of the liquid. The port was then closed and one end of the bulb was attached to the injection port of the chamber and the other to a dry air source. The stopcocks were then opened, and the contents of the bulb were flushed into the chamber with a combination of dry air and heat gun for approximately 5 minutes. Formaldehyde was prepared in a vacuum rack system by heating paraformaldehyde in an evacuated bulb until the pressure corresponded to the desired amount of formaldehyde. The bulb was then closed and detached from the vacuum system and its contents were flushed into the chamber with dry air through the injection port.

Analytical Methods

Ozone and nitrogen oxides (NO_x) were continuously monitored using commercially available continuous analyzers with Teflon sample lines inserted directly into the chambers. The sampling lines from each side of the chamber were connected to solenoids which switched from side to side every 10 minutes, so the instruments alternately collected data from each side. Ozone was monitored using a Dasibi 1003AH UV photometric ozone analyzer and NO and total oxides of nitrogen (including HNO_3 and organic nitrates) were monitored using a Teco Model 14B chemiluminescent NO/NO_x monitor. The output of these instruments, along with that from the temperature sensors and the formaldehyde instrument, were attached to a computer data acquisition system, which recorded the data at 10 minutes intervals for ozone, NO and temperature (and at 15 minutes for formaldehyde), using 30 second averaging times. This yielded a sampling interval of 20 minutes for taking data from each side.

The Teco instrument and Dasibi CO analyzer were calibrated with a certified NO and CO source and CSI gas-phase dilution system. It was done prior to chamber experiment for each run. The NO_2 converter efficiency check was carried out in regular intervals. Dasibi ozone analyzer was calibrated against transfer standard ozone analyzer using transfer standard method in a interval of three months and was check with CSI ozone generator (set to 400 ppb) for each experiment to assure that the instrument worked properly. The details were discussed elsewhere (Carter et al, 1995b)

Organic reactants other than formaldehyde were measured by gas chromatography with FID and ECD detections as described elsewhere (Carter et al. 1993a; 1995b). GC samples were taken for analysis at intervals from 20 minutes to 30 minutes either using 100 ml gas-tight glass syringes or by collecting the 100 ml sample from the chamber onto Tenax-GC solid adsorbent cartridge. These samples were taken from ports directly connected to the chamber after injection and before irradiation and at regular intervals after irradiation. The sampling method employed for injecting the sample onto the GC column depended on the volatility or "stickiness" of the compound. For analysis of the more volatile species, which includes all the organic compounds monitored in this study, the contents of the syringe were flushed through a 2 ml or 3 ml stainless steel or 1/8’ Teflon tube loop and subsequently injected onto the column by turning a gas sample valve.

The calibrations for the GC analyses for most compounds were carried out by sampling from chambers or vessels of known volume into which known amounts of the reactants were injected, as described previously (Carter et al, 1995b).

Characterization Methods

Three temperature thermocouples for each chamber were used to monitor the chamber temperature, two of which were located in the sampling line of continuous analyzers to monitor the temperature in each side. The third one was located in the chamber to monitor chamber temperature. The temperature in these experiment were typically 21-25 C for DTC and 25-30 C for CTC.

The light intensity in the DTC chamber was monitored by periodic NO_2 actinometry experiments utilizing the quartz tube method of Zafonte et al (1977), with the data analysis method modified as discussed by Carter et al. (1995b). The results of these experiments were tracked over time in this chamber since it was first constructed in early 1994, and were fit by a curve where the NO_2 photolysis rate decayed relatively rapidly from its initial values of ~0.31 min^{-1} when the chamber and lights were new, then declining only slowly during the time of these experiments. A curve through the full set of actinometry results predicted NO_2 photolysis rates in the range of 0.202 - 0.193 min^{-1} during the time of these experiments, and the results of the actinometry experiments associated with the runs in this study are consistent with this range. The spectrum of the blacklight light source was measured using a LiCor LI-1200 spectra radiometer, and found to be essentially the same as the general blacklight spectrum recommended by Carter et al (1995b) for use in modeling blacklight chamber experiments.

The dilution of the DTC chamber due to sampling is expected to be small because the flexible reaction bags can collapse as samples are withdrawn for analysis. However, some dilution occurs with the aging of reaction bags because of small leaks. Information concerning dilution in an experiment can be obtained from relative rates of decay of added VOCs which react with OH radicals with differing rate constants (Carter et al., 1993a; 1995b). Most experiments had a more reactive compounds such as m-xylene and n-octane present either as a reactant or added in trace amounts to monitor OH radical levels. Trace amounts (~0.1 ppm) of n-butane were also added to experiments if needed to provide a less reactive compound for monitoring dilution. In addition, specific dilution check experiments such as CO irradiations were carried out. Based on these results, the dilution rates were found to average ~0.5% per hour on both sides.

Reactivity Data Analysis Methods

As indicated above, most of the experiments for this program consisted of simultaneous irradiation of a "base case" reactive organic gas (ROG) surrogate - NO_x mixture in one of the dual reaction chambers, together with an irradiation, in the other reactor, of the same mixture with either 1-propyl bromide or 1-butyl bromide added. The results are analyzed to yield two measures of VOC reactivity: the effect of the added bromide on the amount of NO reacted plus the amount of ozone formed, and integrated OH radical levels. These are discussed in more detail below.

The first measure of reactivity is the effect of the VOC on the change in the quantity $[O_3]$-[NO], or $([O_3]_t$-$[NO]_t)$-$([O_3]_0$-$[NO]_0)$, which is abbreviated as $d(O_3$-NO) in the subsequent discussion. As discussed elsewhere (e.g., Johnson, 1983; Carter and Atkinson, 1987; Carter and Lurmann, 1990, 1991, Carter et al, 1993a, 1995a,c), this gives a direct measure of the amount of conversion of NO to NO_2 by peroxy radicals formed in the photooxidation reactions, which is the process that is directly responsible for ozone formation in the atmosphere. (Johnson calls it "smog produced" or "SP".) The incremental reactivity of the VOC relative to this quantity, which is calculated for each hour of the experiment, is given by

$$IR[d(O_3\text{-NO})]_t^{VOC} = \frac{d(O_3\text{-NO})_t^{test} - d(O_3\text{-NO})_t^{base}}{[VOC]_0} \qquad (I)$$

where $d(O_3\text{-NO})_t^{test}$ is the $d(O_3$-NO) measured at time t from the experiment where the test VOC was added, $d(O_3\text{-NO})_t^{base}$ is the corresponding value from the corresponding base case run, and $[VOC]_0$ is the amount of test VOC added. An estimated uncertainty for IR[$d(O_3$-NO)] is derived based on assuming an ~3% uncertainty or imprecision in the measured $d(O_3$-NO) values. This is consistent with the results of the side equivalency test, where equivalent base case mixtures are irradiated on each side of the chamber.

Note that reactivity relative to $d(O_3$-NO) is essentially the same as reactivity relative to O_3 in experiments where O_3 levels are high, because under such conditions $[NO]_t^{base} \approx [NO]_t^{test} \approx 0$, so a change $d(O_3$-NO) caused by the test compound is due to the change in O_3 alone. However, $d(O_3$-NO) reactivity

has the advantage that it provides a useful measure of the effect of the VOC on processes responsible for O_3 formation even in experiments where O_3 formation is suppressed by relatively high NO levels.

The second measure of reactivity is the effect of the VOC on integrated hydroxyl (OH) radical concentrations in the experiment, which is abbreviated as "IntOH" in the subsequent discussion. This is an important factor affecting reactivity because radical levels affect how rapidly all VOCs present, including the base ROG components, react to form ozone. If a compound is present in the experiment which reacts primarily with OH radicals, then the IntOH at time t can be estimated from

$$\text{IntOH}_t = \int_0^t [\text{OH}]_\tau \, d\tau = \frac{\ln\left(\frac{[\text{tracer}]_0}{[\text{tracer}]_t}\right) - D\,t}{k\text{OH}^{\text{tracer}}}, \qquad \text{(II)}$$

where $[\text{tracer}]_0$ and $[\text{tracer}]_t$ are the initial and time=t concentrations of the tracer compound, $k\text{OH}^{\text{tracer}}$ its OH rate constant, and D is the dilution rate in the experiments. The latter was found to be small and was neglected in our analysis. The concentration of tracer at each hourly interval was determined by linear interpolation of the experimentally measured values. M-xylene was used as the OH tracer in these experiments because it is a base case component present in all incremental reactivity experiments, its OH rate constant is known (the value used was 2.36×10^{-11} cm^3 $molec^{-1}$ s^{-1} [Atkinson, 1989]), and it reacts sufficiently rapidly that its consumption rate can be measured with reasonable precision.

The effect of the VOC on OH radicals can thus be measured by its IntOH incremental reactivity, which is defined as

$$\text{IR}[\text{IntOH}]_t = \frac{\text{IntOH}_t^{\text{test}} - \text{IntOH}_t^{\text{base}}}{[\text{VOC}]_0} \qquad \text{(III)}$$

where $\text{IntOH}_t^{\text{test}}$ and $\text{IntOH}_t^{\text{base}}$ are the IntOH values measured at time t in the added VOC and the base case experiment, respectively. The results are reported in units of 10^6 min. The uncertainties in IntOH and IR[IntOH] are estimated based on assuming an ~2% imprecision in the measurements of the m-xylene concentrations. This is consistent with the observed precision of results of replicate analyses of this compound.

Studies of the HBr and Ozone Reaction

Because model simulations of the results of the chamber experiments suggested that there may be a rapid reaction between ozone and HBr, an exploratory experiment to evaluate this was carried out by Dr. Ernesto Tuazon at the Statewide Air Pollution Research Center (SAPRC). The SAPRC 5800-liter evacuable chamber, containing a multiple reflection optical system interfaced to a Nicolet 7199 Fourier transform infrared (FT-IR) absorption spectrometer, was employed. The chamber walls consist of FEP-Teflon coated aluminum with quartz end windows. The chamber was filled with ultra dry synthetic air made from evaporated liquid nitrogen and ultrahigh purity tank oxygen. Approximately 5 ppm and then

10 ppm of HBr was injected into the chamber and its dark decay was monitored by FT-IR. then approximately 12-13 ppm O_3 was injected and the decay of both O_3 and HBr was monitored by FT-IR. No irradiation was conducted.

CHEMICAL MECHANISMS AND MODELING METHODS

Chemical Mechanism

General Atmospheric Photooxidation Mechanism

Ozone formation in photochemical smog is due to the gas-phase reactions of oxides of nitrogen (NO_x) and various reactive organic gases (ROGs) in sunlight. Various reaction schemes have been developed to represent these processes (e.g., Gery et al., 1988; Carter, 1990; Stockwell et al., 1990), but the one used as the starting point for this work was an updated version of the detailed SAPRC mechanism (Carter, 1990, 1995; Carter et al., 1993b, 1997a). This is detailed in the sense that it explicitly represents a large number of different types of organic compounds, but it uses a condensed representation for most of their reactive products. The major characteristics of this mechanism are described by Carter (1990). The reactions of inorganics, CO, formaldehyde, acetaldehyde, peroxyacetyl nitrate, propionaldehyde, peroxypropionyl nitrate, glyoxal and its PAN analog, methyl glyoxal (model species 'MGLY"), and several other product compounds are represented explicitly. The reactions of unknown photoreactive products formed in the reactions of aromatic hydrocarbons are represented by model species whose yields and photolysis rate are adjusted based on fits of model simulations to environmental chamber experiments. A "chemical operator" approach is used to represent peroxy radical reactions. Generalized reactions with variable rate constants and product yields are used to represent the primary emitted alkane, alkene, aromatic, and other VOCs (with rate constants and product yields appropriate for the individual compounds being represented in each simulation). Most of the higher molecular weight oxygenated product species are represented using the "surrogate species" approach, where simpler molecules such as propionaldehyde or 2-butanone are used to represent the reactions of higher molecular weight analogues that are assumed to react similarly.

The mechanism of Carter (1990) was updated several times prior to this work. A number of changes were made to account for new kinetic and mechanistic information for certain classes of compounds as described by Carter et. al. (1993b) and Carter (1995). Further modifications to the uncertain portions of the mechanisms for the aromatic hydrocarbons were made to satisfactorily simulate results of experiments carried out using differing light sources (Carter et al. 1997a). The latest version of the general mechanism is discussed by Carter et al. (1997a).

Atmospheric Reactions of Propyl and Butyl Bromides

Table 1 gives a listing of the reactions added to the general mechanism to represent the atmospheric reactions of 1-propyl bromide, butyl bromide, and the product and intermediate species they form which were not already in the general mechanism. The latter include the major α-bromo carbonyl products predicted to be formed from propyl and butyl bromides, the reactions of bromine atoms, and

Table 1. Listing of the reactions added to the general atmospheric photooxidation mechanism to represent the atmospheric reactions of 1-propyl bromide, 1-butyl bromide, and bromine containing species. [a]

Kinetic Parameters [b]				Notes	Reactions [c]
k(300)	A	Ea	B	[d]	
Reactions of 1-Propyl and 1-Butyl Bromides					
1.18E-12				1,2	C3-BR + HO. = 0.63 RO2-R. + 0.33 RO2-BR. + 0.04 RO2-N. + RO2. + 0.01 HCHO + 0.51 RCHO + 0.44 MEK + 0.44 BR-KET
2.46E-12				1,3	C4-BR + HO. = 0.68 RO2-R. + 0.26 RO2-BR. + 0.06 RO2-N. + RO2. + 0.94 RCHO + 0.23 MEK + 0.31 BR-ALD + 0.17 BR-KET
(Same k as for RO2.)				4	RO2-BR. + NO = NO2 + BR.
(Same k as for RO2.)					RO2-BR. + HO2. = -OOH
(Same k as for RO2.)					RO2-BR. + RO2. = RO2. + 0.5 BR.
(Same k as for RO2.)					RO2-BR. + RCO3. = RCO3. + 0.5 BR.
Reactions of Bromoacetaldehyde					
(Same k as for RCHO)				5	BR-ALD + HO. = C2CO-O2. + RCO3.
(Phot. Set = CCHOR, varied)				6	BR-ALD + HV = HO2. + CO + HCHO + RO2-BR. + RO2.
(slow)				7	BR-ALD + O3 = products
Reactions of Bromoacetone [e]					
(Phot. Set = KETONE, varied)				8	BR-KET + HV = CCO-O2. + HCHO + RO2-BR. + RO2. + RCO3.
(slow)				9	BR-KET + HO. = products
(slow)				7	BR-KET + O3 = products
BrOx Reactions Added to Mechanism [f]					
(ignored)				10	BR. + NO = BRNO
(fast)				10	BRNO + HV = BR. + NO
(ignored)				10	BR. + NO2 = BRNO2
(fast)				10	BRNO2 + HV = BR. + NO2
1.18E-12	1.70E-11	1.59	0.00		BR. + O3 = BRO. + O2
1.96E-12	1.40E-11	1.17	0.00		BR. + HO2. = HBR + O2
1.60E-11	(No T Dependence)				BR. + NO3 = BRO. + NO2
(Phot. Set = BRO [g])					BRO. + HV = BR. + O
2.07E-11	8.70E-12	-0.52	0.00		BRO. + NO = BR. + NO2
4.69E-31	(Falloff Kinetics)				BRO. + NO2 = BRONO2
k0 =	4.70E-31	0.00	-3.10		
kINF =	1.70E-11	0.00	-0.60		
	F= 0.40	n= 1.00			
1.00E-12	(No T Dependence)			11	BRO. + NO3 = BR. + NO2 + O2
3.28E-11	6.20E-12	-0.99	0.00		BRO. + HO2. = HOBR + O2
2.50E-12	(No T Dependence)				BRO. + BRO. = 2 BR. + O2
kEQ x k(BRO. + NO2)				12	BRONO2 = BRO. + NO2
kEQ =	5.20E+25	23.49	3.40		
(Phot. Set = BRONO2)				13	BRONO2 + HV = 0.9 {BR. + NO3} + 0.1 {BR. + NO2 +O}
(Phot. Set = HOBR)					HOBR + HV = HO. + BR.
1.10E-11	1.10E-11	0.00	-0.80		HBR + HO. = H2O + BR.
(slow)				14	HBR + HO_2 = H2O2 + BR.
1.00E-15	(adjusted - see text)			15	HBR + O3 = HOBR + O2 [h]
Br + VOC and Br + VOC Product Reactions Added to Mechanism					
1.18E-12	1.70E-11	1.59	0.00		BR. + HCHO = HBR + HO2. + CO
3.92E-12	1.30E-11	0.72	0.00		BR. + CCHO = HBR + CCO-O2. + RCO3.
(Same k as for CCHO)				16	BR. + RCHO = HBR + C2CO-O2. + RCO3.
(Same k as for CCHO)				16	BR. + GLY = HBR + 0.6 HO2. + 1.2 CO + 0.4 {HCOCO-O2. + RCH3}

Table 1 (continued)

Kinetic Parameters [b]				Notes	Reactions [c]
k(300)	A	Ea	B	[d]	
	(Same k as for CCHO)			16	BR. + MGLY = HBR + CO + CCO-O2. + RCO3.
	(Same k as for CCHO)			16	BR. + BALD = HBR + BZ-CO-O2. + RCO3.
	(slow)			17	BR. + alkanes = HBR + products
	(slow)			18	BR. + aromatics = unknown products
1.60E-13	(T Depend. ignored)			19	BR. + ETHENE = BR-ALD + RO2-R. + RO2.
3.30E-12	(T Depend. ignored)			20	Br. + PROPENE = BR-ALD + RO2-R. + RO2.
9.40E-12	(T Depend. ignored)			21	BR. + T-2-BUTE = 2 CCHO + RO2-BR. + R2O2. + 2 RO2.
Br + Lumped VOC Groups Used in the Ambient Air Simulations					
3.30E-12	(T Depend. ignored)			22	BR. + OLE1 = BR-ALD + RO2-R. + RO2.
9.40E-12	(T Depend. ignored)			23	BR. + OLE2 = 0.86 {RO2-BR. + R2O2.} + 0.14 RO2-N. + 1.86 RO2. + 0.24 HCHO + 0.66 CCHO + 0.51 RCHO + 0.11 ACET + 0.09 MEK + 0.06 BALD

[a] A listing of the general mechanism to which these reactions were added is given in Appendix A.

[b] Except as noted, the expression for rate constant is $k = A\ e^{Ea/RT}\ (T/300)^{B}$. Rate constants and A factor are in ppm, min units. Units of Ea is kcal $mole^{-1}$. For falloff kinetics the rate constants are given by $(k0[M]kINF)/(k0[M]+kINF) \times F^{X}$, where $X = 1/(1+\log_{10}(k0[M]/kINF)^2)$. For photolysis reactions, the rate constants are calculated using the absorption cross sections in the associated photolysis files, which are given in Table 2. Unit quantum yields were assumed unless indicated otherwise in the listing.

[c] See Carter (1990) for a description of the species used in the general mechanism.

[d] Documentation notes are as follows. If no documentation notes are given, the kinetic parameters and absorption coefficient and quantum yields are from the latest IUPAC evaluation (Atkinson et al., 1997).

1 Rate constants from Donaghy et al. (1993). Temperature dependence is unknown but probably is not large. Mechanisms are estimated as discussed in the text.

2 RCHO represents propionaldehyde and $BrCH_2CH_2CHO$. BR-KET represents bromoacetone.

3 RCHO represents propionaldehyde, 4-hydroxy propionaldehyde and 4-bromo propionaldehyde; MEK represents methyl-(2-bromoethyl) ketone; BR-ALD represents bromoacetaldehyde. Product yields were derived by adjusting the branching ratios b_1, b_2, and the overall nitrate yield, $[b_1(a_1+a_4)+b_2(a_2+a_3)]$, to minimize the sum of squares differences between experimental and calculated $d(O_3\text{-NO})$ data for mini-surrogate run DTC-419(B) and high NO_x full surrogate run DTC-432(B), with b_4 not being varied because it corresponds to only a minor process, and with b_3 determined from $1\text{-}b_1\text{-}b_2\text{-}b_4$. (See text for the definition of these parameters). The low NO_x full surrogate run was not used in the optimization because the optimization of these parameters could not yield close fits in any case.

4 The "chemical operator" RO2-Br. represents the effects of reactions of peroxy radicals which ultimately form Br atoms after reacting with NO. Rate constants assumed to be the same as for other similar peroxy radical operators used in the general mechanism (Carter, 1990).

5 Assumed to have same rate constant as analogous reactions of lumped higher aldehyde (e.g., propionaldehyde). Br-containing peroxyacyl radicals, and the Br-containing PAN analogue, are lumped with the other higher peroxyacyl radicals and PAN analogues.

6 Reaction assumed to be analogous to photolysis of acetaldehyde. The photolysis rate was assumed to be the same as for acetaldehyde; assuming higher photolysis rates did not improve fits of model

Table 1 (continued)

simulations to the chamber data (see text). $BrCH_2\cdot$ reacts with O_2 then NO to form $BrCH_2O\cdot$, which decomposes to formaldehyde and Br.

7 No chemically reasonable exothermic reaction route could be found. Any endothermic reaction would be expected to be too slow at ambient temperatures to be significant.

8 Reaction assumed to be analogous to the photolysis of acetone, with scission of the $CO\text{-}CH_2Br$ bond. The photolysis rate was assumed to be the same as for other higher ketones. Assuming higher photolysis rates did not improve fits of model simulations to the chamber data (see text). $BrCH_2\cdot$ reacts with O_2 then NO to form $BrCH_2O\cdot$, which decomposes to formaldehyde and Br.

9 Reaction of OH with bromoacetone is estimated to have a comparable rate constant as the reaction of OH with acetone (Kwok et al, 1995), which would make it of negligible importance in affecting the reactivities of the parent compound(s).

10 These reactions are ignored because they are expected to be rapidly reversed by photolysis of the products to the starting material The IUPAC recommended absorption cross sections and quantum yields for BrNO and $BrNO_2$ (Atkinson et al. 1997) indicate that they would photolyze rapidly under atmospheric conditions.

11 Reaction initially forms BrO_2, which is assumed to rapidly decompose to Br + O_2.

12 The unimolecular decomposition of $BrONO_2$ has not been studied, but may be non-negligible at tropospheric temperatures. It is estimated to be the same as estimated by us previously for the $ClONO_2$ decomposition (Carter et al. 1997b), which also has not been studied. This is highly uncertain, but model simulations are not sensitive to assumptions made concerning the $BrONO_2$ mechanism.

13 IUPAC (Atkinson et al. 1997) gives no recommendation concerning the quantum yield for $BrONO_2$ photolysis, but for the photolysis of $ClONO_2$, they recommend $\Phi(Cl+NO_2)=0.9$ and $\Phi(ClONO+O)=0.1$. The same quantum yields are assumed for the analogous reactions of $BrONO_2$. The BrONO formed in the 10% pathway is assumed to photolyze rapidly to form Br + NO_2, analogous to the IUPAC recommendation for ClONO.

14 Mellouki et al (1994) report an upper limit rate constant of $\leq 3 \times 10^{-17}$ cm^3 $molec^{-1}$ s^{-1} for this reaction.

15 This reaction had to be added to the mechanism to obtain acceptable fits of model simulations to the results of the alkyl bromide reactivity experiments. The rate constant was optimized to minimize the sum of squares difference between experimental and calculated $d(O_3\text{-}NO)$ in propyl bromide runs DTC-421(A), DTC-427(A), and DTC-428(B). The initial concentrations of some base ROG surrogate components in some of these runs were adjusted to optimize fits to the base case runs, to minimize effects of small biases in base case simulations on results of these optimizations. As discussed in the text, direct measurements of O_3 and HBr consumption in the dark indicate a rate constant of no more than 4×10^{-19} cm^3 $molec^{-1}$ s^{-1}, with two moles of HBr being consumed for each mole of O_3 reacting. Therefore, this reaction is included in the model with the 10^{-15} cm^3 $molec^{-1}$ s^{-1} rate constant not to represent an actual elementary reaction between O_3 and HBr, but to represent some other, unknown, process which has the same net effect on the system.

16 There are no data concerning this reaction, which is assumed to occur at the same rate as the reaction of Br with acetaldehyde.

17 The Br + isobutane rate constant at 298K has been measured to be 1.7×10^{-15} cm^3 $molec^{-1}$ s^{-1} (Russell et al. 1988), which would make it of negligible importance in this system. Abstraction from primary or secondary hydrogens should be even slower. Reactions of Br with alkanes are expected to be slow because they are calculated to be endothermic.

Table 1 (continued)

18 Bierbach et al (1996) reported an upper limit of 10^{-14} cm^3 $molec^{-1}$ s^{-1} for the reactions of Br with benzene, toluene, and p-xylene at 298K. This is sufficiently low that the possibility of reactions of Br with aromatics can be neglected in this system.

19 The rate constant is from Barnes et al. (1989). The rate constant was found to be pressure dependent and have a negative temperature dependence, consistent with an addition reaction forming an excited intermediate which can back-decompose to reactants or be stabilized (Barnes et al. 1989). The mechanism is based on the reaction of the adduct with O_2 and NO to form $BrCH_2CH_2O\cdot$, which primarily reacts with O_2 to form bromoacetaldehyde and HO_2. This is consistent with the observation of bromoacetaldehyde as a major product in this reaction (Barnes et al. 1989).

20 The rate constant used is the average of the T = 298K value of 3.85 x 10^{-12} cm^3 $molec^{-1}$ s^{-1} of Wallington et al. (1989) and the T = 298K value of 2.7 x 10^{-12} cm^3 $molec^{-1}$ s^{-1} of Barnes et al (1989). The temperature dependence is unknown and is ignored. It is assumed that most of the Br addition is to the terminal carbon, forming the $CH_3CHBrCH_2\cdot$ radical, when then reacts in the same way as assumed for it in the OH + 1-propyl bromide mechanism (see text).

21 The rate constant used is an average of the T = 298K value of 9.5 x 10^{-12} cm^3 $molec^{-1}$ s^{-1} of Wallington et al. (1989) and the T = 298K value of 9.3 x 10^{-12} cm^3 $molec^{-1}$ s^{-1} of Bierbach et al (1996). The temperature dependence is unknown and is ignored. The mechanism is based on the estimation that β-bromo alkoxy radicals would primarily decompose, ultimately forming Br atoms and 2 acetaldehyde molecules after two NO to NO_2 conversions.

22 OLE1 is the model species used to represent alkanes, other than ethene, which react with OH radicals with a rate constant less than $7x10^4$ ppm^{-1} min^{-1} (see Appendix A). These consist primarily of terminal alkenes. The mechanism and rate constant are assumed to be similar to that for ethene.

23 OLE2 is the model used to represent alkanes which react with OH radicals with a rate constant greater than $7x10^4$ ppm^{-1} min^{-1}. These consist primarily of terminal alkenes. Their rate constant is assumed to be the same as for trans-2-butene, and their mechanism is assumed to be analogous. Since this mechanism predicts that the Br + internal alkene is analogous to the OH reaction, except that RO2-BR. + R2O2. is formed instead of RO2-R., the organic products used are the same as those used for the OH + OLE2 reaction, which are derived based on the mixture of compounds being represented (see Appendix A).

[e] Bromoacetone reactions also used to represent reactions of bromomethyl ethyl ketone.

[f] Unless noted otherwise, rate constant from the 1997 IUPAC evaluation (Atkinson et al. 1997)

[g] Absorption cross sections are listed in Table A-3 in Appendix A. Unless noted otherwise, unit quantum yields were assumed.

[h] This is believed not to be an actual elementary reaction, but is included to represent some unknown process which has the same effect. Ambient simulations were carried out both with and without this reaction included.

the BrO_x species formed from bromine atoms under atmospheric conditions. These are discussed in the following sections.

Atmospheric Reaction Rates

The main atmospheric loss process for the simple alkyl bromides is expected to be reaction with OH radicals. Rate constants for a number of simple alkyl bromides are given in the latest evaluations (Atkinson, 1989, 1994), and based on these data, Kwok and Atkinson (1995) developed group-additivity factors for estimating OH radical rate constants for alkyl bromides in general. Measurements of the rate constants for n-propyl and n-butyl bromides are reported by Donaghy et al. (1993), who gave

$$k_{OH + 1\text{-propyl bromide}} = 1.18 \times 10^{-12} \text{ cm}^3 \text{ molec}^{-1} \text{ s}^{-1}$$

and

$$k_{OH + 1\text{-butyl bromide}} = 2.46 \times 10^{-12} \text{ cm}^3 \text{ molec}^{-1} \text{ s}^{-1}$$

at T=299 K. These are consistent with the rate constants estimated using the group-additivity method of Kwok and Atkinson (1995), which yield 0.9×10^{-12} and 2.2×10^{-12} cm^3 molec^{-1} s^{-1}, respectively, which is well within the uncertainty range of the estimation method. More recently, Nelson et al (1997) measured the OH radical rate constant for n-propyl bromide as a function of temperature, and obtained

$$k_{OH + 1\text{-propyl bromide}} = 5.75 \pm 0.9 \times 10^{-12} \exp(-504 \pm 50/T) \text{ cm}^3 \text{ molec}^{-1} \text{ s}^{-1},$$

which yields a 299K rate constant of 1.07×10^{-12} cm^3 molec^{-1} s^{-1}. This is in excellent agreement with the data of Donaghy et al (1993), especially considering that different experimental techniques were used. The room temperature rate constants of Donaghy et al (1993) were used in all the model simulations discussed in this report.

The absorption cross-sections for methyl bromide (Atkinson et al, 1997, Gillotay and Simon, 1988) indicate that this compound does not absorb light at wavelengths below ~260 nm, which means that it would not undergo significant photodecomposition in the lower atmosphere. One would expect the higher alkyl bromides to have similar absorption cross sections. Based on reported rate constants for other compounds, we would also not expect reaction of the alkyl bromides with ozone (Atkinson and Carter, 1984; Atkinson, 1994) or NO_3 radicals (Atkinson, 1991) to occur at significant rates. Therefore, in the model simulations we assume that OH reaction is be the only significant loss process for these compounds.

Propyl Bromide Reactions

There is no information concerning the mechanisms of the reactions of the alkyl bromides with OH radicals, but the initial reaction pathways can be estimated based on analogous reactions of other compounds (Atkinson, 1989), and their relative rates can be estimated using structure-reactivity methods (Atkinson, 1987; Kwok and Atkinson, 1995). In the case of 1-propyl bromide, the OH radical can attack at each of the three positions, yielding H_2O and the corresponding alkyl radical, as shown below.

$$CH_3CH_2CH_2Br + OH \rightarrow H_2O + \cdot CH_2CH_2CH_2Br \quad 18\% \quad (1)$$
$$CH_3CH_2CH_2Br + OH \rightarrow H_2O + CH_3CH(\cdot)CH_2Br \quad 46\% \quad (2)$$
$$CH_3CH_2CH_2Br + OH \rightarrow H_2O + CH_3CH_2CH(\cdot)Br \quad 35\% \quad (3)$$

The relative importances of reaction at the various positions, estimated using the structure-reactivity method of Kwok and Atkinson (1995), are also shown. Under atmospheric conditions, these alkyl radicals are expected to react rapidly with O_2 to form the corresponding peroxy radical, which, in the presence of NO_x, will react primarily with NO to for NO_2 and the corresponding alkoxy radical.

$$\cdot CH_2CH_2CH_2Br + O_2 \rightarrow \cdot OOCH_2CH_2CH_2Br$$
$$\cdot OOCH_2CH_2CH_2Br + NO \rightarrow NO_2 + \cdot OCH_2CH_2CH_2Br \quad (4)$$

$$CH_3CH(\cdot)CH_2Br + O_2 \rightarrow CH_3CH(OO\cdot)CH_2Br \quad (5)$$
$$CH_3CH(OO\cdot)CH_2Br + NO \rightarrow NO_2 + CH_3CH(O\cdot)CH_2Br$$

$$CH_3CH_2CH(\cdot)Br + O_2 \rightarrow CH_3CH_2CH(OO\cdot)Br \quad (6)$$
$$CH_3CH_2CH(OO\cdot)Br + NO \rightarrow NO_2 + CH_3CH_2CHBrO\cdot$$

However, based on analogous reactions of the alkanes (Carter and Atkinson, 1985, 1989a; Atkinson, 1990), a small fraction of the peroxy radical will also react with NO to form the corresponding alkyl nitrate,

$$\cdot OOCH_2CH_2CH_2Br + NO + M \rightarrow BrCH_2CH_2CH_2ONO_2 + M \quad (7)$$
$$CH_3CH(OO\cdot)CH_2Br + NO + M \rightarrow NO_2OCH(CH_3)CH_2Br + M \quad (8)$$
$$CH_3CH_2CH(OO\cdot)Br + NO + M \rightarrow CH_3CH_2CHBrONO_2 + M \quad (9)$$

in a process whose importance, relative to the formation of NO_2 and the alkoxy radical, tends to increase with the size of the molecule (Carter and Atkinson, 1985; 1989a).

The organic nitrate yields [i.e., $k7/(k_4+k_7)$, etc.] are important factors affecting a VOCs reactivity because nitrate formation is a radical termination process which tends to inhibit the processes of O_3 formation (Carter and Atkinson, 1989b; Carter, 1995). Based on the trends observed with nitrate yields in OH + alkane systems, the estimated nitrate yields are ~2% and ~5% for primary and secondary C_3 radicals, respectively. The effect of Br substitution on nitrate yields is unknown, but one might expect it would increase nitrate yields because it, in effect, increases the size of the molecule. However, chamber data for ethers (Carter et al, 1993a) and esters (unpublished results from this laboratory) suggest that electron withdrawing groups may decrease nitrate yields. In view of this uncertainty, we tentatively assume that -Br substitution has no effect, and thus use the estimates for C_3 alkyl radicals, or $k_7/(k_7+k_4)$ = 2% and $k_8/(k_8+k_5) = k_9/(k_9+k_6)$ = 5%. This gives an overall assumed nitrate yield of 4%. This is

relatively low and would not indicate significant radical inhibition. If this is an underestimate, it will be evident from the model simulations of the results of the reactivity experiments (Carter, 1995).

Most of the complexity and uncertainty in atmospheric photooxidation mechanism for VOCs come from the reactions of alkoxy radicals, which, depending on their structure, can react with O_2 to form HO_2 and the corresponding carbonyl, undergo β-scission decomposition to form a smaller carbonyl compound and a new alkyl radical, or, if the radical is large enough, undergo 1,4-internal hydrogen abstraction to form a Δ-hydroxy-substituted alkyl radical (Carter and Atkinson, 1985; Atkinson, 1990; 1997). However, the C_3 radicals cannot undergo 1,4-H shift reactions, so only the O_2 and decomposition reactions need to be considered. For the three alkoxy radicals initially formed in the propyl bromide system, the possible reactions are:

$$\cdot OCH_2CH_2CH_2Br + O_2 \rightarrow HCOCH_2CH_2Br + HO_2\cdot \quad (10)$$

$$\cdot OCH_2CH_2CH_2Br \rightarrow \cdot CH_2CH_2Br + HCHO \quad \text{Minor} \quad (11)$$

$$CH_3CH(O\cdot)CH_2Br + O_2 \rightarrow CH_3\text{-}CO\text{-}CH_2Br + HO_2\cdot \quad (12)$$

$$CH_3CH(O\cdot)CH_2Br \rightarrow CH3\cdot + BrCH_2CHO \quad \text{Very minor} \quad (13)$$

$$CH_3CH(O\cdot)CH_2Br \rightarrow CH3CHO + CH_2Br\cdot \quad \text{Minor} \quad (14)$$

$$CH_3CH_2CHBrO\cdot + O_2 \rightarrow CH_3CH2\text{-}CO\text{-}Br + HO_2 \quad \text{Very minor} \quad (15)$$

$$CH_3CH_2CHBrO\cdot \rightarrow CH_3CH_2CHO + Br\cdot \quad (16)$$

$$CH_3CH_2CHBrO\cdot \rightarrow CH_3CH_2\cdot + BrCHO\cdot \quad \text{Very minor} \quad (17)$$

Atkinson (1997) recently developed methods for estimating relative importances of these competing processes based on the limited kinetic available concerning alkoxy + O_2 and alkoxy β-scission decomposition reactions, and relative rate constants obtained from product yield studies. This involves examining relationships between rate constants and estimated heats of reaction for the O_2 reactions, and relationships between heats of reaction and ionization potentials of the leaving radical for the β-scission processes (Choo and Benson, 1981; Atkinson, 1997). Based on these methods, we estimate that O_2 reaction will dominate over decomposition for $\cdot OCH_2CH_2CH_2Br$ and $CH_3CH(O\cdot)CH_2Br$ radicals, but that decomposition to form Br atoms (Reaction 16) will dominate for $CH_3CH_2CHBrO\cdot$. These estimates must be considered to have relatively large uncertainty factors, though the conclusions that Reaction (16) dominates over (15) and (17), and that Reaction (13) is unimportant are probably not uncertain. On the other hand, given the uncertainties of these estimates, the possibilities that Reactions (11) and (14) are non-negligible cannot be strictly ruled out. However, for modeling purposes, we assume that Reactions (10), (12), and (16) dominate, as indicated above.

Neglecting the pathways which are assumed to be minor, the overall process of the OH + 1-propyl bromide reaction in the presence of O_2 and NO_x can be represented as follows,

$$OH + CH_3CH_2CH_2Br \xrightarrow{O_2,\ NO} \rightarrow \rightarrow - NO + 0.95\ NO_2 + 0.62\ HO_2 + 0.33\ Br\cdot + 0.05\ C_3H_6BrONO_2 + 0.45\ CH_3\text{-}CO\text{-}CH_2Br + 0.33\ CH_3CH_2CHO + 0.17\ BrCH_2CH_2CHO$$

where $C_3H_6BrONO_2$ represents the three possible bromoalkyl nitrate isomers. In terms of model species used in the simulations, this is represented as

$$OH + \text{Propyl Bromide} \rightarrow 0.62\ RO2\text{-}R. + 0.33\ RO2\text{-}BR. + 0.05\ RO2\text{-}N. + 0.5\ RCHO + 0.45\ BR\text{-}KET$$

where RO2-R., RO2-N., and RO2-BR. are chemical "operators" representing the effects peroxy radicals reacting with NO to form HO_2, an unreactive organic nitrate, or Br atoms, respectively, RCHO represents propionaldehyde and is also used to represent the reactions of $BrCH_2CH_2CHO$, and BR-KET represents bromoacetone, which is represented separately, as discussed below. See Carter (1990) for a more detailed discussion of how peroxy radical reactions are represented in the SAPRC mechanisms, and how chemical operators such as RO2-R. and RO2-N. are used. Note that RO2-BR. is a new chemical operator which is added to the mechanism to represent the effects of bromine atom formation, and, other than the fact that it forms Br atoms instead of HO_2 when it reacts with NO, is exactly analogous to the RO2-R. operator. The reactions of RO2-BR. and BR-KET are given in Table 1, and the reactions of RO2-R., RO2-N., and RCHO are given in Appendix A.

Note that the above mechanism is applicable only in the presence of NO_x and sunlight, which is required for O_3 formation to occur. In the absence of NO (or NO_x and sunlight, where NO is formed from the photolysis of NO_2), reactions (4-9) will not occur, and instead the peroxy radical will either react with HO_2 to form hydroperoxides, or with other peroxy radicals to form, in varying yields, various carbonyls, alcohols, or alkoxy radicals. These processes, which are not important in affecting O_3 formation, are represented using the same approach as employed for peroxy radicals formed from other VOC's, as discussed in detail elsewhere (Carter, 1990). This involves representing the overall process using various chemical operators and assuming that the organic products ultimately formed are the same as formed in the presence of NO_x and sunlight.

Note also that this mechanism, and the assumed product yields, are based entirely on estimates and not on experimental measurements of actual product yields. Obtaining product yield information necessary to directly verify these estimates was beyond the scope of this study. However this represents our best estimate given the data currently available.

Butyl Bromide Reactions

The considerations involved in estimating the atmospheric reaction mechanism for 1-butyl bromide are essentially the same as discussed above for propyl bromide, though the system is somewhat more complex. The initial OH reaction can occur at the four different positions, as follows,

$$CH_3CH_2CH_2CH_2Br + \cdot OH \rightarrow H_2O + CH_3CH_2CH_2CH(\cdot)Br \qquad 15\% \quad (18)$$

$$CH_3CH_2CH_2CH_2Br + \cdot OH \rightarrow H_2O + CH_3CH_2CH(\cdot)CH_2Br \quad 24\% \quad (19)$$

$$CH_3CH_2CH_2CH_2Br + \cdot OH \rightarrow H_2O + CH_3CH(\cdot)CH_2CH_2Br \quad 53\% \quad (20)$$

$$CH_3CH_2CH_2CH_2Br + \cdot OH \rightarrow H_2O + \cdot CH_2CH_2CH_2CH_2Br \quad 8\% \quad (21)$$

The relative importances of these competing processes, estimated using the structure-reactivity methods of Kwok and Atkinson (1995), are also shown. Note that these estimated relative importances are somewhat uncertain, and adjusting them to improve fits of model simulations to the chamber data may not be inappropriate. The radicals formed will then react with O_2 to form the corresponding peroxy radical, which, in the presence of NO_x and sunlight, will react with NO to form either NO_2 and the alkoxy radical, or, to a lesser but non-negligible extent, to form the corresponding alkyl nitrate.

$$CH_3CH_2CH_2CH(\cdot)Br + O_2 \rightarrow CH_3CH_2CH_2CH(OO\cdot)Br$$

$$CH_3CH_2CH_2CH(OO\cdot)Br + NO \rightarrow NO_2 + CH_3CH_2CH_2CHBrO\cdot \quad (22)$$

$$CH_3CH_2CH_2CH(OO\cdot)Br + NO \rightarrow CH_3CH_2CH_2CHBrONO_2 \quad (23)$$

$$CH_3CH_2CH(\cdot)CH_2Br + O_2 \rightarrow CH_3CH_2CH(OO\cdot)CH_2Br$$

$$CH_3CH_2CH(OO\cdot)CH_2Br + NO \rightarrow NO_2 + CH_3CH_2CH(O\cdot)CH_2Br \quad (24)$$

$$CH_3CH_2CH(OO\cdot)CH_2Br + NO \rightarrow CH_3CH_2CH(ONO_2)CH_2Br \quad (25)$$

$$CH_3CH(\cdot)CH_2CH_2Br + O_2 \rightarrow CH_3CH(OO\cdot)CH_2CH_2Br$$

$$CH_3CH(OO\cdot)CH_2CH_2Br + NO \rightarrow NO_2 + CH_3CH(O\cdot)CH_2CH_2Br \quad (26)$$

$$CH_3CH(OO\cdot)CH_2CH_2Br + NO \rightarrow CH_3CH(ONO_2)CH_2CH_2Br \quad (27)$$

$$BrCH_2CH_2CH_2CH_2O\cdot + O_2 \rightarrow BrCH_2CH_2CH_2CH_2OO\cdot$$

$$BrCH_2CH_2CH_2CH_2OO\cdot + NO \rightarrow NO_2 + BrCH_2CH_2CH_2CH_2O\cdot \quad (28)$$

$$BrCH_2CH_2CH_2CH_2OO\cdot + NO \rightarrow BrCH_2CH_2CH_2CH_2ONO_2 \quad (29)$$

As with the propyl bromide system, the nitrate yields are assumed to be the same as estimated by Carter and Atkinson (1989a) for primary or secondary alkyl peroxy radicals with the same number of carbons. For primary and secondary C_4 alkylperoxy radicals, Carter and Atkinson estimate nitrate yields of 3.5% and 8.5%, respectively. Therefore, we estimate that $k_{23}/(k_{22}+k_{23}) = k_{29}/(k_{28}+k_{29}) = 3.5\%$ and $k_{25}/(k_{24}+k_{25}) = k_{27}/(k_{26}+k_{27}) = 8.5\%$. This corresponds to an overall estimated nitrate yield of 8%. This is sufficiently large that the assumed nitrate yield will have a non-negligible effect on model simulations of the chamber experiments (Carter, 1995). Since this is uncertain, the nitrate yield is treated as an adjustable parameter if necessary to improve fits of model simulation to the results of the chamber experiments.

As discussed above, the alkoxy radicals formed in the above reactions could react with O_2, or undergo β-scission decomposition. In addition, the 1- or 4-alkoxy radicals formed Reaction (28) and (22),

can also undergo an internal 1,5-H shift isomerization via a six-member ring transition state. The possible reactions are listed below.

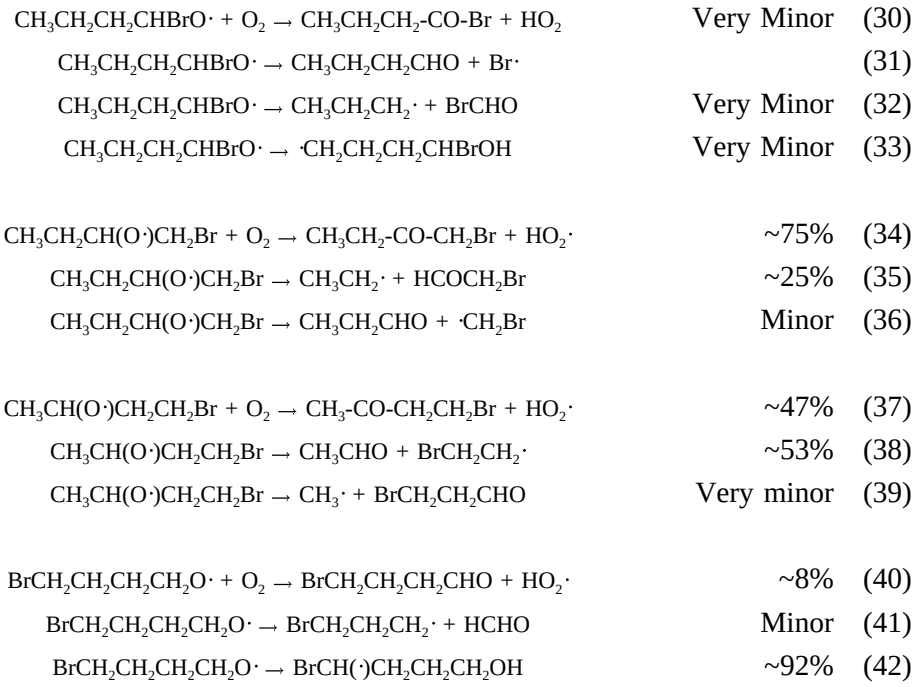

Also shown are our estimates of relative importances of these reactions, derived using the methods recently developed by Atkinson (1997). Based on the thermochemistry, it is reasonable to expect that Reaction 35 is unimportant and Reaction (40) dominates over the competing processes. However, the k_{33}/k_{34} and k_{36}/k_{37} rate constant rations are probably uncertain by at least a factor of ~3, and the k_{30}/k_{32} rate constant ratio is probably uncertain by at least an order of magnitude. Because of this uncertainty, these branching ratios can be treated as adjustable parameters if necessary to improve fits of model simulations to the results of the chamber experiments.

The Δ-hydroxy alkoxy radical formed in the 1,4-H shift isomerization reaction (32) is expected to react as follows, ultimately giving rise to additional Br atoms.

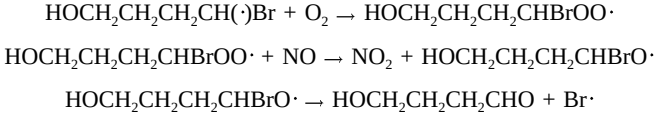

The competing reactions of the $HOCH_2CH_2CH_2CHBrO\cdot$ alkoxy radical are expected to be minor. The ethyl radicals formed in Reaction (37) will react to yield HO_2 and acetaldehyde, and the $BrCH_2CH_2\cdot$ radicals will be expected to react analogously,

$$CH_3CH_2\cdot + O_2 \rightarrow CH_3CH_2OO\cdot$$
$$CH_3CH_2OO\cdot + NO \rightarrow NO_2 + CH_3CH_2O\cdot$$
$$CH_3CH_2O\cdot + O_2 \rightarrow CH_3CHO + HO_2\cdot$$

$$BrCH_2CH_2\cdot + O_2 \rightarrow BrCH_2CH_2OO\cdot$$
$$BrCH_2CH_2OO\cdot + NO \rightarrow NO_2 + BrCH_2CH_2O\cdot$$
$$BrCH_2CH_2O\cdot + O_2 \rightarrow BrCH_2CHO + HO_2\cdot$$

Note that in all these cases the formation of these additional radicals via β-scission decomposition or 1,4-H shift isomerization result in additional NO to NO_2 conversions, which tend to increase the amount of ozone which can be formed in the overall process.

The above reactions can be combined, and recast in terms of model species used in the mechanism, as follows:

OH + Butyl Bromide → $(1-b_1)(a_1+a_4)$ RO2-R. + $(1-b_2)(a_2+a_3)$ RO2-R. + $[b_1(a_1+a_4)+b_2(a_2+a_3)]$ RO2-Br. + $(1-b_1)a_1(1-d_2)$ R2O2. + $(1-b_1)a_4(1-d_3)$ R2O2. + $(1-b_2)a_3(1-d_2)$ R2O2. + $(1-b_2)a_2(1-d_2)$ BR-KET + $[b_1(a_1+a_4)+b_2(a_2+a_3)]$ RO2-N.

where

$$a_1 = k_{18}(k_{18}+k_{19}+k_{20}+k_{21});\quad a_2 = k_{19}(k_{18}+k_{19}+k_{20}+k_{21});$$
$$a_3 = k_{20}(k_{18}+k_{19}+k_{20}+k_{21});\quad a_4 = k_{21}(k_{18}+k_{19}+k_{20}+k_{21});$$
$$b_1 = k_{22}/(k_{22}+k_{23}) = k_{29}/(k_{28}+k_{29});$$
$$b_2 = k_{25}/(k_{24}+k_{25}) = k_{27}/(k_{26}+k_{27});$$
$$d_2 = k_{35}/(k_{34}+k_{35});\quad d_3 = k_{38}/(k_{37}+k_{38});$$

and RO2-R., RO2-N., and RO2-Br. are the same as discussed above for the propyl bromide mechanism; R2O2. is an operator used to represent the effect of the extra NO to NO_2 conversions caused by formation of peroxy radicals in secondary reactions (Carter, 1990); CCHO represents acetaldehyde; RCHO represents lumped higher aldehydes, which in this case includes propionaldehyde, 4-hydroxy propionaldehyde and 4-bromo propionaldehyde; MEK represents lumped higher ketones, which in this case represents methyl-(2-bromoethyl) ketone; BR-ALD represents bromoacetaldehyde, which is represented explicitly as discussed below; and BR-KET represents bromomethyl ethyl ketone, which is lumped with bromoacetone, as also discussed below.

If the initially estimated branching ratios are assumed, then the overall reaction would be,

OH + Butyl Bromide → 0.21 RO2-BR. + 0.71 RO2-R. + 0.38 R2O2. + 0.31 CCHO + 0.31 BR-ALD + 0.21 RCHO + 0.23 MEK + 0.17 BR-KET + 0.08 RO2-N.

However, this estimated mechanism is more uncertain than the estimated mechanism for propyl bromide because of the larger number of branching ratios with competing processes, particularly those where one process does not dominate over all the others. For that reason, some of these branching ratios are treated as adjustable parameters to improve the fits of the model simulations to the chamber experiments. The reaction as written in Table 1 incorporates the adjusted branching ratios, derived as discussed later.

Reactions of α-Bromo Carbonyl Products

The bromine-containing organic products predicted to be formed from the reactions of 1-propyl and 1-butyl bromides include bromoacetaldehyde, β-bromo propionaldehyde, γ-bromo butyraldehyde, bromoacetone, bromomethyl ethyl ketone, and methyl 2-bromoethyl ketone. When the bromine is two or more carbons away from the carbonyl it is assumed not to significantly affect reactions at the carbonyl center, and the product is represented in the model in the same manner as similar carbonyl products without the bromine (see above). However, compounds with the bromine on the carbon adjacent to the carbonyl group are represented separately because the bromine may affect the reactivity characteristics of the carbonyl, and because the reaction is more likely to release bromine into the system. These include bromoacetaldehyde, represented as BR-ALD, and bromoacetone and bromomethyl ethyl ketone, lumped together as BR-KET. This was done primarily to allow for determining the effects of making alternative assumptions concerning their mechanisms on results of simulations of the chamber experiments.

The reactions assumed for bromoacetaldehyde (BR-ALD) and bromoacetone (BR-KET) are shown on Table 1, and footnotes to the table indicate the source of the assumed rate constants and mechanism. The mechanisms are generally direct analogies of the mechanisms for the corresponding unbrominated compound, except that when $CH_2Br\cdot$ is formed, it is assumed to react to form Br atoms via

$$BrCH_2\cdot + O_2 \rightarrow BrCH_2OO\cdot$$
$$BrCH_2OO\cdot + NO \rightarrow NO_2 + BrCH_2O\cdot$$
$$BrCH_2O\cdot \rightarrow Br\cdot + HCHO$$

This is represented in the model as RO2-BR. + HCHO. The $BrCH_2(CO)OO\cdot$ formed from the OH + bromoacetaldehyde reaction are lumped with $CH_3CH_2(CO)OO\cdot$ (model species C2CO-O2.), since, once ozone formation begins, most of it reacts to form the corresponding PAN analogue (e.g., $BrCH_2(CO)OO$-NO_2), which is relatively stable on the time scale of the experiments. The OH + bromoketone reactions are not expected to occur at sufficiently high rates to significantly affect model simulations on the time scale of these one-day simulations, so are ignored. The photolysis reactions are assumed to proceed via the scission of the C-CO bond involving the bromonated carbon, forming $BrCH_2\cdot$ radicals which react as indicated above.

The effects of Br substitution on the photolysis rates of these α-bromo carbonyl products are uncertain. For lack of available information, we assume that the photolysis rates are not significantly

affected by Br substitution, so the photolysis rate used in most of the calculations were the same as for the corresponding unbromonated species. However, sensitivity calculations were carried out to assess if assuming higher α-bromocarbonyl photolysis rates improved fits of the model simulations to the chamber data.

As discussed later, certain aspects of the chamber data suggest that there are reactions, not accounted for in the initially estimated model, causing accelerated O_3 formation and later accelerated O_3 loss in the chamber experiments. One possible cause of this is reactions of O_3 with the bromine-containing products, forming radicals which initially enhance O_3 formation to a greater extent than the O_3 lost by the direct reactions, but then causing net O_3 loss when NO_x levels are lower and O_3 formation is less efficient. However, O_3 reacts slowly if at all with simple carbonyl compounds (Atkinson and Carter, 1984), thermochemical considerations indicate that O_3 cannot react significantly at C-Br bonds at ambient temperatures, and no endothermic and mechanistically reasonable reaction route between O_3 and these products could be devised. Therefore, the possibility of O_3 reaction with these products being important in this system is not considered.

Br and BrO_x Reactions

A number of the reaction pathways discussed above involve the formation of bromine atoms. Prior to this study, the general mechanism did not include provision for representing reactions of Br atoms or the inorganic BrO_x species they form, so they had to be added to the mechanism for this study. These reactions are given in Table 1, with the absorption cross sections for the photoreactive species being given in Appendix A. Some reactions, such as BrO + BrO or BrO_2 reactions, are omitted from the listing because they are expected or calculated to be of negligible importance under lower atmospheric conditions. Footnotes to the table indicate sources for rate constants or mechanistic assumptions which were not based on IUPAC (Atkinson et al. 1997) recommendations. Most of rate constants for the inorganic Br and BrO_x reactions, all the absorption cross sections, and the rate constants for the reactions of Br with formaldehyde and propionaldehyde, are taken from the most recent IUPAC evaluation (Atkinson et al. 1997).

Although many of the BrO_x reactions appear to be reasonably well studied because of their potential relevance to the stratospheric ozone problem, there are a number of potentially significant uncertainties. These include reactions of $BrONO_2$, possible reactions of Br atoms with aromatics and olefins, and possible wall or other reactions of HBr. These are discussed below.

$BrONO_2$ is expected to be formed when BrO, formed in the reaction of Br atoms with O_3, reacts with NO_2. As indicated on Table 1, it can react in a number of ways, including photolysis and thermal decomposition. The thermal decomposition reaction has not been studied, presumably because thermochemical considerations indicate it would be negligible at stratospheric temperatures, but is estimated to have a non-negligible thermal decomposition rate at tropospheric temperatures. There are

also no data concerning the quantum yields for its photolysis, which, based on analogy with $ClONO_2$ (Atkinson et al., 1992; 1997) are expected to be relatively high. However, model simulations of the chamber experiments were found to be relatively insensitive to assumptions made concerning $BrONO_2$ reactions, with calculations incorporating alternative (and in some cases extreme) assumptions concerning these reactions yielding essentially the same result. This is because most of the Br is consumed by the reactions of Br with the aldehydes and other the organic species present in these experiments, so formation of BrO and $BrONO_2$ following the reaction of Br with O_3 is a relatively minor process.

As indicated on Table 1, Br atoms are known to react relatively rapidly with formaldehyde and acetaldehyde, and trans-2-butene, and at slower rates with propene and ethene, but its reactions with alkanes and aromatics appear to be slow. The reactions of Br with the aldehydes are expected involve H-atom abstraction, forming HBr and acyl radicals. In the case of the alkenes, the reaction is expected to involve initial addition to the double bond, with the subsequent reactions being as follows, where R_n refer to H- or Alkyl- groups, depending on the compound.

$$Br + R_1R_2C{=}CR_3R_4 \rightarrow R_1R_2C(Br)\text{-}CR_3R_4\cdot$$
$$R_1R_2C(Br)\text{-}CR_3R_4\cdot + O_2 \rightarrow R_1R_2C(Br)\text{-}CR_3R_4OO\cdot$$
$$R_1R_2C(Br)\text{-}CR_3R_4OO\cdot + NO \rightarrow NO_2 + R_1R_2C(Br)\text{-}CR_3R_4O\cdot$$

$$R_1R_2C(Br)\text{-}CHR_3O\cdot + O_2 \rightarrow R_1R_2C(Br)\text{-}CO\text{-}R_3 \qquad (R_4{=}H) \quad (43)$$
$$R_1R_2C(Br)\text{-}CR_3R_4O\cdot \rightarrow R_1R_2(Br)C\cdot + R_3\text{-}CO\text{-}R_4 \qquad (44)$$

$$R_1R_2C(Br)C\cdot + O_2 \rightarrow R_1R_2C(Br)COO\cdot$$
$$R_1R_2C(Br)COO\cdot + NO \rightarrow R_1R_2C(Br)CO\cdot$$
$$R_1R_2C(Br)CO\cdot \rightarrow R_1\text{-}CO\text{-}R_2 + Br\cdot$$

Based on alkoxy radical reaction estimation methods recently developed by Atkinson (1997), we would expect O_2 reaction (Reaction 43) to dominate over decomposition (Reaction 44) for ethene and propene; this is consistent with the observation that bromoacetaldehyde is a major product in the Br + ethene system (Barnes et al. 1989). However, the same estimation method predicts that decomposition would dominate in the case of the internal olefins such as trans-2-butene. The mechanisms used for the Br + alkene reactions, given in terms of SAPRC model species on Table 1, are based on these estimates. Note that the assumption that decomposition dominates in the case of trans-2-butene is somewhat uncertain, but test calculations indicate that the model results are not highly sensitive to this uncertainty.

The major uncertainty concerns the fact that, as discussed below, the results of the chamber experiments could not be adequately simulated by the model unless it was assumed that there is a significant reaction between O_3 and some major reactive product which both initiates radicals and destroys ozone. The reaction of Br with O_3 does not appear to be significantly rapid for $BrO/BrONO_2$ chemistry to account for these observations. As indicated above, no thermochemically reasonable reaction between O_3 and the expected bromocarbonyl products could be devised to account for the observed results. The

only remaining bromine-containing product predicted to be formed in significant yields in this system, for which reaction with ozone cannot be ruled out *a-priori*, is HBr, the dominant product formed when free Br atoms react with aldehydes or internal alkenes. The only known gas-phase reaction of HBr relevant to this system is its reaction with OH radicals (see Table 1) which, while relatively rapid, is not so fast that it prevents HBr from building up in concentration.

The only information we are aware of concerning a possible reaction between O_3 and HBr comes from Mellouki et al. (1994), who observed that HO_2 is not formed when O_3 and HBr are mixed. This rules out not only

$$HBr + O_3 \rightarrow BrO\cdot + HO_2 \qquad (45)$$

but also

$$HBr + O_3 \rightarrow OH + Br\cdot + O_2 \qquad (46)$$

because if OH radicals were formed, they would react with O_3 to form HO2. Reactions (45) and (46) are not expected to be rapid in any case, since they are calculated to be endothermic. However, the data of Mellouki et al. (1994) do not eliminate the possibility of

$$HBr + O_3 \rightarrow HOBr + O_2 \qquad (47)$$

which is exothermic and might possibly occur on surfaces if not in the gas phase. HOBr would photolyze relatively rapidly to form OH and Br,

$$HOBr + h\nu \rightarrow OH + Br \qquad (48)$$

since, based on the absorption cross sections recommended in the IUPAC evaluation (Atkinson et al. 1997), and assuming unit quantum yields, the photolysis of HOBr (Reaction 46) is calculated to have a half life of ~30 minutes under the conditions of our experiments. Thus, this reaction represents a radical initiation process as well as an ozone sink. Model simulations of our environmental chamber experiments, discussed below, give much better fits to our data if Reaction (47) is assumed to occur at a significant rate. Because of this, the possibility that this reaction may occur at a significant rate was investigated in exploratory experiments carried out at SAPRC as part of this project.

Modeling Methods

Environmental Chamber Simulations

The ability of the chemical mechanisms to appropriately simulate the atmospheric impacts of the alkyl bromides was evaluated by conducting model simulations of the environmental chamber experiments from this study. This requires including in the model appropriate representations of chamber-dependent effects such as wall reactions and characteristics of the light source. The methods used are based on those

discussed in detail by Carter and Lurmann (1990, 1991), updated as discussed by Carter et al. (1995b,d; 1997a). The photolysis rates were derived from results of NO_2 actinometry experiments and measurements of the relative spectra of the light source. In the case of the xenon arc lights used in the CTC, the spectra were derived from those measured during the individual experiments, assuming continuous linear changes in relative intensity at the various wavelengths, as discussed by Carter et al. (1997a). The thermal rate constants were calculated using the temperatures measured during the experiments, with the small variations in temperature with time during the experiment being taken into account. The computer programs and modeling methods employed are discussed in more detail elsewhere (Carter et al, 1995b). The specific values of the chamber-dependent parameters used in the model simulations of the experiments for this study are given in Table A-4 in Appendix A. Various alternative assumptions were made concerning different aspects of the mechanism, as discussed below.

The initial reactant concentrations used when modeling the experiments were based on the measured initial concentrations except as noted. The toluene and m-xylene data in some of the experiments were judged to be unreliable because they disagreed with the amount injected, and because using the measured initial concentrations of these species resulted in more variability in the model simulations of the replicate base case runs than were observed experimentally. This variability was due to a GC problem which was subsequently corrected. More consistent and better model performance in simulating the base case experiments was obtained if average values of initial base ROG surrogate reactants, taken from runs where the analytical data were considered more reliable, were used in the model simulations. Therefore, an average initial m-xylene was used in the model simulations of the mini-surrogate experiments, and a single base surrogate composition was used in the simulations of all the full surrogate runs. The base surrogate composition chosen for the latter purpose was that measured during run DTC-423, which was consistent with the expected amounts injected and gave good fits to the simulations of the base case runs.

Some uncertain mechanistic parameters were derived by using a non-linear optimization method to determine the value of the parameter(s) which minimized the sum of squares differences between experimental and model calculation d(O_3-NO) results. Footnotes to Table 1 indicate the runs and data which were used in those optimizations. (Generally the runs used were those with the largest amount of added alkyl bromide.) In some reactivity experiments, the model tended to slightly underpredict the d(O_3-NO) data in the base case experiment, due to uncertainties in initial base case reactant concentrations. In these cases, the initial m-xylene concentrations were adjusted slightly to improve the fits to the base case experiment, and the same adjustment was made to the added bromide side, which was used in the optimization. This was done to minimize biases in the optimizations due to discrepancies in the simulations of the base ROG - NO_x reactions being compensated for by inappropriate adjustments to the alkyl bromide parameters.

Atmospheric Reactivity Simulations

To estimate its effects on ozone formation under conditions more representative of polluted urban atmospheres, incremental reactivities, defined as the change in O_3 caused by adding small amounts of a compound to the emissions, were calculated for the alkyl bromides for various simulated atmospheric pollution scenarios. These are compared with ozone impacts calculated for ethane under the same conditions. The airshed scenarios and modeling approach employed were based on that previously employed by Carter (1994a), and are discussed later in this report. The chemical mechanisms used were the same those used to simulate the chamber experiments, except that the reactions representing chamber effects were removed, and the reactions for the full variety of VOCs emitted into the scenarios (Carter, 1994a) were represented (see Appendix A). Most of the emitted VOCs (other than the test compound whose reactivity is being calculated) are not represented in the model explicitly, but are represented using lumped model species whose rate constants and product yield parameters are derived based on the mixture of compounds they represent. The rate constants and mechanistic parameters for the emitted species in the scenarios were the same as those used previously (Carter et al, 1993b), except for the aromatics, whose unknown photoreactive product yields were reoptimized in a manner analogous to that discussed above for toluene and m-xylene (Carter et al. 1997a). The listings on Appendix A give the lumped model species used to represent the emissions into the scenarios, indicate the types of species each is used to represent, and give their rate constants and product yield parameters.

In the case of the alkyl bromides, calculations were carried out both with and without the speculative O_3 + HBr reaction, which may or may not be heterogeneous. The other alkyl bromide and BrO_3 reactions were assumed to be the same in all the atmospheric simulations, and are given in Table 1.

RESULTS AND DISCUSSION

Summary of Experiments

Table 2 gives a chronological listing of all the experiments carried out for this program, and the conditions and results of the incremental reactivity experiments are summarized in more detail on Table 2. In addition to the reactivity experiments, control experiments were conducted to assure consistency with previous results, and side equivalency tests were conducted to assure that essentially equivalent results were obtained when equal mixtures were simultaneously irradiated in each of the dual reaction bags.

The relevant results of the individual control and characterization runs are summarized on Table 1. These results were as expected based on our previous experience with these and similar chambers in our laboratories (Carter et al. 1995b and references therein). Good side equivalency was observed when equivalent surrogate - NO_x (not shown on Table 1), propene - NO_x, CO - NO_x, or n-butane - NO_x mixtures were simultaneously irradiated in the dual reactors. The results of the CO - NO_x and n-butane - NO_x experiments, which are highly sensitive to the magnitude of the chamber radical source assumed in the model (see Table A-4 in Appendix A), were sufficiently well simulated by the model to indicate that the model was appropriately representing this effect for these runs. The actinometry results agreed with the extrapolated values based on results of previous determinations, to within the variability of these determinations.

Because of a problem with a GC instrument which has since been corrected, unreliable results were obtained in our analyses of toluene and m-xylene for a number of experiments, as indicated by the measured initial concentrations not agreeing with the amounts injected. For those experiments, which are noted on Table 1, the m-xylene data had to be rejected, resulting in no IntOH data being available. However, good reproducibility in amounts of base ROG reactant injections were obtained in replicate runs of the same type, so the initial reactant concentrations for modeling could be estimated reasonably reliably using the average concentrations measured in similar experiments where the initial reactant concentrations were less uncertain.

Results of The Reactivity Experiments and Mechanism Evaluations

Summaries of the conditions and results of the incremental reactivity experiments are given on Table 2, and Figures 1 through 12 give time series plots for relevant measurements used for mechanism evaluation. These include concentrations of O_3, NO, and m-xylene in the base case and test experiments, concentrations of the alkyl bromide in the test experiment, and the d(O_3-NO) and IntOH incremental reactivities derived from the differences between the two sides. Results of model calculations, discussed below, are also shown in these figures.

Table 2. Criminological listing of the environmental chamber experiments carried out for this program.

RunID	Date	Title	Comments
DTC392	8/5/96	NO2 and Cl_2 Actinometry	The NO_2 photolysis rate was measured using the quartz tube method was 0.19 min^{-1}, in good agreement with other actinometry results in this chamber.
DTC393	8/6/96	Propene + NOx	Control run for comparison with other propene runs carried out in this and other chambers. Good side equivalency was observed. The results were in good agreement with model predictions.
DTC401	8/22/96	Mini-Surrogate + Butyl Bromide (A)	See Table 2 and Figure 8. No reliable m-xylene data available due to analytical problems.
DTC404	8/28/96	Mini-Surrogate + Butyl Bromide (A: 5 ppm and B: 2ppm)	Due to a miscommunication, butyl bromide was injected into both sides of the chamber. Results, summarized on Table 2, are consistent with the other mini-surrogate + butyl bromide runs.
DTC405	8/29/96	Propene + NOx	Control run to determine if prior exposure to alkyl bromides had any effect on subsequent runs. Good side equivalency was observed. The results were in good agreement with model predictions.
DTC407	9/4/96	NO2 and Cl_2 Actinometry	The NO_2 photolysis rate was measured using the quartz tube method was 0.18 min^{-1}, and the Cl_2 consumption rate corresponded to an NO2 photolysis rate of 0.20 min^{-1}. These are in good agreement with other actinometry results in this chamber.
DTC416	9/19/96	n-Butane + NOx	Control run to measure the chamber radical source. The NO consumption rate was in good agreement with the predictions of the chamber model.
DTC417	9/20/96	Propene + NOx	Control run for comparison with other propene runs carried out in this and other chambers. The results were essentially the same as run DTC405.

Table 2 (continued)

RunID	Date	Title	Comments
DTC419	9/25/96	Full surrogate + Butyl bromide (B)	See Table 2 and Figure 10.
DTC420	9/26/96	Low NOx full surrogate + Butyl bromide (B)	See Table 2 and Figure 11.
DTC421	9/27/96	Mini surrogate + Propyl bromide (a)	See Table 2 and Figure 2. M-xylene measurements were inconsistent with amount injected, and were not used for model evaluation.
DTC423	10/2/96	Full surrogate + Propyl bromide (B)	See Table 2 and Figure 3.
DTC424	10/3/96	Low NOx full surrogate + Propyl Bromide (a)	See Table 2 and Figure 5.
DTC425	10/4/96	CO + NOx	Control run to measure the chamber radical source. NO consumption rate slightly slower than predictions of the chamber model, but within the expected range. CO data indicated that dilution was negligible.
DTC426	10/8/96	Mini surrogate + Butyl Bromide (B)	See Table 2 and Figure 7.
DTC427	10/9/96	Full surrogate + Propyl Bromide (a)	See Table 2 and Figure 4. M-xylene measurements were inconsistent with amount injected, and were not used for model evaluation.
DTC428	10/10/96	Low NOx full surrogate + Propyl Bromide (B)	See Table 2 and Figure 6. M-xylene measurements were inconsistent with amount injected, and were not used for model evaluation.
DTC429	10/14/96	NO_2 Actinometry	The NO_2 photolysis rate was measured using the quartz tube method was 0.18 min^{-1}, in good agreement with other actinometry results in this chamber.
DTC430	10/15/96	Full surrogate + Butyl Bromide (a)	See Table 2 and Figure 9. M-xylene measurements were inconsistent with amount injected, and were not used for model evaluation.

Table 2 (continued)

RunID	Date	Title	Comments
DTC431	10/16/96	Propene + NOx	Control run for comparison with other propene runs carried out in this and other chambers. The results were similar to run DTC405.
DTC432	10/17/96	Low NOx full Surrogate + Butyl Bromide (B)	See Table 2 and Figure 12. M-xylene measurements were inconsistent with amount injected, and were not used for model evaluation.
DTC433	10/18/96	Mini-Surrogate + Propyl Bromide (A)	See Table 2 and Figure 1.
DTC434	10/21/96	n-Butane + NOx	Control run to measure the chamber radical source. Results were similar to run DTC416. Run could not be modeled because of lack of n-butane data.
DTC435	10/22/96	pure air irradiation	After 6 hours of irriadiation, approximately 24 ppb O_3 formed on side A and 22 on side B. Results are within the normal range, and were consistent with the predictions of the chamber effects model.
DTC436	10/23/96	Ozone decay	Measured O_3 decay rate was ~1% per hour, in good agreement with the default value used in the chamber model.

Table 3. Summary of conditions and results of the environmental chamber experiments.

Run	Initial Reactants (ppm)			t=6 Max. d(O_3-NO) (ppm)			t=6 IntOH (10^{-6} min)		
	NOx	Surg [a]	Bromide	Base	Test	IR [b]	Base	Test	IR
1-Bromopropane									
Mini-Surrogate									
DTC-433 (A)	0.37	5.5	3.0	0.66	0.82	0.0517	22	28	2.2
DTC-421 (A)	0.37	5.8	4.8	0.64	0.77	0.0269	33	30	-0.6
Full Surrogate - High NOx									
DTC-423 (B)	0.30	5.2	2.3	0.56	0.59	0.0126	37	43	2.3
DTC-427 (A)	0.29	4.7	5.4	0.59	0.58	-0.0013	31	20	-2.0
Full Surrogate - Low NOx									
DTC-424 (A)	0.12	4.9	2.1	0.35	0.32	-0.0159	33	25	-3.9
DTC-428 (B)	0.11	4.8	5.7	0.36	0.31	-0.0082	-72	14	15.0
1-Bromobutane									
Mini-Surrogate									
DTC-426 (B)	0.39	5.6	6.4	0.56	0.79	0.0359	16	17	0.2
DTC-401 (A)	0.36	5.3	12.3	0.54	0.74	0.0160	27	19	-0.6
DTC-404 (B) [c]	0.35	5.7	2.2	-	0.78	-	-	22	-
DTC-404 (A) [c]	0.34	5.6	6.0	-	0.76	-	-	17	-
Full Surrogate - High NOx									
DTC-430 (A)	0.28	4.5	5.7	0.58	0.60	0.0035	30	14	-2.8
DTC-419 (B)	0.27	5.1	6.9	0.58	0.61	0.0054	38	23	-2.2
Full Surrogate - Low NOx									
DTC-420 (B)	0.12	5.1	7.0	0.35	0.32	-0.0043	31	16	-2.1
DTC-432 (B)	0.15	4.6	11.9	0.37	0.33	-0.0034	27	8	-1.6

Notes

[a] Total base ROG surrogate in ppmC. For some runs the initial toluene and/or m-xylene were estimated based on averages for other similar runs.

[b] Incremental reactivity

[c] Butyl bromide injected into both sides of chamber. No base case.

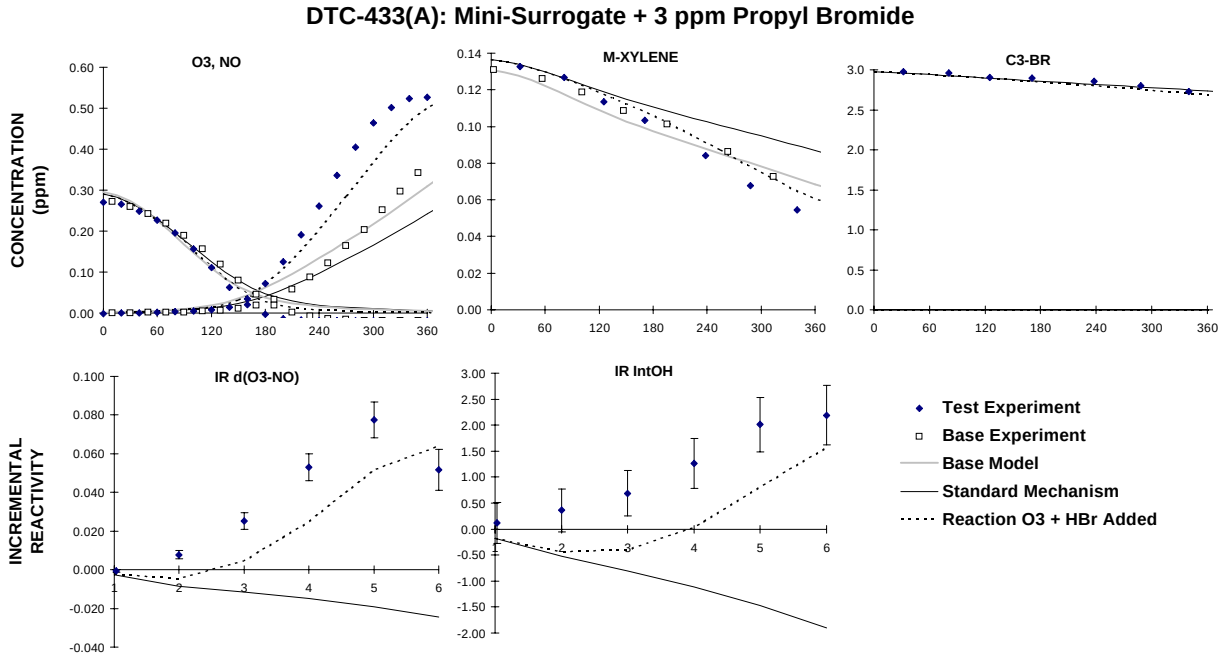

Figure 1. Plots of selected results of the mini-surrogate + propyl bromide run DTC-433.

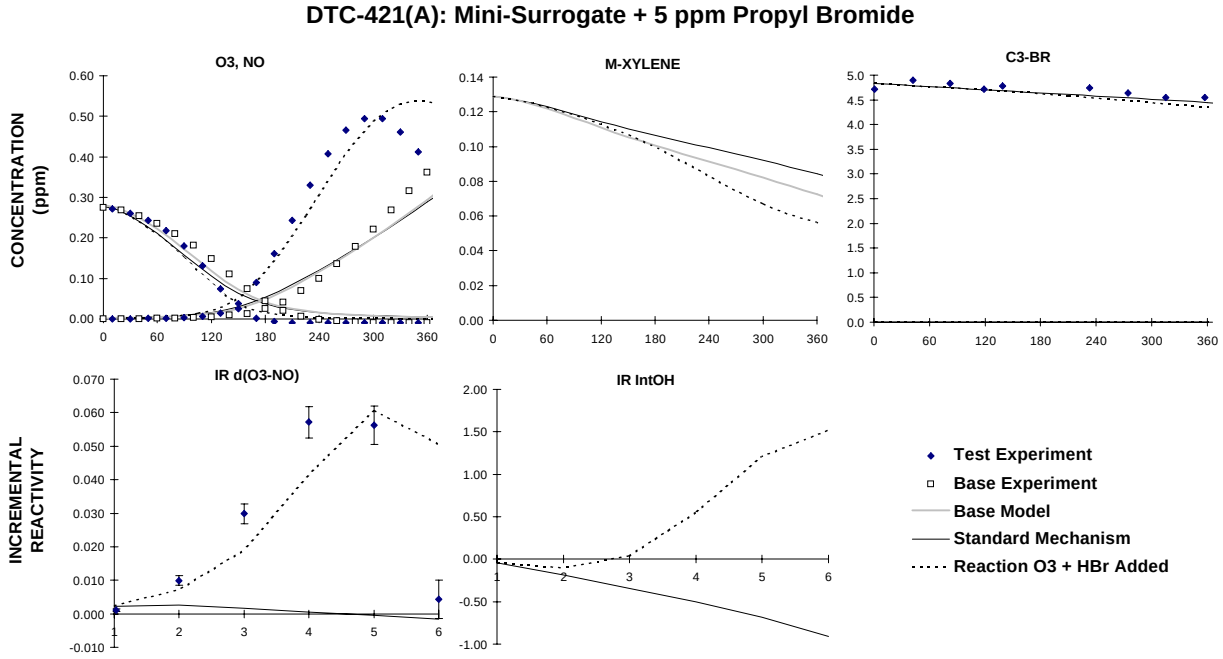

Figure 2. Plots of selected results of the mini-surrogate + propyl bromide run DTC-421.

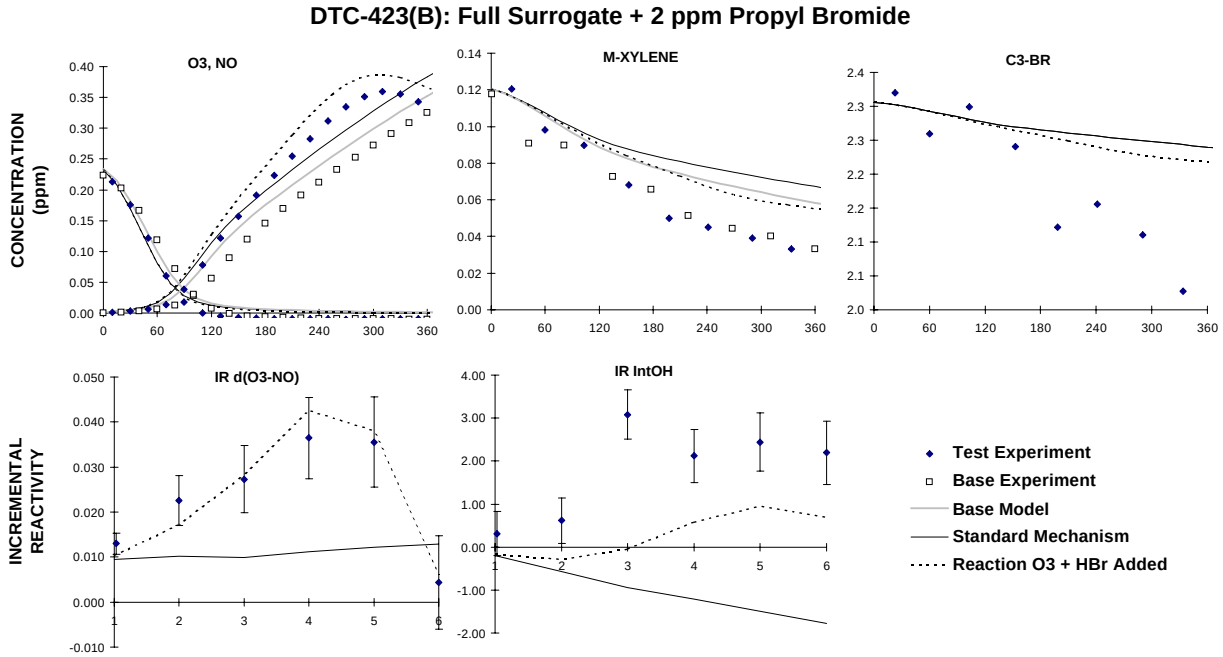

Figure 3. Plots of selected results of the full surrogate + propyl bromide run DTC-423.

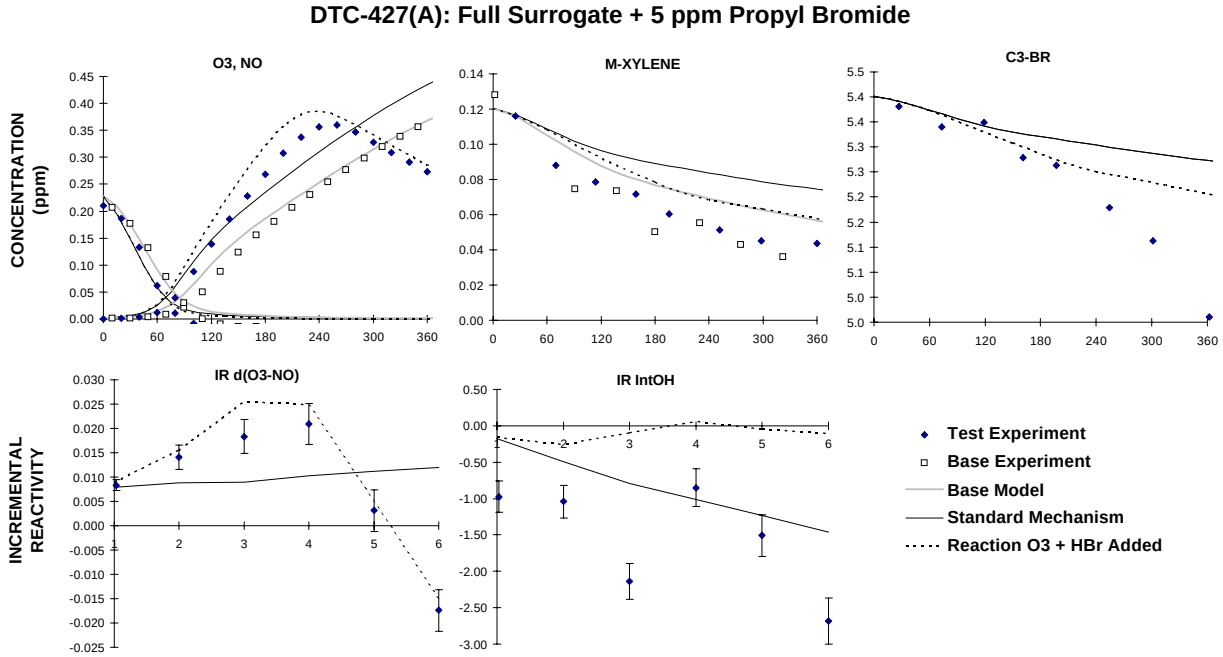

Figure 4. Plots of selected results of the full surrogate + propyl bromide run DTC-427.

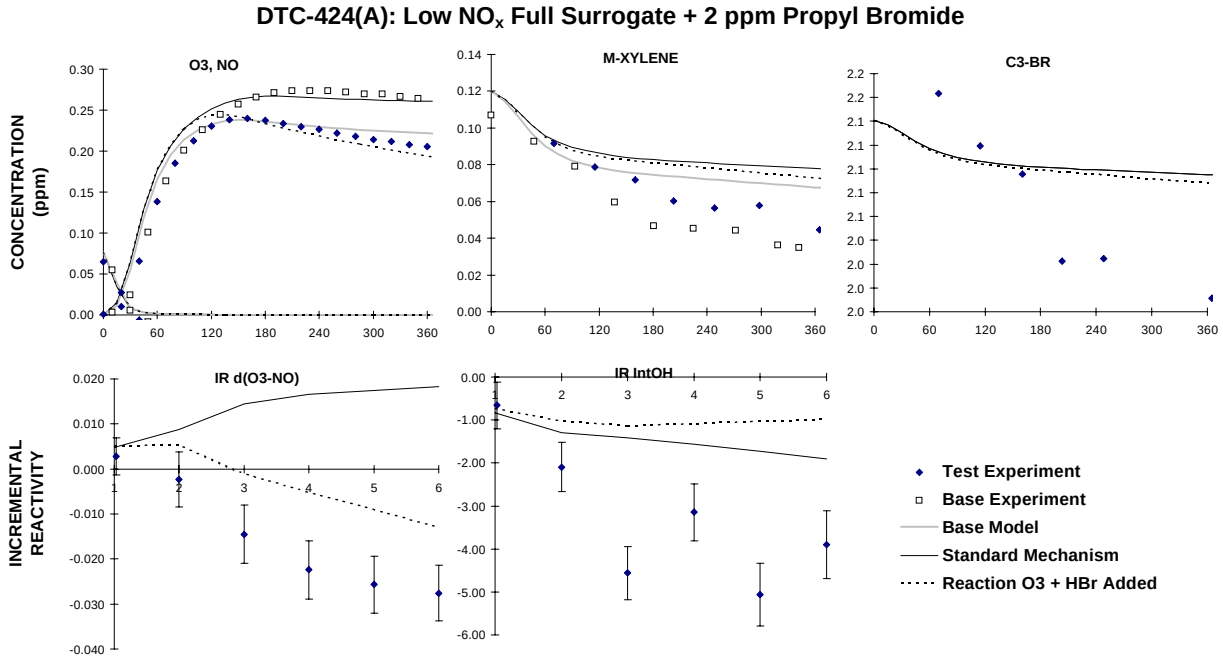

Figure 5. Plots of selected results of the low NO_x full surrogate + propyl bromide run DTC-424.

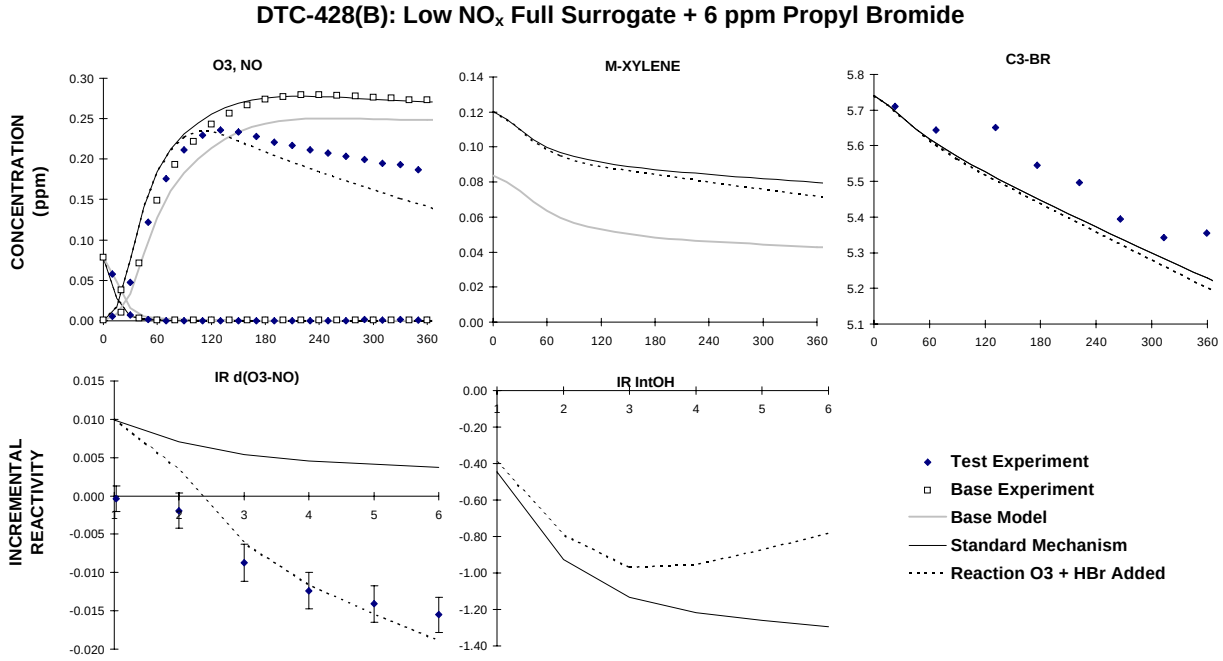

Figure 6. Plots of selected results of the low NOx full surrogate + propyl bromide run DTC-428.

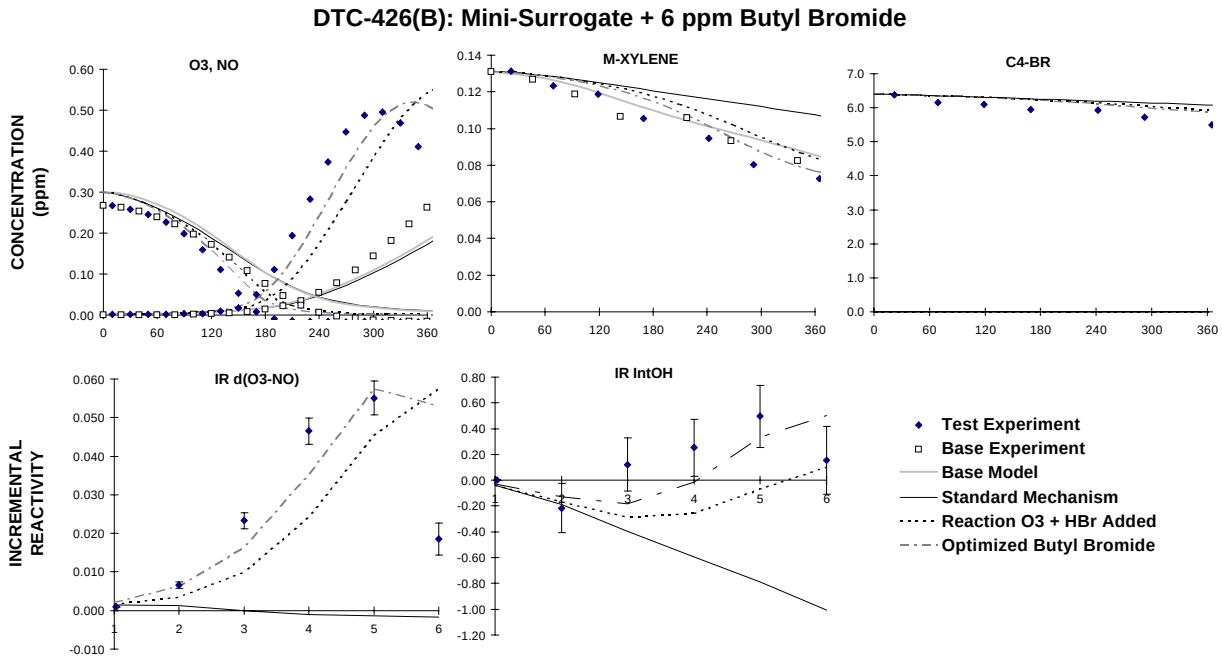

Figure 7. Plots of selected results of the mini-surrogate + butyl bromide run DTC-426.

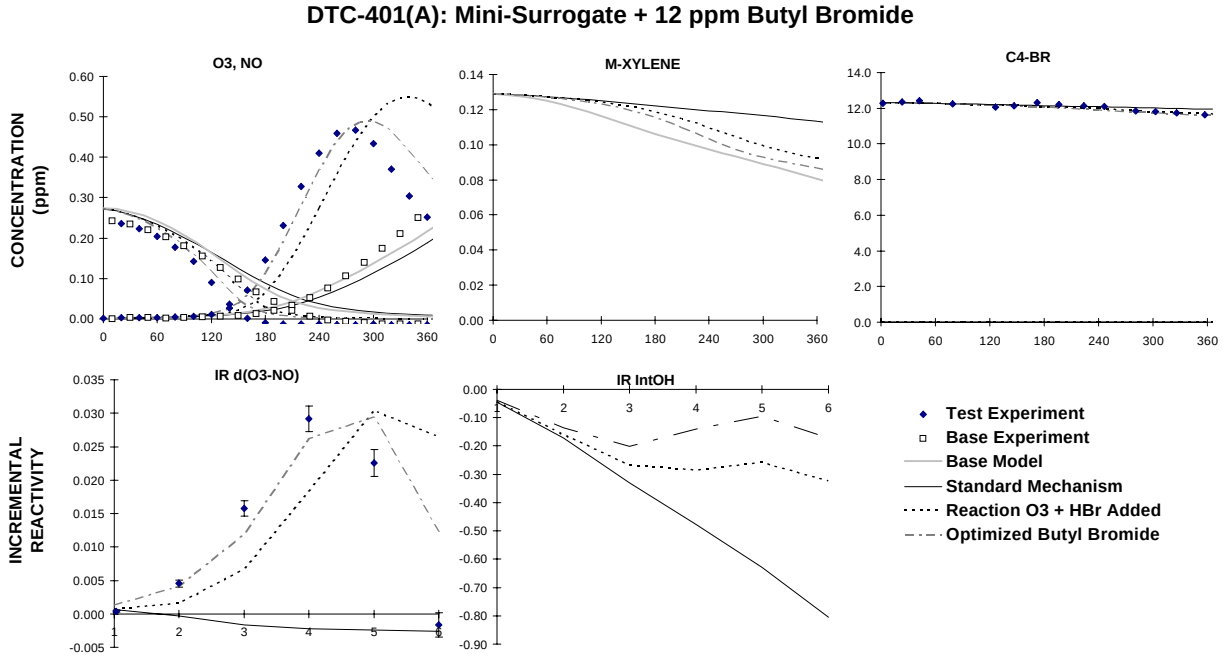

Figure 8. Plots of selected results of the mini-surrogate + butyl bromide run DTC-401.

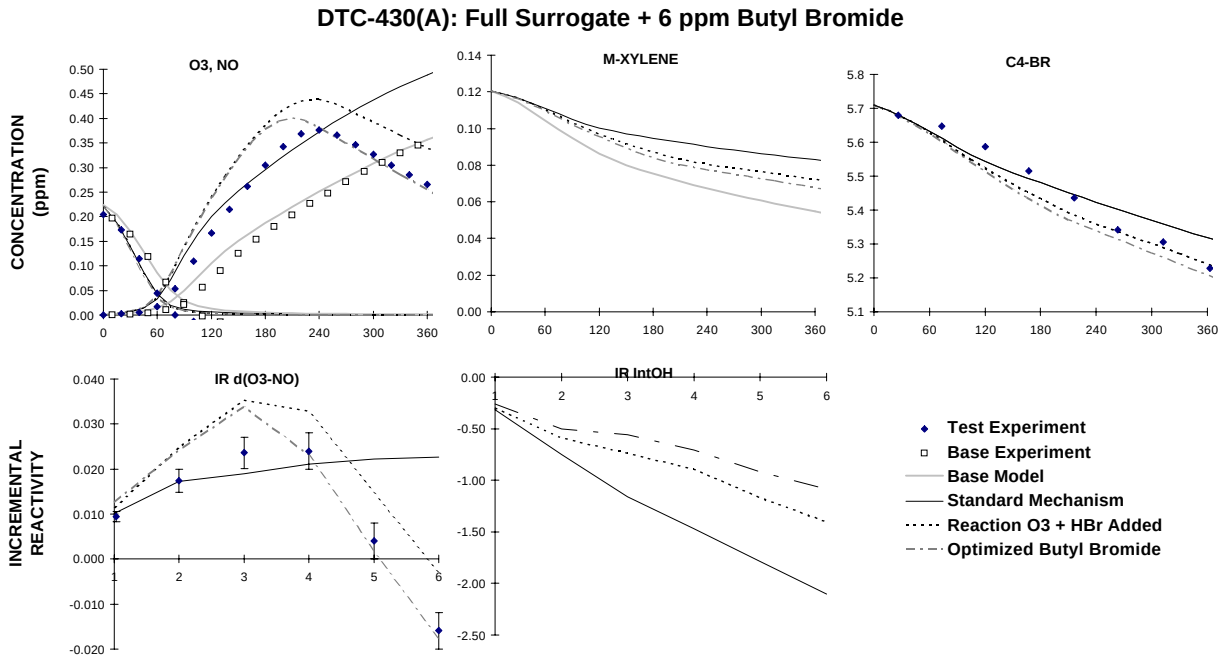

Figure 9. Plots of selected results of the full surrogate + butyl bromide run DTC-430.

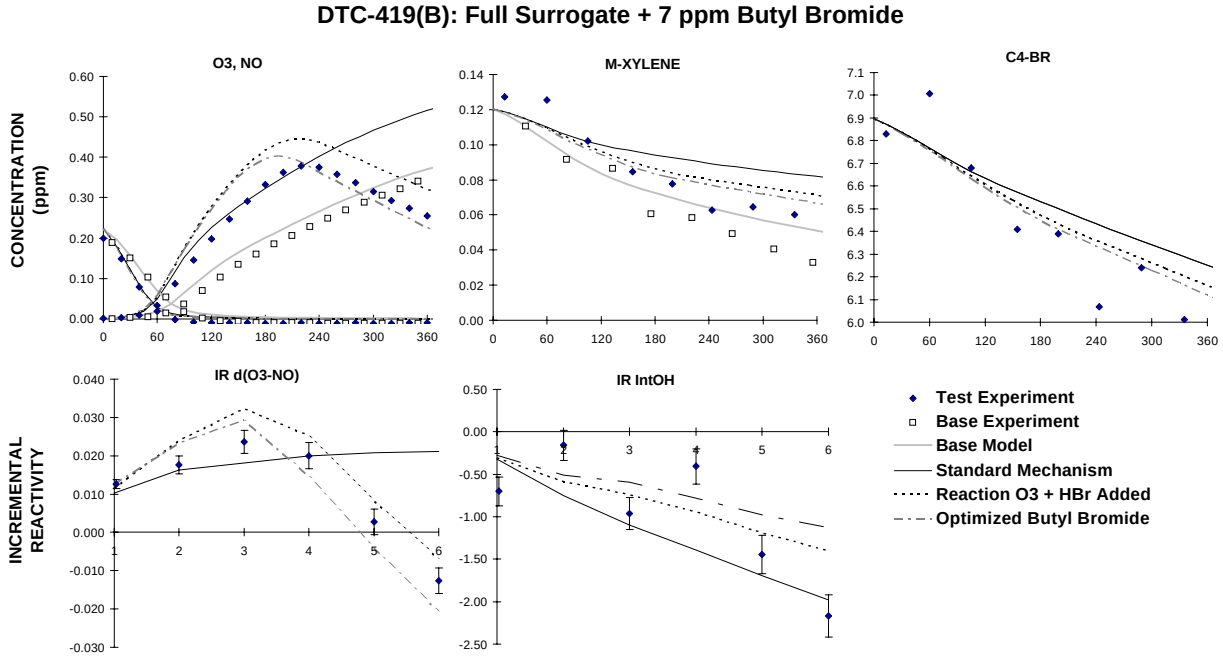

Figure 10. Plots of selected results of the full surrogate + butyl bromide run DTC-419.

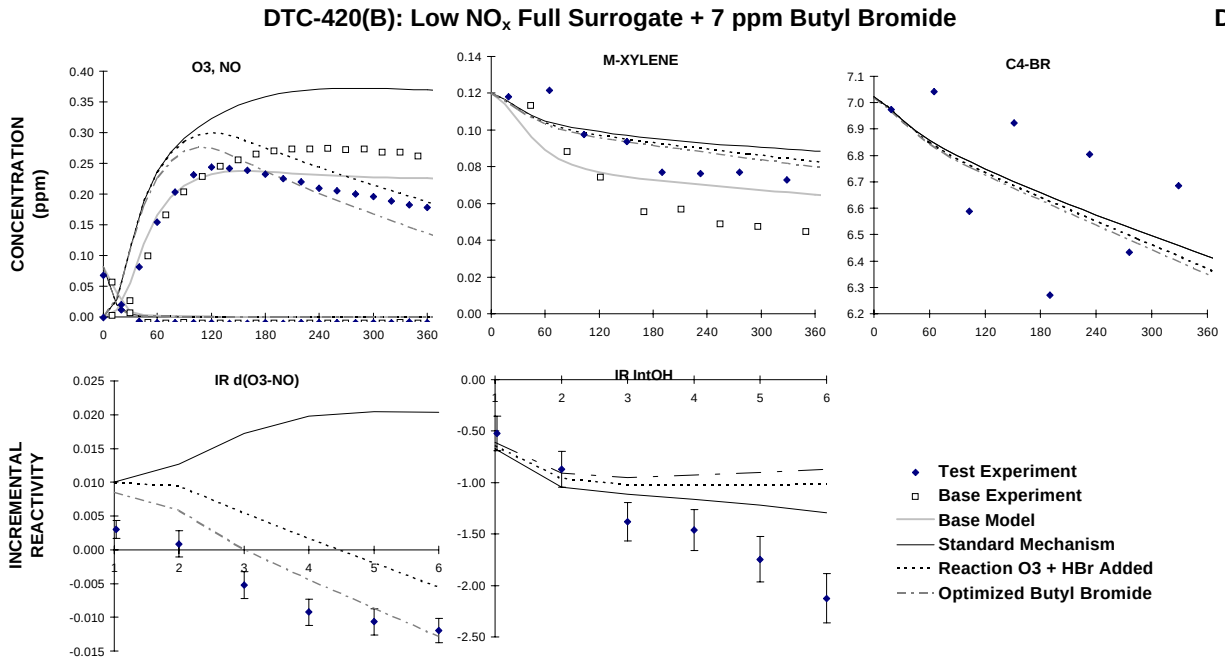

Figure 11 Plots of selected results of the low NOx full surrogate + butyl bromide run DTC-420.

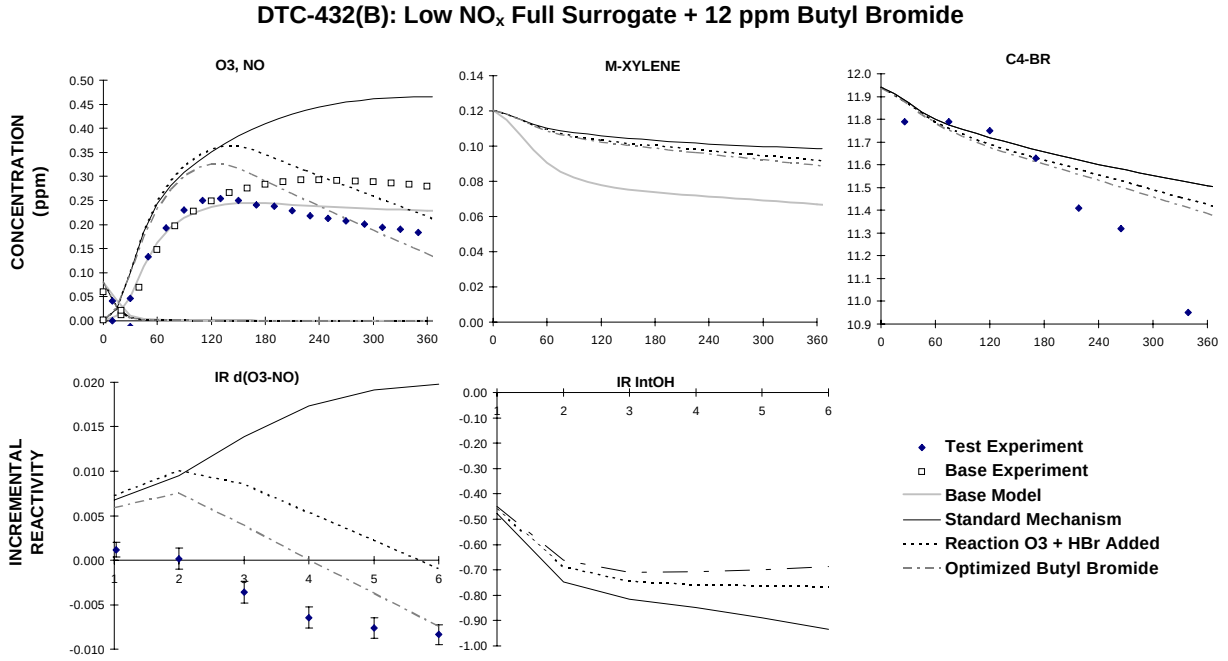

Figure 12. Plots of selected results of the low NOx full surrogate + butyl bromide run DTC-432.

Figures 1 and 2 show that although the addition of 3-5 ppm of propyl bromide to the mini-surrogate experiments does not have a large effect on the initial NO oxidation rate, it causes a significant increase in the initial rates of ozone formation. In addition, if enough bromide is added to the experiment, the O_3 goes through a maximum and starts a relatively rapid decline. Figures 7 and 8 show that the effects of adding butyl bromide to the mini-surrogate is similar. The addition of propyl bromide to the mini-surrogate causes a slight increase in the OH radical levels beginning around the time the O_3 formation begins, but the butyl bromide has only a small effect on OH radical levels.

The results of the high NO_x full surrogate experiments are similar to the mini-surrogate runs except that the effect on O_3 formation for the addition of comparable amounts of bromide are somewhat less. Again, ozone in the added bromide side is observed to reach a maximum and decline, with the final O_3 concentrations becoming comparable to or less than the O_3 on the base case side. The data concerning IntOH reactivities in the full surrogate runs are somewhat scattered for propyl bromide, but do not indicate strong overall radical initiation or termination effects. On the other hand, run DTC-419 indicates that butyl bromide tends to suppress radical levels in the full surrogate experiments.

In contrast to the data from the higher NO_x runs, the added bromides were observed not to significantly enhance the O_3 formation rates in the low NO_x full surrogate experiments, but instead tended to inhibit ozone formation. This is because the added bromide caused the O_3 formation to end earlier than on the base case side, resulting in a lower net ozone yield. In addition, the O_3 on the added bromide side declined more rapidly following the O_3 maximum than was the case on the base case side. The more rapid decline in O_3 following the maximum on the added bromide side is consistent with the results of the higher NO_x added bromide experiments, though the O_3 declined at somewhat lower rates in the lower NO_x runs.

A lower IntOH reactivity for butyl bromide is expected because, as discussed above, radical termination caused by organic nitrate formation in the peroxy + NO reaction is expected to become relatively more important as the size of the molecule increases. Experimental and modeling results for similar experiments with other VOCs indicate that in general the mini-surrogate experiments are more sensitive to radical initiation and inhibition effects (Carter et al, 1995a; Carter, 1995), making these runs most useful for assessing this aspect of the mechanism. The fact that the IntOH reactivities in the mini-surrogate runs are positive for propyl bromide, and not significantly negative for butyl bromide, indicates that there must be radical initiation processes in the photooxidations of these bromides. The fact that the bromides have relatively large effects on O_3 formation rates while having only small effects on initial NO oxidation rates suggests that O_3 is involved in this radical initiation process.

Model simulations of these reactivity experiments are also shown on Figures 1-12. The curves labeled "standard mechanism" were calculated using only the known or estimated reactions for the alkyl bromides and BrO_x systems, without any speculative reactions added or parameters adjusted to improve

the fits to the model simulations to the chamber data. Although the standard mechanism correctly predicts that the alkyl bromides have only very small effects on the NO oxidation rates and OH radical levels in the initial stages of the experiment, it performs very poorly in simulating the data once ozone formation begins. In particular, the standard mechanism fails to predict the increase in ozone formation rates and integrated OH radical levels observed in the mini-surrogate experiments beginning when O_3 formation starts, does not predict the decline in ozone concentrations in the later stages of the mini-surrogate runs with the higher levels of added bromide in the higher NO_x full surrogate runs, and incorrectly predicts that the added bromides enhance, rather than suppress, the peak O_3 levels in the low NO_x full surrogate runs. Clearly, there is some important process occurring in the alkyl bromide photooxidation or BrO_x reaction system which this mechanism is not capturing.

The effects of varying various uncertain aspects of the mechanism were examined to determine possible causes for the poor performance of the standard mechanism. Most of these modifications either had no significant effect, or caused the simulation to change in a way which was not consistent with the data, or could only fit the data if chemically unreasonable or thermodynamically or kinetically impossible rate constants or mechanisms were used. The major modifications examined are summarized below.

Product Photolysis Rates. Significant yields of α-bromo carbonyl products are predicted, and the effects of the bromine substitution on the carbonyl photolysis rates are uncertain. To determine whether the discrepancy may be due to the standard model using inappropriately low photodecomposition rates for these compounds, simulations were carried out where the photolysis rates for BR-ALD and BR-KET were increased by a factor of 100. The results are shown on Figure 13, which gives experimental and calculated concentration-time plots for O_3 and NO in selected mini-surrogate and full-surrogate + propyl bromide reactivity runs. The results for butyl bromide are similar. It can be seen that although assuming higher photolysis rates for these products can results in improved simulations of ozone formation rates in the mid-periods of the experiments, and also improved simulations of the maximum ozone in the low NO_x full surrogate runs, this model significantly overpredicts the initial NO oxidation rates in the higher NO_x runs, and does not predict the peaking and decline in O_3 concentrations in the higher NO_x experiments. Thus, high photolysis rates for the photooxidation products does not appear to be the source of the observed excess reactivity.

Uncertain $BrONO_2$ or BrO Reactions. A number of rate constants involving $BrONO_2$ and BrO are uncertain. In particular, assuming a more rapid decomposition of $BrONO_2$ or other reactions where BrO or $BrONO_2$ are recycled back to Br atoms will result in an increased O_3 destruction rate and help explain the ozone loss observed in the later stages of many of the experiments. However, varying uncertain rate constants involved in these reactions, or adding speculative reactions to enhance recycling of BrO or $BrONO_2$ to Br, had relatively little effects on the results of model simulations of these experiments. This is because most of the Br atoms formed in this system react with aldehydes and other organics, rather than with ozone.

Figure 13. Effects of assuming faster product photolysis rates on model simulations of ozone and NO for selected propyl bromide reactivity experiments.

Reactions of O_3 With Bromo-Carbonyl Products. Although it is not anticipated that O_3 would react sufficiently rapidly with bromoacetone or the other bromocarbonyl products formed in these systems, such reactions would account for radical initiation at the time of O_3 formation and possibly O_3 loss later in the experiments. Therefore, the effects of assuming various O_3 + bromocarbonyl reactions were examined. Satisfactory fits to the chamber experiments could not be obtained unless it was assumed that O_3 + bromocarbonyl reactions involved OH formation without any NO to NO_2 conversions, for which no chemically reasonable mechanism could be written. If any NO to NO_2 conversions are assumed to occur in the reaction sequence, the model predicts no net O_3 loss and significantly overpredicts the final O_3 yield in the full surrogate experiments.

Reactions of NO_3 Radicals with Bromo-Carbonyl Products. Although it is not anticipated that NO_3 would react sufficiently rapidly with bromoacetone or the other bromocarbonyl products formed in these systems, such reactions could also account for radical initiation at the time of O_3 formation. NO_3 radicals are formed from the reactions of O_3 with NO_2, and thus become important only when O_3 formation begins. In addition, NO_3 + organic reactions can result in both radical source and NO_x sink processes. However,

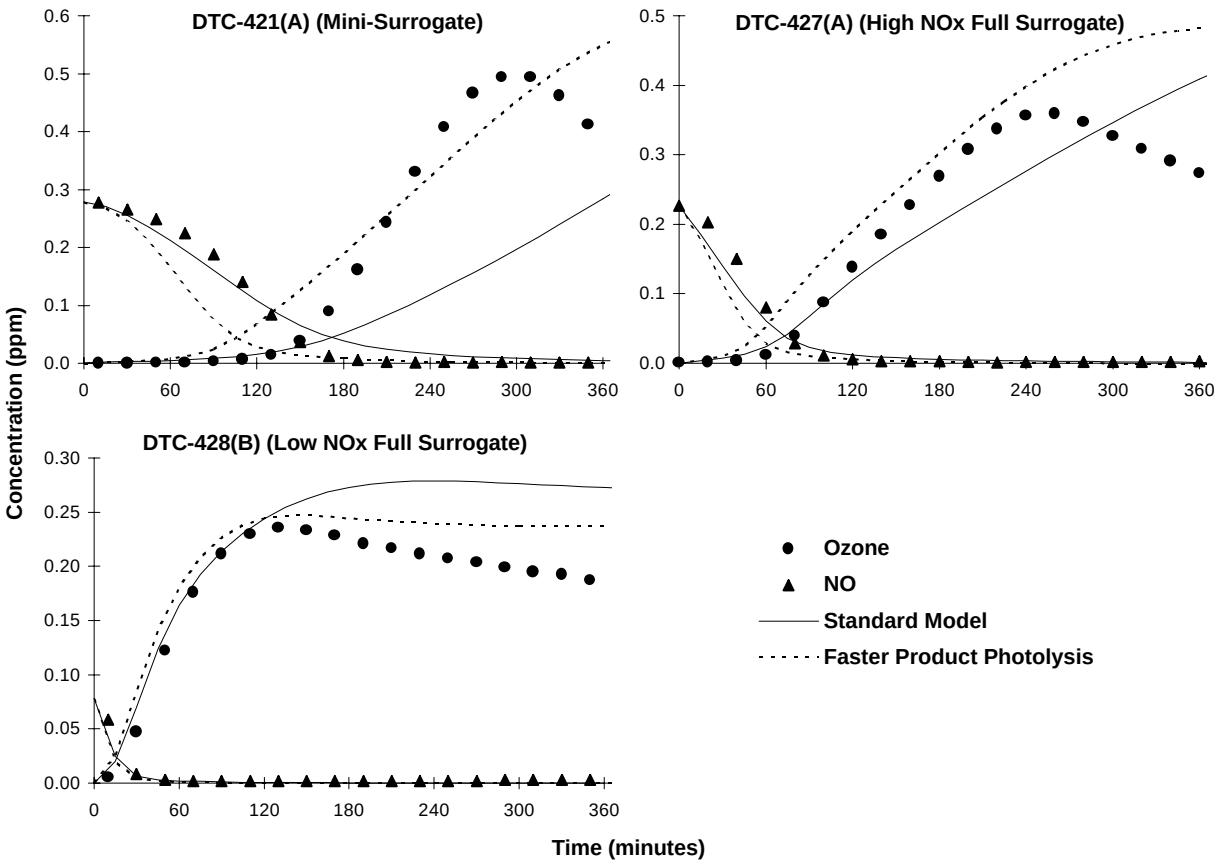

Figure 13. Effects of assuming faster product photolysis rates on model simulations of ozone and NO for selected propyl bromide reactivity experiments.

including such reactions in the model did not result in correct simulations of the O_3 loss at the end of the lower NO_x experiments, and the rate constants required to fit the enhanced reactivity when O_3 formation began were greater than the gas kinetic upper limits.

HBr + NO_x Reactions. The possibility of reactions of HBr with NO_2, NO_3, N_2O_5, or HNO_3 causing recycling of Br atoms was examined. Reaction of HBr with NO_2, N_2O_5 and HNO_3 were ruled out on the basis of thermochemistry. However, the reactions

$$HBr + NO_3 \rightarrow HONO + Br$$

is thermochemically possible, and could account for the radical initiation after O_3 formation began. Model simulations indicated that including this reaction indeed could account for the enhanced reactivity after O_3 formation began, though a rate constant of $>5 \times 10^{-11}$ cm^3 $molec^{-1}$ s^{-1} had to be assumed. However, including this reaction tended to result in the final O_3 yields being underpredicted, and also it did not predict the relatively rapid O_3 consumption rate observed in the later stages of most of the added bromide runs.

HBr + BrO_2NO_2 Reaction. The reaction

$$HBr + BrONO_2 \rightarrow Br_2 + HNO_3$$

may well occur as a heterogeneous process, with the Br_2 rapidly being photolyzed to form Br atoms. However, as with other mechanism modifications involving $BrONO_2$, including this reaction had essentially no effect on the results of the model simulations.

Reactions of HBr with Ozonolysis Intermediates. The possibility that the excess reactivity in the presence of O_3 could be due to a reaction between HBr and the biradical intermedicate formed in the O_3 + alkene reactions was examined. The only alkene present in the mini-surrogate experiment is ethene. As shown in Appendix A, in the standard model ethene reacts with O_3 to form an intermediate designated (HCHO2), which is assumed to primarily decompose to form stable and (to a lesser extent) radical products. For testing purposes, the reaction

$$(HCHO2) + HBr \rightarrow OH + Br\cdot + HCHO$$

was added, and given a sufficiently high rate constant that this would be the major fate of (HCHO2) if HBr were present. Although there was an effect of adding this reaction, it was too small to account for the observed excess initiation rate observed in the mini-surrogate experiments.

Reactions of HBr + O_3. The only exothermic and chemically reasonable reaction we could come up which could even approximately simulate our data was the reaction of O_3 with HBr, forming HOBr, which rapidly photolyzes to form OH and Br.

$$O_3 + HBr \rightarrow HOBr + O_2 \quad (47)$$

$$HOBr + h\nu \rightarrow OH + Br \quad (48)$$

Figures 1-12 show the effects of adding this reaction in the model, using a rate constant of

$$k_{47} = k(OH + Br \rightarrow BrOH + O_2) = 1 \times 10^{-15} \text{ cm}^3 \text{ molec}^{-1} \text{ s}^{-1},$$

which was optimized based on simulations of selected propyl bromide reactivity experiments as indicated in footnotes to Table 1. It can be seen that adding this reaction causes significant improvements to the simulations of the chamber data.

Since the mechanisms assuming that the HBr + O_3 reaction occurs with a rate constant, k_{47}, of 1 x 10^{-15} cm^3 $molec^{-1}$ s^{-1} give the best performance when simulating the chamber data, they are referred to as the "base fit" or "adjusted" mechanisms in the subsequent discussions. The propyl bromide runs were used to determine the best fit value of k_{47} because its mechanism has somewhat fewer competing processes, and thus the Br atom yield in its photooxidation is somewhat less uncertain. The adjusted propyl bromide mechanism gives the best fits to the experiments with the full surrogate, but tends to somewhat underpredict the ozone formation rates in the mini-surrogate runs. Somewhat better fits can be obtained if higher rate constants were assumed for the Br + alkene reactions, but since these rate constants have already been measured (see Table 1), this adjustment is not made. Better fits to the mini-surrogate experiments can also be obtained if higher values of k_{47} are used, but at the expense of the model having a greater tendency to overpredict the O_3 consumption rates at the end of the low NO_x full surrogate runs. The lower value of k_{47} are considered to be more appropriate for ambient modeling applications because the full surrogate experiments are somewhat more representative of ambient conditions.

Figures 7-12 show that the model with only k_{47} adjusted does not perform quite as well simulating the butyl bromide experiments as those with propyl bromide. This may be due to the greater uncertainty for the branching ratios for the various reactions of the radicals formed in the OH + butyl bromide system, and in the higher predicted overall organic nitrate yields, which are also uncertain. The branching ratios affecting the more important overall processes in the OH + butyl bromide system were adjusted to see the extent to which this would improve the fits (see footnote to Table 1). As indicated on Table 1, best fits were obtained by reducing the number of NO to NO_2 conversions to the minimum by assuming that $b_2 \approx b_3 \approx 0$, increasing slightly the Br atom yield by increasing b_1 from 15% to 19%, and decreasing the overall organic nitrate yield from ~8% to ~6%. Although this adjustment is highly uncertain and to some

extent is probably compensating for other errors in the mechanism, it is not outside of the relatively large range of uncertainty of the initial estimates. The results of the model simulations using this optimized butyl bromide mechanisms are shown on Figures 7-12. This optimization improves the fits to the high NO_x mini-surrogate and full surrogate runs, but does not significantly improve the fits to the low NO_x full surrogate runs. No reasonable adjustments to the butyl bromide mechanism could be found which gave fully satisfactory simulations of those runs. Therefore, no butyl bromide mechanism was developed which satisfactorily fit all the data.

Results of Exploratory Studies of the HBr + O_3 Reaction

Since the chamber model simulations suggested that there was a rapid reaction between HBr and O_3, exploratory experiments were carried out to measure this rate constant in the SAPRC evacuable chamber with in-situ FT-IR spectroscopy. This experiment was carried out in 1 atm of dry, synthetic air in the dark. First ~5 ppm of HBr was injected into the chamber and monitored for approximately 16 minutes. It was observed to decay with a unimolecular rate constant of 7.6×10^{-3} min^{-1}. Then an additional ~10 ppm of HBr was added and monitored for an additional 44 minutes. The HBr decay rate during this second period was 2.84×10^{-3} min^{-1}, with the decline in the decay rate indicating a possible wall conditioning effect. Finally ~12-13 ppm of O_3 was added, and the O_3 and HBr were monitored for somewhat over an hour. The concentration-time plots for both O_3 and HBr are shown on Figure 14.

Figure 14 shows that the decay rate of both O_3 and HBr are relatively slow, though HBr decays somewhat more rapidly than O_3. If HBr and O_3 dark decay rates of respectively 2.84×10^{-3} and 5.5×10^{-4} min^{-1} are assumed [the latter being based on results of previous O_3 dark decay rates measured in this chamber (Carter et al, 1995b], then the data are well fit by representing the O_3 + HBr reaction as

$$HBr + O_3 \rightarrow \rightarrow \text{-HBr} + \text{(products)} \qquad (51)$$

where

$$k_{51} = 3.8 \times 10^{-19} \text{ cm}^3 \text{ molec}^{-1} \text{ s}^{-1}.$$

The lines on Figure 14 show the results of the model simulations of this experiment using this model. Note that two molecules of HBr are consumed for each molecule of O_3, indicating that the reaction is a one-step elementary process. However, the data are consistent with the rate determining step being first order in both O_3 and HBr.

These results are inconsistent with the rapid O_3 + HBr reaction assumed in the adjusted model which best fit the environmental chamber data, which assumes a reaction which is over three orders of magnitude faster. However, the possibility of a light-induced reaction between O_3 and HBr, forming the same overall products (i.e, OH + Br) has not been ruled out.

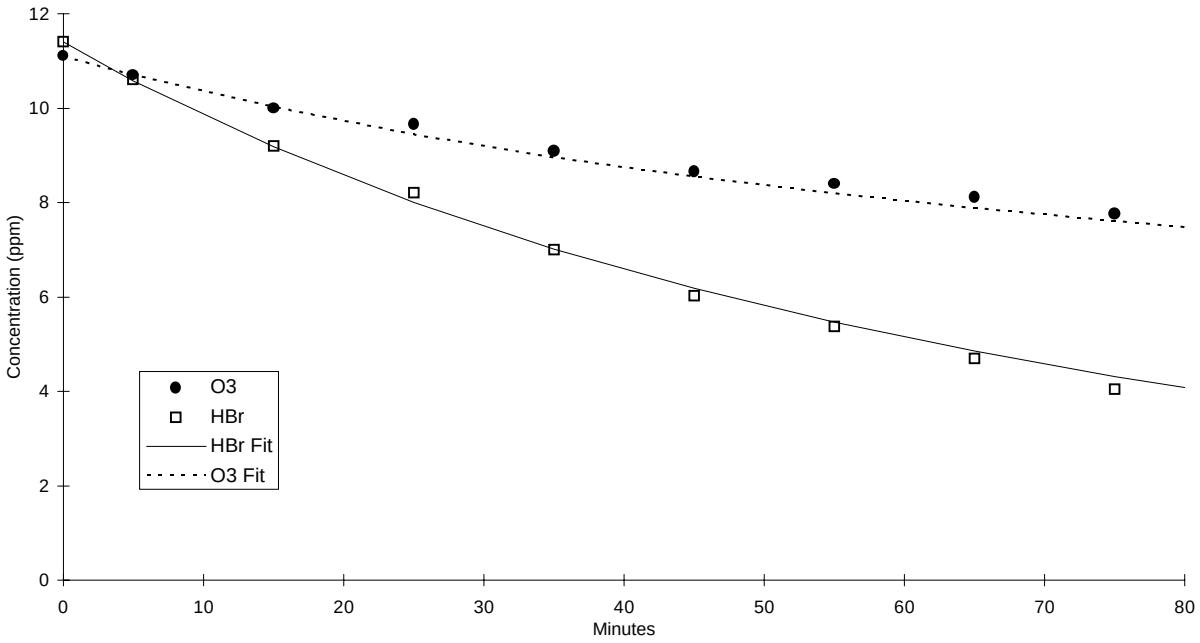

Figure 14. Experimental and calculated concentration-time plots for O_3 and HBr as monitored by FT-IR in the SAPRC Evacuable chamber.

ATMOSPHERIC REACTIVITY CALCULATIONS

Incremental reactivities of VOCs have been shown to be highly dependent on environmental conditions, so reactivities measured in environmental chamber experiments cannot necessarily be assumed to be exactly the same as those under atmospheric conditions (Carter and Atkinson, 1989b; Carter et al, 1995a). The only method available to obtain quantitative estimates of incremental reactivities of VOCs in ambient air pollution episodes is to conduct airshed model simulations of the episodes. Since these simulations cannot be any more reliable than the chemical mechanisms used, the major objective of this program was to develop and evaluate alkyl bromide mechanisms for use in such simulations. This was discussed in the previous sections. In this section, we discuss the results of model simulations of its incremental reactivities in a variety of model scenarios representing ozone exceedence episodes in various areas in the United States (Baugues, 1990), and compare the results to incremental reactivities calculated for ethane, the compound used by the EPA as the criterion for determining "negligible" reactivity, and for the base ROG, the mixture representing total ROG emissions from all sources.

Although it is clear that the rapid reaction between O_3 and HBr, forming HOBr, does not occur as a simple dark reaction as written, it must be assumed in the model in order to even approximately fit the chamber data. Therefore, even though this reaction does not occur as written, it must represent some process which is actually occurring in the system which has the same net effect. Since the exact nature of this process is not known, it is uncertain whether it represents a gas phase reaction which will also occur in the atmosphere, or some sort of a chamber artifact. If it is the former, then including the O_3 + HBr reaction with the rate constant which fit the chamber data may be an appropriate way to model this process in the atmosphere. If it is a heterogeneous or chamber-dependent process, it may be more appropriate to assume that it does not occur when conducting atmospheric simulations, or to model the process with a significantly reduced rate constant.

Therefore, to assess the likely range of uncertainties in the atmospheric ozone impacts of these alkyl bromides, the atmospheric model simulations using two different models for their reactions: one assuming the process represented by the O_3 + HBr reaction occurs in the atmosphere at the same rate it does in the chamber, and the other where that process is assumed not to occur, i.e., where k_{47}=0. The differences between the results of the simulations using these two models give an indication of the importance of this unknown process in affecting the ozone impacts of these compounds.

Scenarios Used for Reactivity Assessment

The set of airshed scenarios employed to assess the alkyl bromide reactivities for this study is the same as those used for calculating the MIR and other reactivity scales (Carter, 1994a; Carter et al, 1993b). The objective is to use a set of scenarios which represents, as much as possible, a comprehensive

distribution of the environmental conditions where unacceptable levels of ozone are formed. Although a set of scenarios has not been developed for the specific purpose of VOC reactivity assessment, the EPA developed an extensive set of scenarios for conducting analyses of effects of ROG and NO_x controls on ozone formation using the EKMA modeling approach (Gipson et al. 1981; Gipson and Freas, 1983; EPA, 1984; Gery et al. 1987; Baugues, 1990). The EKMA approach involves the use of single-cell box models to simulate how the ozone formation in one day episodes is affected by changes in ROG and NO_x inputs. Although single-cell models cannot represent realistic pollution episodes in great detail, they can represent dynamic injection of pollutants, time-varying changes of inversion heights, entrainment of pollutants from aloft as the inversion height raises, and time-varying photolysis rates, temperatures, and humidities (Gipson and Freas, 1981; EPA, 1984; Gipson, 1984; Hogo and Gery, 1988). Thus, they can be used to simulate a wide range of the chemical conditions which affect ozone formation from ROG and NO_x, and which affect VOC reactivity. Therefore, at least to the extent they are suitable for their intended purpose, an appropriate set of EKMA scenarios should also be suitable for assessing reactivities over a wide range of conditions.

Base Case Scenarios

The set of EKMA scenarios used in this study were developed by the United States EPA for assessing how various ROG and NO_x control strategies would affect ozone nonattainment in various areas of the country (Baugues, 1990). The characteristics of these scenarios and the methods used to derive their input data are described in more detail elsewhere (Baugues, 1990; Carter, 1994b). Briefly, 39 urban areas in the United States were selected based on geographical representativeness of ozone nonattainment areas and data availability, and a representative high ozone episode was selected for each. The initial non-methane organic carbon (NMOC) and NO_x concentrations, the aloft O_3 concentrations, and the mixing height inputs were based on measurement data for the various areas, the hourly emissions in the scenarios were obtained from the National Acid Precipitation Assessment Program emissions inventory (Baugues, 1990), and biogenic emissions were also included. Table 4 gives a summary of the urban areas represented and other selected characteristics of the scenarios.

Several changes to the scenario inputs were made based on discussions with the California ARB staff and others (Carter, 1994b). Two percent of the initial NO_x and 0.1% of the emitted NO_x in all the scenarios was assumed to be in the form of HONO. The photolysis rates were calculated using solar light intensities and spectra calculated by Jeffries (1991) for 640 meters, the approximate mid-point of the mixed layer during daylight hours. The composition of the NMOCs entrained from aloft was based on the analysis of Jeffries et al. (1989). The composition of the initial and emitted reactive organics was derived as discussed below. Complete listings of the input data for the scenarios are given elsewhere (Carter, 1994b).

This set of 39 EKMA scenarios are referred to as "base case" to distinguish them from the scenarios derived from them by adjusting NO_x inputs to yield standard conditions of NO_x availability as

Table 4. Summary of conditions of base case scenarios used for atmospheric reactivity assessment.

City, State	Calc. Max O_3 (ppb)	ROG /NO_x	NO_x /NO_x^{MOR}	Final Height (km)	Init.+Emit Base ROG (mmol m^{-2})	Aloft O_3 (ppb)
Atlanta, GA	179	7.3	0.7	2.1	12	63
Austin, TX	175	9.3	0.5	2.1	11	85
Baltimore, MD	326	5.2	1.0	1.2	17	84
Baton Rouge, LA	247	6.8	0.8	1.0	11	62
Birmingham, AL	238	6.9	0.5	1.8	13	81
Boston, MA	195	6.5	0.6	2.6	14	105
Charlotte, NC	143	7.8	0.3	3.0	7	92
Chicago, IL	281	11.6	0.5	1.4	25	40
Cincinnati, OH	198	6.4	0.7	2.8	17	70
Cleveland, OH	251	6.6	0.9	1.7	16	89
Dallas, TX	213	4.7	1.2	2.3	18	75
Denver, CO	211	6.3	1.0	3.4	29	57
Detroit, MI	238	6.8	0.7	1.8	17	68
El Paso, TX	188	6.6	0.9	2.0	12	65
Hartford, CT	169	8.4	0.5	2.3	11	78
Houston, TX	307	6.1	0.9	1.7	25	65
Indianapolis, IN	211	6.6	0.8	1.7	12	52
Jacksonville, FL	156	7.6	0.6	1.5	8	40
Kansas City, MO	154	7.1	0.6	2.2	9	65
Lake Charles, LA	291	7.4	0.6	0.5	7	40
Los Angeles, CA	580	7.6	0.8	0.5	23	100
Louisville, KY	210	5.5	0.8	2.5	14	75
Memphis, TN	225	6.8	0.6	1.8	15	58
Miami, FL	133	9.6	0.4	2.7	9	57
Nashville, TN	166	8.1	0.4	1.6	7	50
New York, NY	363	8.1	0.7	1.5	39	103
Philadelphia, PA	242	6.2	0.9	1.8	19	53
Phoenix, AZ	275	7.6	0.8	3.3	40	60
Portland, OR	165	6.5	0.7	1.6	6	66
Richmond, VA	233	6.2	0.7	1.9	16	64
Sacramento, CA	202	6.6	0.8	1.1	7	60
St Louis, MO	322	6.1	1.0	1.6	26	82
Salt Lake City, UT	184	8.5	0.6	2.2	11	85
San Antonio, TX	132	3.9	1.0	2.3	6	60
San Diego, CA	196	7.1	0.9	0.9	8	90
San Francisco, CA	325	4.8	1.5	0.7	25	70
Tampa, FL	232	4.4	1.0	1.0	8	68
Tulsa, OK	225	5.3	0.9	1.8	15	70
Washington, DC	276	5.3	0.8	1.4	13	99

discussed below. No claim is made as to the accuracy of these scenarios in representing any real episode, but they are a result of an effort to represent, as accurately as possible given the available data and the limitations of the formulation of the EKMA model, the range of conditions occurring in urban areas throughout the United States. When developing general reactivity scales it is more important that the scenarios employed represent a realistic distribution of chemical conditions than accurately representing the details of any one particular episode.

The Base ROG mixture is the mixture of reactive organic gases used to represent the chemical composition of the initial and emitted anthropogenic reactive organic gases from all sources in the scenarios. Consistent with the approach used in the original EPA scenarios, the same mixture was used for all scenarios. The speciation for this mixture was derived by Croes (1991) based on an analysis of the EPA database (Jeffries et al. 1989) for the hydrocarbons and the 1987 Southern California Air Quality Study (SCAQS) database for the oxygenates (Croes et al. 1994; Lurmann et al. 1992). This mixture consists of 52% (by carbon) alkanes, 15% alkenes, 27% aromatics, 1% formaldehyde, 2% higher aldehydes, 1% ketones, and 2% acetylene. The detailed composition of this mixture is given elsewhere (Carter, 1994b).

Adjusted NO_x scenarios

Incremental reactivities in the base case scenarios is expected to vary widely because they depend on the ROG/NO_x ratio, which varies from scenario to scenario. To obtain reactivity scales for specified NO_x conditions, separate sets of scenarios, designated MIR (for maximum incremental reactivity), MOR (for maximum ozone reactivity), and Equal Benefit Incremental Reactivity (EBIR) were developed (Carter, 1994a). In the MIR scenarios, the NO_x inputs were adjusted so the base ROG mixture (and most other VOCs) have their highest incremental reactivity. This is representative of the highest NO_x conditions of relevance to VOC reactivity assessment because at higher NO_x levels O_3 yields become significantly suppressed, but is also the condition where O_3 is most sensitive to VOC emissions. In the MOR scenarios, the NO_x inputs were adjusted to yield the highest ozone concentration. In the EBIR scenarios, the NO_x inputs were adjusted so that the relative effects of NO_x reductions and total ROG reductions on peak ozone levels were equal. This represents the lowest NO_x condition of relevance for VOC reactivity assessment, because O_3 formation becomes more sensitive to NO_x emissions than VOC emissions at lower NO_x levels. The changes in the base case ROG/NO_x ratios which yielded the MOR scenarios are given in Table 4. As discussed by Carter (1994a) the MIR and EBIR ROG/NO_x ratios are respectively ~1.5 and ~0.7 times those for the MOR scenarios in all cases.

For this study, the MIR, MOIR, and EBIR reactivities were calculated using the "averaged conditions" scenarios with the corresponding adjusted NO_x conditions. As discussed by Carter (1994a), averaged conditions scenarios have all inputs derived by averaging the corresponding inputs of the base case scenarios, except that the NO_x inputs were adjusted to yield the specified NO_x conditions as discussed above. This is slightly different than the approach used by Carter (1994a) to derive the MIR, MOIR, and

EBIR scales, which involved adjusting NO_x conditions separately for each of the 39 base case scenarios, and then averaging the reactivities derived from them. Since Carter (1994a) showed that both approaches yield essentially the same result. For this work use of the averaged conditions approach was preferred because it is computationally much more straightforward, and gives an equally a good indication of how the relative reactivities of compounds vary with varying NO_x conditions. Calculations were also performed where the NO_x inputs in the averaged conditions scenarios were continuously varied, to provide additional information on how relative reactivities varied with changing NO_x conditions.

NO_x Conditions in the Base Case Scenarios

The variability of ROG/NO_x ratios in the base case scenarios suggest a variability of reactivity characteristics in the base case scenarios. However, as discussed previously (Carter, 1994a), the ROG/NO_x ratio is also variable in the MIR or MOR scenarios, despite the fact that the NO_x inputs are adjusted to yield a specified reactivity characteristic. Thus, the ROG/NO_x ratio, by itself, is not necessarily a good predictor of reactivity characteristics of a particular scenario. The NO_x/NO_x^{MO} ratio is a much better predictor of this, with values greater than 1 indicating relatively high NO_x conditions where ozone formation is more sensitive to VOCs, and values less than 1 indicating NO_x-limited conditions. NO_x/NO_x^{MO} ratios less than 0.7 represent conditions where NO_x control is a more effective ozone control strategy than ROG control (Carter, 1994a). Note that more than half of the base case scenarios represent NO_x-limited conditions, and ~25% of them represent conditions where NO_x control is more beneficial than VOC control. A relatively small number of scenarios represent MIR or near MIR conditions. However, as discussed elsewhere (Carter, 1994a), this set of scenarios is based on near-worst-case conditions for ozone formation in each of the airsheds. Had scenarios representing less-than-worst-case conditions been included, one might expect a larger number of MIR or near MIR scenarios. This is because NO_x is consumed more slowly on days with lower light intensity or temperature, and thus the scenario is less likely to become NO_x-limited.

Incremental and Relative Reactivities

The incremental reactivity of a VOC in an airshed scenario is the change in ozone caused by adding the VOC to the emissions, divided by the amount of VOC added, calculated for sufficiently small amounts of added VOC that the incremental reactivity is independent of the amount added. The procedure used to calculate incremental reactivities in a scenario was as discussed in detail elsewhere (Carter, 1994a,b). The incremental reactivities depend on how the amount of VOC added are quantified. In this work, the added VOC was quantified on a mass basis, since this is how VOCs are regulated. In addition, the incremental reactivities also depend on how ozone impacts are quantified (Carter, 1994a). In this work, two different ozone quantifications were used, resulting in two different incremental reactivities being calculated for a VOC in a scenario. These are discussed below.

The "Ozone Yield" incremental reactivities measure the effect of the VOC on the total amount of ozone formed in the scenario at the time of its maximum concentration. In this work, this is quantified

as grams O_3 formed per gram VOC added. This gives the same ratios of incremental reactivities as reactivities calculated from peak ozone concentrations, but is preferred because it permits magnitudes of reactivities in scenarios with differing dilutions to be compared on the same basis. Most previous recent studies of incremental reactivity (Dodge, 1984; Carter and Atkinson, 1987, 1989b, Chang and Rudy, 1990; Jeffries and Crouse, 1991) have all been based on ozone yield or peak ozone concentration reactivities.

The ozone yield incremental reactivities do not necessarily measure the effect of the VOC on exposure to unacceptable levels of ozone because it does not measure how long high levels of ozone are present. A quantification which reflects this is integrated ozone over the standard, which is defined as the sum of the hourly ozone concentrations for the hours when ozone exceeds the standard in the base case scenarios (Carter 1994a). In the previous work (Carter, 1994a), we used the California ozone standard of 90 ppb, but in this work we will use the national standard of 0.12 ppm. Reactivities relative to this quantification of ozone are referred to by the abbreviation "IntO_3>0.12" reactivities.

Relative reactivities are ratios of incremental reactivities to incremental reactivities of some standard VOC or mixture. Since these are the quantities which usually are the most relevant to control strategy applications, the results in this work will be given in terms of relative reactivities. In our previous work (Carter 1991, 1994a), we used the incremental reactivity of the base ROG mixture, i.e., the mixture representing ROG pollutants from all sources, as the standard to define relative reactivities. However, because of the tendency within the EPA to consider ethane as the standard to define exempt vs controlled VOCs, in this work we will present reactivity ratios where ethane is used as the standard.

Calculated Relative Reactivities of Propyl and Butyl Bromides

Table 5 lists the reactivities, relative to the average reactivity of the total mixture of all ROGs emitted into the atmosphere, calculated for ethane, 1-propyl bromide and 1-butyl bromide for the various scenarios and mechanisms discussed above. Plots of the reactivities of the bromides relative to ethane against the NO_x levels in the scenarios, as measured by the NO_x/NO_x^{MO} ratio, are shown on Figure 15, where the points show the data for the base case scenarios, and the lines show the effects of continuously varying the NO_x levels in the averaged conditions scenario. The bromide reactivities were calculated both with and without the O_3 + HBr reaction which was required for the model to approximately fit the chamber data, and in both cases the butyl bromide reactivities were calculated using the optimized butyl bromide mechanism. The reactivities are given on an ozone formed per gram VOC basis, with the ozone quantified either as peak ozone yield or as integrated ozone over the U.S. standard of 0.12 ppm. The dotted horizontal lines on the plots show the relative reactivity of ethane (i.e. 1), so points or curves above those line correspond to scenarios or NO_x conditions where the bromides are calculated to be more reactive than ethane.

Table 5. Summary of calculated incremental reactivities (gram basis) for ethane and the alkyl bromides relative to the average of all ROG emissions.

Scenario	O_3 Yield Relative Reactivities					$IntO_3$ >0.12 Relative Reactivities				
	Ethane	Propyl Bromide		Butyl Bromide		Ethane	Propyl Bromide		Butyl Bromide	
		Std.	O_3 + HBr	Std.	O_3 + HBr		Std.	O_3 + HBr	Std.	O_3 + HBr
Averaged Conditions										
Max React	0.08	0.07	0.23	0.15	0.34	0.07	0.06	0.21	0.14	0.31
Max Ozone	0.15	0.04	0.00	0.18	0.15	0.10	0.04	0.07	0.13	0.18
Equal Benefit	0.19	-0.07	-0.36	0.11	-0.20	0.12	-0.02	-0.15	0.08	-0.05
Base Case										
Average	**0.17**	**-0.03**	**-0.23**	**0.13**	**-0.07**	**0.11**	**0.00**	**-0.07**	**0.10**	**0.03**
St.Dev	**0.04**	**0.07**	**0.25**	**0.07**	**0.25**	**0.03**	**0.05**	**0.16**	**0.04**	**0.17**
ATL GA	0.17	-0.05	-0.25	0.10	-0.10	0.12	-0.02	-0.13	0.07	-0.04
AUS TX	0.19	-0.09	-0.39	0.09	-0.25	0.14	-0.05	-0.24	0.05	-0.17
BAL MD	0.15	0.06	-0.03	0.22	0.14	0.09	0.05	0.09	0.14	0.19
BAT LA	0.15	-0.01	-0.11	0.12	0.02	0.10	0.00	-0.03	0.08	0.05
BIR AL	0.23	-0.04	-0.38	0.20	-0.16	0.13	0.00	-0.13	0.12	-0.01
BOS MA	0.20	-0.11	-0.34	0.08	-0.16	0.12	-0.03	-0.12	0.07	-0.02
CHA NC	0.20	-0.16	-0.51	0.03	-0.36	0.16	-0.11	-0.35	0.02	-0.25
CHI IL	0.27	-0.15	-0.97	0.06	-0.83	0.14	-0.05	-0.38	0.04	-0.34
CIN OH	0.19	0.00	-0.18	0.20	0.00	0.12	0.03	-0.02	0.15	0.10
CLE OH	0.15	0.01	-0.13	0.15	0.02	0.09	0.03	0.03	0.11	0.12
DAL TX	0.12	0.07	0.15	0.18	0.29	0.09	0.05	0.14	0.13	0.24
DEN CO	0.11	0.02	-0.04	0.12	0.06	0.07	0.03	0.08	0.10	0.16
DET MI	0.20	0.00	-0.19	0.20	0.01	0.11	0.03	0.00	0.14	0.11
ELP TX	0.11	0.02	-0.01	0.13	0.10	0.08	0.02	0.05	0.09	0.13
HAR CT	0.20	-0.08	-0.41	0.13	-0.23	0.15	-0.03	-0.21	0.10	-0.10
HOU TX	0.18	0.03	-0.08	0.21	0.10	0.11	0.03	0.02	0.14	0.14
IND IN	0.16	-0.01	-0.15	0.14	0.00	0.11	0.02	0.00	0.11	0.11
JAC FL	0.16	-0.11	-0.37	0.03	-0.25	0.13	-0.07	-0.27	0.03	-0.18
KAN MO	0.19	-0.03	-0.26	0.17	-0.07	0.14	0.00	-0.11	0.13	0.01
LAK LA	0.22	-0.19	-0.61	-0.02	-0.45	0.14	-0.10	-0.33	-0.02	-0.27
LOS CA	0.15	0.05	-0.14	0.19	-0.02	0.08	0.04	0.03	0.12	0.11
LOU KY	0.19	-0.03	-0.15	0.15	0.03	0.13	0.00	-0.04	0.12	0.08
MEM TN	0.20	-0.11	-0.39	0.09	-0.20	0.13	-0.04	-0.16	0.08	-0.05
MIA FL	0.18	-0.16	-0.58	-0.01	-0.47	0.17	-0.14	-0.52	-0.01	-0.43
NAS TN	0.23	-0.10	-0.49	0.12	-0.27	0.19	-0.07	-0.37	0.10	-0.22
NEW NY	0.17	-0.16	-0.86	-0.04	-0.80	0.09	-0.01	-0.17	0.05	-0.13
PHI PA	0.17	0.01	-0.13	0.17	0.03	0.11	0.03	0.01	0.13	0.12
PHO AZ	0.16	0.07	-0.03	0.24	0.14	0.09	0.05	0.07	0.15	0.18
POR OR	0.17	-0.05	-0.23	0.12	-0.07	0.14	-0.03	-0.15	0.09	-0.03
RIC VA	0.18	0.00	-0.23	0.18	-0.05	0.12	0.03	-0.03	0.14	0.09
SAC CA	0.17	0.03	-0.06	0.20	0.11	0.12	0.03	0.02	0.14	0.14
SAI MO	0.14	0.05	-0.03	0.18	0.11	0.08	0.04	0.08	0.12	0.17
SAL UT	0.19	-0.02	-0.26	0.17	-0.09	0.12	0.01	-0.08	0.12	0.03
SAN TX	0.13	0.05	0.08	0.17	0.22	0.12	0.04	0.07	0.15	0.20
SDO CA	0.12	0.01	-0.08	0.11	0.02	0.09	0.02	-0.01	0.09	0.07
SFO CA	0.05	0.06	0.23	0.11	0.32	0.05	0.05	0.19	0.10	0.27
TAM FL	0.13	0.03	0.03	0.14	0.16	0.09	0.03	0.08	0.11	0.17
TUL OK	0.18	-0.04	-0.17	0.13	0.00	0.11	0.02	0.00	0.12	0.12
WAS DC	0.19	0.00	-0.16	0.19	0.03	0.11	0.02	-0.01	0.13	0.10

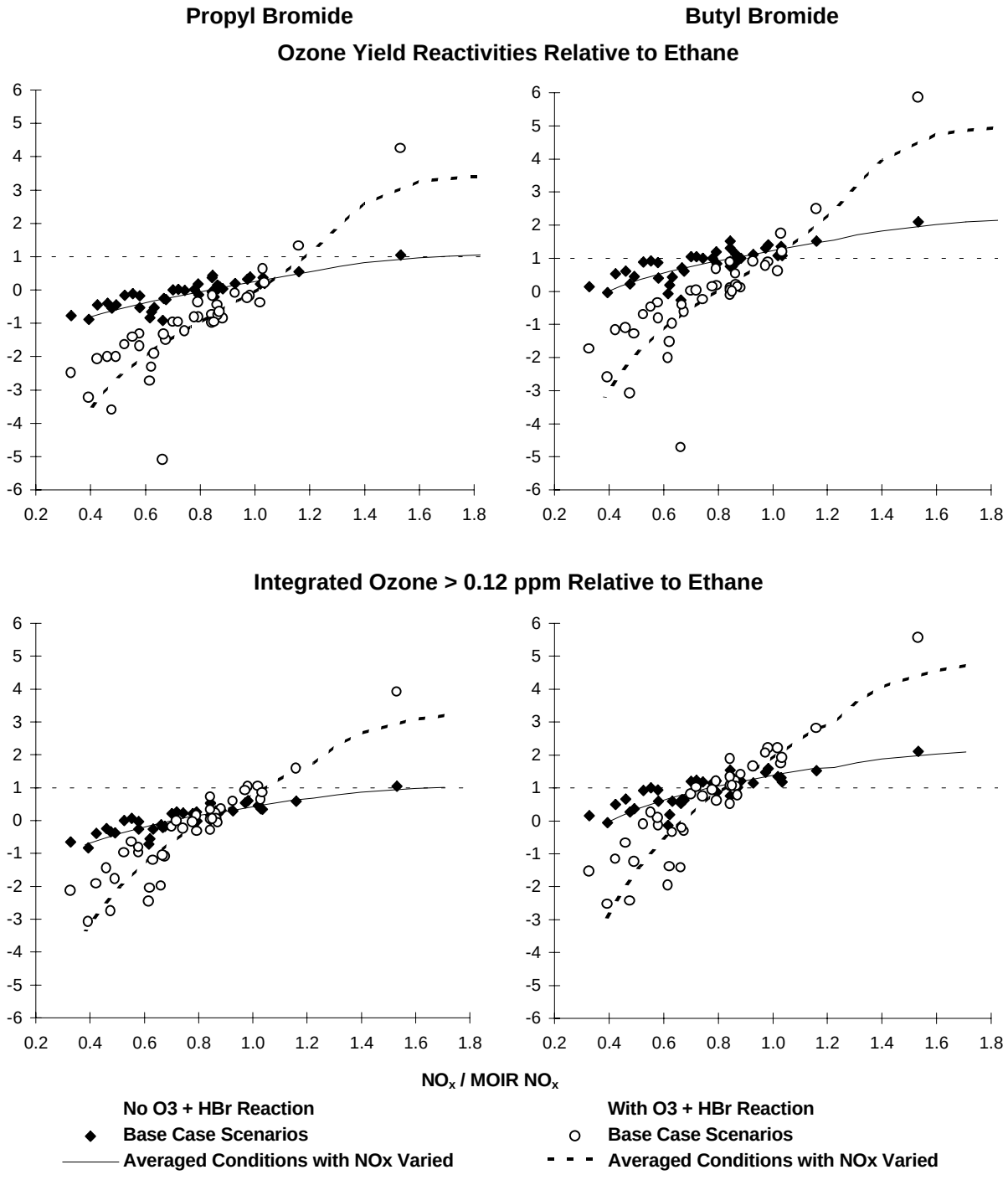

Figure 15. Calculated reactivities of 1-propyl bromide and 1-butyl bromide, relative to ethane as a function of NO_x conditions in the ambient pollution scenarios.

The results show a strong dependence of the alkyl bromide relative reactivities on NO_x conditions, being highest under high NO_x or maximum reactivity conditions, and becoming lower or even negative in scenarios where ozone is NO_x limited. This dependence on NO_x conditions is the greatest if the process represented by the O_3 + HBr reaction is assumed to be important, being less but still non-negligible if that process is assumed to be unimportant in the atmosphere.

If the process represented by the O_3 + HBr reaction is assumed to occur in the same way in the ambient atmosphere as in the chamber experiments, then propyl and butyl bromides are calculated to be respectively 3 or 4.5 times more reactive than ethane, on a gram emitted basis, in the high NO_x or MIR scenarios, regardless of whether ozone is quantified by peak ozone yield or integrated O_3 over the 0.12 ppm standard. However, the reactivity of propyl bromide is still less, by a factor of four, than the average reactivity of all ROG emissions, indicating that the maximum ozone impact of this compounds are still relatively low. The reactivity of butyl bromide under these conditions is a factor of three less than the average for all ROG emissions. The relative reactivities decline rapidly as the NO_x levels are reduced, though the rate of decline is somewhat less for integrated O_3 reactivities than is the case for reactivities based on O_3 yields. In the case of propyl bromide, the ozone yield reactivities approach zero as NO_x conditions approach MOR levels, and become significantly negative for scenarios that are NO_x limited. On the other hand, the integrated ozone reactivities of propyl bromide approach those of ethane for MOR conditions, and become negative only as NO_x approaches or becomes lower than EBIR levels. In the case of butyl bromide, the ozone yield reactivities approach those of ethane as NO_x goes down to MOR levels, and become negative at NO_x levels between MOR and EBIR. The butyl bromide integrated ozone reactivities are greater than those of ethane for most scenarios where NO_x levels are greater than EBIR, becoming lower or negative only for scenarios with EBIR or lower NO_x scenarios.

This strong NO_x dependence which is predicted if the process represented by the O_3 + HBr reaction is included can be readily explained by the fact that this reaction is both a radical source and an ozone sink. Under relatively high NO_x or MIR conditions, ozone yields (and integrated O_3 levels) are determined primarily by how rapidly ozone is formed, which is highly sensitive to radical initiation processes. The amounts of additional ozone formation caused by the radicals initiated by the photolysis of the HOBr formed in the O_3 + HBr reaction is more than enough to compensate for the direct O_3 destruction caused by this reaction. However, under lower NO_x conditions, the ozone yields are less sensitive to how rapidly ozone is formed and more sensitive to the ultimate ozone formation potential of the system. The latter is less sensitive to radical initiation processes, and more sensitive to NO_x or O_3 sinks. Therefore, the O_3 sink aspects of this reaction become the more important factor influencing the net effect of this reaction, with the result being that it causes negative incremental reactivities of the alkyl bromides in scenarios where NO_x is sufficiently low.

The dependence of the relative reactivities of the alkyl bromides on NO_x levels is considerably less if it is assumed that the process represented by the O_3 + HBr reaction is a chamber effect which does

not occur in ambient air scenarios. In this case, the MIR reactivities of the bromides are calculated to be considerably less, but the low NO_x reactivities to be considerably greater (i.e., less negative), than is calculated if the O_3 + HBr reaction is included. In the case of propyl bromide, the MIR or high NO_x reactivities are approximately the same as those for ethane, regardless of whether the reactivities are derived from ozone yields or integrated O_3 over the standard. For lower NO_x conditions, including all but one of the base case scenarios, the propyl bromide ozone yield or integrated O_3 reactivities are calculated to be less than that of ethane, and become slightly negative for scenarios where NO_x is lower than EBIR levels. In the case of butyl bromide, the ozone yield and integrated O_3 reactivities are very similar, are about twice that of ethane for high NO_x or MIR scenarios, and become less than those for ethane only for scenarios where NO_x at or below EBIR levels.

Although the bromide reactivities are calculated to be less strongly sensitive to NO_x levels if the process represented by the O_3 + HBr reaction is assumed to be unimportant in the atmosphere, there is still a much greater calculated NO_x dependence than is the case for most VOCs. In this case, there is no significant radical initiation process enhancing bromide reactivities under high NO_x conditions, so the NO_x dependence must be primarily due to moderate NO_x or O_3 sinks causing lower reactivities under low NO_x conditions. The reaction of bromine atoms with O_3 clearly must be playing a role, because much higher alkyl bromide reactivities are calculated for low NO_x scenarios if that reaction is removed from the mechanism. This could be due to the direct removal of ozone by that reaction, combined with the NO_x sink caused by the subsequent formation of BrONO2. These reactions may be more important under ambient conditions than they are in the chamber experiments, and thus the uncertainties in their rate constants may also be more important.

CONCLUSIONS

The decision whether it is appropriate to regulate a compound as an ozone precursor requires a qualitative assessment of its ozone impacts under a variety of environmental conditions. This involves developing a chemical mechanism for the compounds atmospheric reactions which can be reliably used in airshed models to predict its atmospheric reactivity. Until this study, there was no mechanism available for simulating the atmospheric reactions of any bromine containing compounds, and thus quantitative ozone impact estimates for the alkyl bromides could not be made. The objective of this study was to develop such a mechanism and provide the data needed to verify its predictive capabilities. This program made progress towards this objective. Experimental information was obtained for the first time on how these compounds affect ozone formation in simulated photochemical smog systems allowing mechanisms for the atmospheric reactions of these compounds to be evaluated. However, we were not successful in developing a mechanism which could satisfactorily simulate the results of the experiments, without adding a speculative reaction to represent a process whose exact nature is unknown. Therefore, although we could make estimates of possible ozone impacts of these compounds if various assumptions about this unknown process are made, it is unknown which assumptions are correct.

The problem is that the known or predicted reactions of the alkyl bromides, bromine atoms, or the predicted bromine-containing products could not explain the enhanced rates of O_3 formation and radical levels caused by the alkyl bromides in simulated photochemical smog systems around the time that ozone formation begins, nor could they explain the enhanced rates of O_3 removal they cause once ozone formation has completed. Although a number of possibilities were examined, satisfactory simulations of these observations could be obtained only if it is assumed that O_3 reacts rapidly with HBr, forming HOBr, which then photolyzes rapidly to form OH radicals and Br atoms. The formation of the OH radicals and Br atoms allows the enhanced rates of ozone formation in the initial stages of the experiments to be simulated, while the destruction of O_3 by the reaction with HBr accounts for the loss of ozone in the later stages of the experiment, and the lower ozone reactivities under lower NO_x conditions. However, direct measurements of O_3 mixed with HBr in the dark indicate that there is no such rapid reaction of these compounds, at least in the absence of light and other reactants. Therefore, there is likely some other process which is occurring in this system which has the same net effect. The exact nature of this process, and the extent to which it occurs in atmospheric scenarios, is unknown. Regardless of the nature of this process, it apparently is successfully modeled by assuming this rapid O_3 + HBr reaction, at least for the conditions of the environmental chamber experiments.

If the unknown process represented by the HBr + ozone reaction is assumed to be as important in the atmosphere as it appears to be in our chamber experiments, then the ozone formation potentials of the alkyl bromide, and their reactivities relative to ethane, are calculated to be highly dependent on NO_x

conditions. Under the relatively high NO_x such as those used to derive the Maximum Incremental Reactivity (MIR) scale, propyl bromide is calculated to form approximately 1/4 as much ozone as the average of all ROG emissions, or approximately three times more ozone than ethane. Butyl bromide is calculated to form ~50% more ozone under these conditions. On the other hand, because of the strong O_3 sink caused by the process represented by the O_3 + HBr reaction, then both these alkyl bromides are calculated to be ozone inhibitors under lower NO_x conditions, including the majority of the scenarios used to represent "worst case" ozone episodes throughout the United States.

If the enhanced rates of O_3 formation and destruction in our chamber experiments are due to a surface process which is not important in the atmosphere, then the alkyl bromides are calculated to have much lower reactivities under MIR conditions, with propyl bromide having a MIR reactivity about the same as that of ethane, and having lower reactivities than ethane in most other scenarios. Butyl bromide would have somewhat higher reactivities, generally between one to two times that of ethane in scenarios where ozone formation is not NO_x limited.

It is clear that elucidating the unknown process which is represented by the O_3 + HBr reaction in our model calculations would significantly reduce the uncertainties in making quantitative estimates of the ozone impacts of these compounds. However, it is not unreasonable to assume that the "best fit" model, which assumes that this process is as important in the atmosphere as it appears to be in the chamber, may give appropriate near-upper-limit reactivity estimates for these compounds under high NO_x conditions. Likewise, it is not unreasonable to assume that the model which assumes that this process does not occur in the atmosphere may be appropriate for upper limit reactivity estimates under low NO_x conditions. Based on this, it is concluded that propyl bromide probably has no more than 1/4 the ozone impact as the average of all ROG emissions under high NO_x conditions, and it has much lower reactivity, or is an ozone inhibitor, under low NO_x conditions. Likewise, it is concluded that butyl bromide probably has no more than 1/3 the ozone impact of the average of all VOC emissions, with the impact also declining or becoming negative as NO_x is reduced.

REFERENCES

Atkinson, R. (1987): "A Structure-Activity Relationship for the Estimation of Rate Constants for the Gas-Phase Reactions of OH Radicals with Organic Compounds," Int. J. Chem. Kinet., 19, 799-828.

Atkinson, R. (1989): "Kinetics and Mechanisms of the Gas-Phase Reactions of the Hydroxyl Radical with Organic Compounds," J. Phys. Chem. Ref. Data, Monograph no 1.

Atkinson, R. (1991): "Kinetics and Mechanisms of the Gas-Phase Reactions of the NO_3 Radical with Organic Compounds," J. Phys. Chem. Ref. Data, 20, 459-507.

Atkinson, R. (1994): "Gas-Phase Tropospheric Chemistry of Organic Compounds," J. Phys. Chem. Ref. Data, Monograph No. 2.

Atkinson, R. (1997): "Gas Phase Tropospheric Chemistry of Volatile Organic Compounds: 1. Alkanes and Alkenes," J. Phys. Chem. Ref. Data, in press.

Atkinson, R. and W. P. L. Carter (1984): "Kinetics and Mechanisms of the Gas-Phase Reactions of Ozone with Organic Compounds under Atmospheric Conditions," Chem. Rev. 1984, 437-470.

Atkinson, R., D. L. Baulch, R. A. Cox, R. F. Hampson, Jr., J. A. Kerr, and J. Troe (1992): "Evaluated Kinetic and Photochemical Data for Atmospheric Chemistry. Supplement IV. IUPAC Subcommittee on Gas Kinetic Data Evaluation for Atmospheric Chemistry," J. Phys. Chem. Ref. Data 21, 1125-1568.

Atkinson, R., D. L. Baulch, R. A. Cox, R. F. Hampson, Jr., J. A. Kerr, M. J. Rossi, and J. Troe (1997): "Evaluated Kinetic, Photochemical and Heterogeneous Data for Atmospheric Chemistry: Supplement V., IUPAC Subcommittee on Gas Kinetic Data Evaluation for Atmospheric Chemistry," J. Phys. Chem. Ref. Data, in press.

Barnes, I., V. Bastian, K. H. Becker, R. Overath, and Z. Tong (1989): "Rate Constants for the Reactions of Br Atoms with a Series of Alkanes, Alkenes, and Alkynes in the Presence of O_2," Int. J. Chem. Kinet. 21, 499-517.

Baugues, K. (1990): "Preliminary Planning Information for Updating the Ozone Regulatory Impact Analysis Version of EKMA," Draft Document, Source Receptor Analysis Branch, Technical Support Division, U. S. Environmental Protection Agency, Research Triangle Park, NC, January.

Bierbach, A., I. Barnes, and K. H. Becker (1996): "Rate Coefficients for the Gas-Phase Reactions of Bromine Radicals with a Series of Alkenes, Dienes, and Aromatic Hydrocarbons at 298 ± 2K," Int. J. Chem. Kinet., 28, 565-577.

CARB (1993): "Proposed Regulations for Low-Emission Vehicles and Clean Fuels — Staff Report and Technical Support Document," California Air Resources Board, Sacramento, CA, August 13, 1990. See also Appendix VIII of "California Exhaust Emission Standards and Test Procedures for 1988 and Subsequent Model Passenger Cars, Light Duty Trucks and Medium Duty Vehicles," as last amended September 22, 1993. Incorporated by reference in Section 1960.1 (k) of Title 13, California Code of Regulations.

Carter, W. P. L. (1990): "A Detailed Mechanism for the Gas-Phase Atmospheric Reactions of Organic Compounds," Atmos. Environ., 24A, 481-518.

Carter, W. P. L. (1991): "Development of Ozone Reactivity Scales for Volatile Organic Compounds", EPA-600/3-91/050, August.

Carter, W. P. L. (1994a): "Development of Ozone Reactivity Scales for Volatile Organic Compounds," J. Air & Waste Manage. Assoc., 44, 881-899.

Carter, W. P. L. (1994b): "Calculation of Reactivity Scales Using an Updated Carbon Bond IV Mechanism," Draft Report Prepared for Systems Applications International Under Funding from the Auto/Oil Air Quality Improvement Research Program, April 12.

Carter, W. P. L. (1995): "Computer Modeling of Environmental Chamber Measurements of Maximum Incremental Reactivities of Volatile Organic Compounds," Atmos. Environ., 29, 2513-2517.

Carter, W. P. L., and R. Atkinson (1985): "Atmospheric Chemistry of Alkanes", J. Atmos. Chem., 3, 377-405, 1985.

Carter, W. P. L. and R. Atkinson (1987): "An Experimental Study of Incremental Hydrocarbon Reactivity," Environ. Sci. Technol., 21, 670-679

Carter, W. P. L. and R. Atkinson (1989b): "Alkyl Nitrate Formation from the Atmospheric Photooxidation of Alkanes; a Revised Estimation Method," J. Atm. Chem. 8, 165-173.

Carter, W. P. L. and R. Atkinson (1989b): "A Computer Modeling Study of Incremental Hydrocarbon Reactivity", Environ. Sci. Technol., 23, 864.

Carter, W. P. L., and F. W. Lurmann (1990): "Evaluation of the RADM Gas-Phase Chemical Mechanism," Final Report, EPA-600/3-90-001.

Carter, W. P. L. and F. W. Lurmann (1991): "Evaluation of a Detailed Gas-Phase Atmospheric Reaction Mechanism using Environmental Chamber Data," Atm. Environ. 25A, 2771-2806.

Carter, W. P. L., J. A. Pierce, I. L. Malkina, D. Luo and W. D. Long (1993a): "Environmental Chamber Studies of Maximum Incremental Reactivities of Volatile Organic Compounds," Report to Coordinating Research Council, Project No. ME-9, California Air Resources Board Contract No. A032-0692; South Coast Air Quality Management District Contract No. C91323, United States Environmental Protection Agency Cooperative Agreement No. CR-814396-01-0, University Corporation for Atmospheric Research Contract No. 59166, and Dow Corning Corporation. April 1.

Carter, W. P. L, D. Luo, I. L. Malkina, and J. A. Pierce (1993b): "An Experimental and Modeling Study of the Photochemical Ozone Reactivity of Acetone," Final Report to Chemical Manufacturers Association Contract No. KET-ACE-CRC-2.0. December 10.

Carter, W. P. L., D. Luo, I. L. Malkina, and J. A. Pierce (1995a): "Environmental Chamber Studies of Atmospheric Reactivities of Volatile Organic Compounds. Effects of Varying ROG Surrogate and NO_x," Final report to Coordinating Research Council, Inc., Project ME-9, California Air Resources Board, Contract A032-0692, and South Coast Air Quality Management District, Contract C91323. March 24.

Carter, W. P. L., D. Luo, I. L. Malkina, and D. Fitz (1995b): "The University of California, Riverside Environmental Chamber Data Base for Evaluating Oxidant Mechanism. Indoor Chamber Experiments through 1993," Report submitted to the U. S. Environmental Protection Agency, EPA/AREAL, Research Triangle Park, NC., March 20..

Carter, W. P. L., J. A. Pierce, D. Luo, and I. L. Malkina (1995c): "Environmental Chamber Study of Maximum Incremental Reactivities of Volatile Organic Compounds," Atmos. Environ. 29, 2499-2511.

Carter, W. P. L., D. Luo, I. L. Malkina, and J. A. Pierce (1995d): "Environmental Chamber Studies of Atmospheric Reactivities of Volatile Organic Compounds. Effects of Varying Chamber and Light Source," Final report to National Renewable Energy Laboratory, Contract XZ-2-12075, Coordinating Research Council, Inc., Project M-9, California Air Resources Board, Contract A032-0692, and South Coast Air Quality Management District, Contract C91323, March 26.

Carter, W. P. L., D. Luo, and I. L. Malkina (1997a): "Environmental Chamber Studies for Development of an Updated Photochemical Mechanism for VOC Reactivity Assessment," Draft final report to California Air Resources Board Contract 92-345, Coordinating Research Council Project M-9, and National Renewable Energy Laboratory Contract ZF-2-12252-07. March 10.

Carter, W. P. L., D. Luo and I. L. Malkina (1997b): "Investigation of that Atmospheric Reactions of Chloropicrin," Atmos. Environ. 31, 1425-1439.

Chang, T. Y. and S. J. Rudy (1990): "Ozone-Forming Potential of Organic Emissions from Alternative-Fueled Vehicles," Atmos. Environ., 24A, 2421-2430.

Choo, K. Y. and S. W. Benson (1981): Int. J. Chem. Kinet. 13, 883.

Croes, B. E., Technical Support Division, California Air Resources Board, personal communication (1991).

Croes, B. E., et al. (1994): "Southern California Air Quality Study Data Archive," Research Division, California Air Resources Board.

Dodge, M. C. (1984): "Combined effects of organic reactivity and NMHC/NOx ratio on photochemical oxidant formation -- a modeling study," Atmos. Environ., 18, 1657.

Donaghy, T., I. Shanahan, M. Hande and S. Fitzpatrick (1993): Int. J. Chem. Kinet. 25, 273.

EPA (1984): "Guideline for Using the Carbon Bond Mechanism in City-Specific EKMA," EPA-450/4-84-005, February.

Gery, M. W., R. D. Edmond and G. Z. Whitten (1987): "Tropospheric Ultraviolet Radiation. Assessment of Existing Data and Effects on Ozone Formation," Final Report, EPA-600/3-87-047, October.

Gery, M. W., G. Z. Whitten, and J. P. Killus (1988): "Development and Testing of the CBM-IV For Urban and Regional Modeling,", EPA-600/ 3-88-012, January.

Gillosay, D. and P. C. Simon (1988): Annales Geophysicae. 6, 211.

Gipson, G. L., W. P. Freas, R. A. Kelly and E. L. Meyer (1981): "Guideline for Use of City-Specific EKMA in Preparing Ozone SIPs, EPA-450/4-80-027, March.

Gipson, G. L. and W. P. Freas (1983): "Use of City-Specific EKMA in the Ozone RIA," U. S. Environmental Protection Agency, July.

Gipson, G. L. (1984): "Users Manual for OZIPM-2: Ozone Isopleth Plotting Package With Optional Mechanism/Version 2," EPA-450/4-84-024, August.

Hogo, H. and M. W. Gery (1988): "Guidelines for Using OZIPM-4 with CBM-IV or Optional Mechanisms. Volume 1. Description of the Ozone Isopleth Plotting Package Version 4", Final Report for EPA Contract No. 68-02-4136, Atmospheric Sciences Research Laboratory, Research Triangle Park, NC. January.

Jeffries, H. E., K. G. Sexton, J. R. Arnold, and T. L. Kale (1989): "Validation Testing of New Mechanisms with Outdoor Chamber Data. Volume 2: Analysis of VOC Data for the CB4 and CAL Photochemical Mechanisms," Final Report, EPA-600/3-89-010b.

Jeffries, H. E. and R. Crouse (1991): "Scientific and Technical Issues Related to the Application of Incremental Reactivity. Part II: Explaining Mechanism Differences," Report prepared for Western States Petroleum Association, Glendale, CA, October.

Jeffries, H. E. (1991): "UNC Solar Radiation Models," unpublished draft report for EPA Cooperative Agreements CR813107, CR813964 and CR815779".

Johnson, G. M. (1983): "Factors Affecting Oxidant Formation in Sydney Air," in "The Urban Atmosphere -- Sydney, a Case Study." Eds. J. N. Carras and G. M. Johnson (CSIRO, Melbourne), pp. 393-408.

Kwok, E. S. C., and R. Atkinson (1995): "Estimation of Hydroxyl Radical Reaction Rate Constants for Gas-Phase Organic Compounds Using a Structure-Reactivity Relationship: An Update," Atmos. Environ 29, 1685-1695.

Lurmann, F. W. and H. H. Main (1992): "Analysis of the Ambient VOC Data Collected in the Southern California Air Quality Study," Final Report to California Air Resources Board Contract No. A832-130, February.

Mellouki, A., R. K. Talukdar, and C. J. Howard (1994): "Kinetics of the Reactions of HBr with O_3 and HO_2: The yield of HBr from HO_2 + BRO," J. Geophys. Res. 99, 22,949-22,954.

Nelson, D. D., J. C. Wormhoudt, M. S. Zahniser, C. E. Kolb, M. K. W. Ko, and D. K. Weisenstein (1997): "OH Reaction Kinetics and Atmospheric Impact of 1-Bromopropane," J. Phys. Chem. A, 1997, 4879-4990.

Pitts, J. N., Jr., E. Sanhueza, R. Atkinson, W. P. L. Carter, A. M. Winer, G. W. Harris, and C. N. Plum (1984): "An Investigation of the Dark Formation of Nitrous Acid in Environmental Chambers," Int. J. Chem. Kinet., 16, 919-939.

Russell, J. J., J. A. Seetula, R. S. Timonen, D. Gutman, and D. F. Nava (1988): J. Am. Chem. Soc. 110, 3084.

Stockwell, W. R., P. Middleton, J. S. Chang, and X. Tang (1990): "The Second Generation Regional Acid Deposition Model Chemical Mechanism for Regional Air Quality Modeling," J. Geophys. Res. 95, 16343- 16376.

Tuazon, E. C., R. Atkinson, C. N. Plum, A. M. Winer, and J. N. Pitts, Jr. (1983): "The Reaction of Gas-Phase N_2O_5 with Water Vapor," Geophys. Res. Lett. 10, 953-956.

Wallington, T. J., L. M. Skewes, W. O. Siegl, and S. M. Japar (1989): "A Relative Rate Study of the Reaction of Bromine Atmos with a Variety of Organic Compounds at 295 K," Int. J. Chem. Kinet., 21, 1069-1076.

Zafonte, L., P. L. Rieger, and J. R. Holmes (1977): "Nitrogen Dioxide Photolysis in the Los Angeles Atmosphere," Environ. Sci. Technol. 11, 483-487.

APPENDIX A
LISTING OF THE CHEMICAL MECHANISM

The chemical mechanism used in the environmental chamber and atmospheric model simulations discussed in this report is given in Tables A-1 through A-4. Table A-1 lists the species used in the mechanism, Table A-2 gives the reactions and rate constants, Table A-3 gives the parameters used to calculate the rates of the photolysis reactions, and Table A-4 gives the values and derivations of the chamber-dependent parameters used when modeling the environmental chamber experiments. Footnotes to Table A-2 indicate the format used for the reaction listing.

Table A-1. List of species in the standard chemical mechanism used in the model simulations for this study. [a]

Name	Description
Constant Species.	
O2	Oxygen
M	Air
H2O	Water
Active Inorganic Species.	
O3	Ozone
NO	Nitric Oxide
NO2	Nitrogen Dioxide
NO3	Nitrate Radical
N2O5	Nitrogen Pentoxide
HONO	Nitrous Acid
HNO3	Nitric Acid
HNO4	Peroxynitric Acid
HO2H	Hydrogen Peroxide
Active Radical Species and Operators.	
HO2.	Hydroperoxide Radicals
RO2.	Operator to Calculate Total Organic Peroxy Radicals
RCO3.	Operator to Calculate Total Acetyl Peroxy Radicals
Active Reactive Organic Product Species.	
CO	Carbon Monoxide
HCHO	Formaldehyde
CCHO	Acetaldehyde
RCHO	Lumped C3+ Aldehydes
ACET	Acetone

Table A-1, (continued)

Name	Description
MEK	Lumped Ketones
PHEN	Phenol
CRES	Cresols
BALD	Aromatic aldehydes (e.g., benzaldehyde)
GLY	Glyoxal (formed from aromatics an SAPRC-90 acetylene model)
GLY-A	Glyoxal (formed from acetylene Model A)
GLY-B	Glyoxal (formed from acetylene Model B)
GLY-C	Glyoxal (formed from acetylene Model C)
MGLY	Methyl Glyoxal
AFG1	Reactive Aromatic Fragmentation Products from benzene and naphthalene
AFG2	Other Reactive Aromatic Fragmentation Products
RNO3	Organic Nitrates
NPHE	Nitrophenols
PAN	Peroxy Acetyl Nitrate
PPN	Peroxy Propionyl Nitrate
GPAN	PAN Analogue formed from Glyoxal
PBZN	PAN Analogues formed from Aromatic Aldehydes
-OOH	Operator Representing Hydroperoxy Groups
ISOPROD	Lumped reactive isoprene products
Non-Reacting Species	
CO2	Carbon Dioxide
-C	"Lost Carbon"
-N	"Lost Nitrogen"
H2	Hydrogen
Steady State Species and Operators.	
HO.	Hydroxyl Radicals
O	Ground State Oxygen Atoms
O*1D2	Excited Oxygen Atoms
RO2-R.	Peroxy Radical Operator representing NO to NO_2 conversion with HO_2 formation.
RO2-N.	Peroxy Radical Operator representing NO consumption with organic nitrate formation.
RO2-NP.	Peroxy Radical Operator representing NO consumption with nitrophenol formation
R2O2.	Peroxy Radical Operator representing NO to NO_2 conversion.
CCO-O2.	Peroxy Acetyl Radicals
C2CO-O2.	Peroxy Propionyl Radicals
HCOCO-O2.	Peroxyacyl Radical formed from Glyoxal
BZ-CO-O2.	Peroxyacyl Radical formed from Aromatic Aldehydes
HOCOO.	Intermediate formed in Formaldehyde + HO_2 reaction
BZ-O.	Phenoxy Radicals
BZ(NO2)-O.	Nitratophenoxy Radicals
HOCOO.	Radical Intermediate formed in the HO_2 + Formaldehyde system.
(HCHO2)	Excited Criegee biradical formed from $=CH_2$ groups
(CCHO2)	Excited Criegee biradical formed from $=CHCH_3$ groups

Table A-1, (continued)

Name	Description
(RCHO2)	Excited Criegee biradicals formed from =CHR groups, where R not CH_3
(C(C)CO2)	Excited Criegee biradical formed from $=C(CH_3)_2$ groups
(C(R)CO2)	Excited Criegee biradicals formed from $=C(CH_3)R$ or CR_2 groups
(BZCHO2)	Excited Criegee biradicals formed from styrenes
(C:CC(C)O2)	Excited Criegee biradical formed from ISOPROD
(C:C(C)CHO2)	Excited Criegee biradical formed from ISOPROD
(C2(O2)CHO)	Excited Criegee biradical formed from ISOPROD
(HOCCHO2)	Excited Criegee biradical formed from ISOPROD
Hydrocarbon species represented explicitly	
ETHANE	Ethane
N-C4	n-Butane
N-C6	n-Hexane
N-C8	n-Octane
ETHE	Ethene
PROPENE	Propene
T-2-BUTE	trans-2-Butene
TOLUENE	Toluene
M-XYLENE	m-Xylene
Hydrocarbon species represented explicitly in EKMA model simulations	
CH4	Methane (EKMA simulations only)
ISOP	Isoprene (EKMA simulations only)
APIN	α-Pinene (EKMA simulations only)
UNKN	Unknown biogenics (EKMA simulations only)
Lumped species used to represent the Base ROG mixture in the EKMA model simulations.	
ALK1	Alkanes and other saturated compounds with $k_{OH} < 10^4$ ppm^{-1} min^{-1}.
ALK2	Alkanes and other saturated compounds with $k_{OH} \geq 10^4$ ppm^{-1} min^{-1}.
ARO1	Aromatics with $k_{OH} < 2x10^4$ ppm^{-1} min^{-1}.
ARO2	Aromatics with $k_{OH} \geq 2x10^4$ ppm^{-1} min^{-1}.
OLE1	Alkenes (other than ethene) with $k_{OH} < 7x10^4$ ppm^{-1} min^{-1}.
OLE2	Alkenes with $k_{OH} \geq 7x10^4$ ppm^{-1} min^{-1}.

[a] See Table 1 for species added to the mechanism to represent the alkyl bromides and BrO_x species.

Table A-2. List of reactions in the chemical mechanism used in the model simulations for this study.

Rxn. Label	Kinetic Parameters [a] k(300)	A	Ea	B	Reactions [b]
Inorganic Reactions					
1	(Phot. Set = NO2)				NO2 + HV = NO + O
2	6.00E-34	6.00E-34	0.00	-2.30	O + O2 + M = O3 + M
3A	9.69E-12	6.50E-12	-0.24	0.00	O + NO2 = NO + O2
3B	1.55E-12	(Falloff Kinetics)			O + NO2 = NO3 + M
	k0 =	9.00E-32	0.00	-2.00	
	kINF =	2.20E-11	0.00	0.00	
		F= 0.60	n= 1.00		
4	1.88E-14	2.00E-12	2.78	0.00	O3 + NO = NO2 + O2
5	3.36E-17	1.40E-13	4.97	0.00	O3 + NO2 = O2 + NO3
6	2.80E-11	1.70E-11	-0.30	0.00	NO + NO3 = 2 NO2
7	1.92E-38	3.30E-39	-1.05	0.00	NO + NO + O2 = 2 NO2
8	1.26E-12	(Falloff Kinetics)			NO2 + NO3 = N2O5
	k0 =	2.20E-30	0.00	-4.30	
	kINF =	1.50E-12	0.00	-0.50	
		F= 0.60	n= 1.00		
9	5.53E+10	9.09E+26	22.26	0.00	N2O5 + #RCON8 = NO2 + NO3
10	1.00E-21	(No T Dependence)			N2O5 + H2O = 2 HNO3
11	4.17E-16	2.50E-14	2.44	0.00	NO2 + NO3 = NO + NO2 + O2
12A	(Phot. Set = NO3NO)				NO3 + HV = NO + O2
12B	(Phot. Set = NO3NO2)				NO3 + HV = NO2 + O
13A	(Phot. Set = O3O3P)				O3 + HV = O + O2
13B	(Phot. Set = O3O1D)				O3 + HV = O*1D2 + O2
14	2.20E-10	(No T Dependence)			O*1D2 + H2O = 2 HO.
15	2.92E-11	1.92E-11	-0.25	0.00	O*1D2 + M = O + M
16	4.81E-12	(Falloff Kinetics)			HO. + NO = HONO
	k0 =	7.00E-31	0.00	-2.60	
	kINF =	1.50E-11	0.00	-0.50	
		F= 0.60	n= 1.00		
17	(Phot. Set = HONO)				HONO + HV = HO. + NO
18	1.13E-11	(Falloff Kinetics)			HO. + NO2 = HNO3
	k0 =	2.60E-30	0.00	-3.20	
	kINF =	2.40E-11	0.00	-1.30	
		F= 0.60	n= 1.00		
19	1.03E-13	6.45E-15	-1.65	0.00	HO. + HNO3 = H2O + NO3
21	2.40E-13	(No T Dependence)			HO. + CO = HO2. + CO2
22	6.95E-14	1.60E-12	1.87	0.00	HO. + O3 = HO2. + O2
23	8.28E-12	3.70E-12	-0.48	0.00	HO2. + NO = HO. + NO2
24	1.37E-12	(Falloff Kinetics)			HO2. + NO2 = HNO4
	k0 =	1.80E-31	0.00	-3.20	
	kINF =	4.70E-12	0.00	-1.40	
		F= 0.60	n= 1.00		
25	7.92E+10	4.76E+26	21.66	0.00	HNO4 + #RCON24 = HO2. + NO2
27	4.61E-12	1.30E-12	-0.75	0.00	HNO4 + HO. = H2O + NO2 + O2
28	2.08E-15	1.10E-14	0.99	0.00	HO2. + O3 = HO. + 2 O2
29A	1.73E-12	2.20E-13	-1.23	0.00	HO2. + HO2. = HO2H + O2
29B	5.00E-32	1.90E-33	-1.95	0.00	HO2. + HO2. + M = HO2H + O2
29C	3.72E-30	3.10E-34	-5.60	0.00	HO2. + HO2. + H2O = HO2H + O2 + H2O
29D	2.65E-30	6.60E-35	-6.32	0.00	HO2. + HO2. + H2O = HO2H + O2 + H2O
30A	1.73E-12	2.20E-13	-1.23	0.00	NO3 + HO2. = HNO3 + O2
30B	5.00E-32	1.90E-33	-1.95	0.00	NO3 + HO2. + M = HNO3 + O2
30C	3.72E-30	3.10E-34	-5.60	0.00	NO3 + HO2. + H2O = HNO3 + O2 + H2O
30D	2.65E-30	6.60E-35	-6.32	0.00	NO3 + HO2. + H2O = HNO3 + O2 + H2O
31	(Phot. Set = H2O2)				HO2H + HV = 2 HO.
32	1.70E-12	3.30E-12	0.40	0.00	HO2H + HO. = HO2. + H2O
33	9.90E-11	4.60E-11	-0.46	0.00	HO. + HO2. = H2O + O2
Peroxy Radical Operators					
B1	7.68E-12	4.20E-12	-0.36	0.00	RO2. + NO = NO
B2	2.25E-11	(Falloff Kinetics)			RCO3. + NO = NO
	k0 =	5.65E-28	0.00	-7.10	
	kINF =	2.64E-11	0.00	-0.90	
		F= 0.27	n= 1.00		
B4	1.04E-11	(Falloff Kinetics)			RCO3. + NO2 = NO2
	k0 =	2.57E-28	0.00	-7.10	
	kINF =	1.20E-11	0.00	-0.90	
		F= 0.30	n= 1.00		
B5	4.90E-12	3.40E-13	-1.59	0.00	RO2. + HO2. = HO2. + RO2-HO2-PROD
B6	4.90E-12	3.40E-13	-1.59	0.00	RCO3. + HO2. = HO2. + RO2-HO2-PROD
B8	1.00E-15	(No T Dependence)			RO2. + RO2. = RO2-RO2-PROD
B9	1.09E-11	1.86E-12	-1.05	0.00	RO2. + RCO3. = RO2-RO2-PROD
B10	1.64E-11	2.80E-12	-1.05	0.00	RCO3. + RCO3. = RO2-RO2-PROD

Table A-2 (continued)

Rxn. Label	Kinetic Parameters [a] k(300)	A	Ea	B	Reactions [b]
B11	(Same k as for RO2.)				RO2-R. + NO = NO2 + HO2.
B12	(Same k as for RO2.)				RO2-R. + HO2. = -OOH
B13	(Same k as for RO2.)				RO2-R. + RO2. = RO2. + 0.5 HO2.
B14	(Same k as for RO2.)				RO2-R. + RCO3. = RCO3. + 0.5 HO2.
B19	(Same k as for RO2.)				RO2-N. + NO = RNO3
B20	(Same k as for RO2.)				RO2-N. + HO2. = -OOH + MEK + 1.5 -C
B21	(Same k as for RO2.)				RO2-N. + RO2. = RO2. + 0.5 HO2. + MEK + 1.5 -C
B22	(Same k as for RO2.)				RO2-N. + RCO3. = RCO3. + 0.5 HO2. + MEK + 1.5 -C
B15	(Same k as for RO2.)				R2O2. + NO = NO2
B16	(Same k as for RO2.)				R2O2. + HO2. =
B17	(Same k as for RO2.)				R2O2. + RO2. = RO2.
B18	(Same k as for RO2.)				R2O2. + RCO3. = RCO3.
B23	(Same k as for RO2.)				RO2-XN. + NO = -N
B24	(Same k as for RO2.)				RO2-XN. + HO2. = -OOH
B25	(Same k as for RO2.)				RO2-XN. + RO2. = RO2. + 0.5 HO2.
B26	(Same k as for RO2.)				RO2-XN. + RCO3. = RCO3. + HO2.
G2	(Same k as for RO2.)				RO2-NP. + NO = NPHE
G3	(Same k as for RO2.)				RO2-NP. + HO2. = -OOH + 6 -C
G4	(Same k as for RO2.)				RO2-NP. + RO2. = RO2. + 0.5 HO2. + 6 -C
G5	(Same k as for RO2.)				RO2-NP. + RCO3. = RCO3. + HO2. + 6 -C
Excited Criegee Biradicals					
RZ1	(fast)				(HCHO2) = 0.7 HCOOH + 0.12 "HO. + HO2. + CO" + 0.18 "H2 + CO2"
RZ2	(fast)				(CCHO2) = 0.25 CCOOH + 0.15 "CH4 + CO2" + 0.6 HO. + 0.3 "CCO-O2. + RCO3." + 0.3 "RO2-R. + HCHO + CO + RO2."
RZ3	(fast)				(RCHO2) = 0.25 CCOOH + 0.15 CO2 + 0.6 HO. + 0.3 "C2CO-O2. + RCO3." + 0.3 "RO2-R. + CCHO + CO + RO2." + 0.55 -C
RZ4	(fast)				(C(C)CO2) = HO. + R2O2. + HCHO + CCO-O2. + RCO3. + RO2.
RZ5	(fast)				(C(R)CO2) = HO. + CCO-O2. + CCHO + R2O2. + RCO3. + RO2.
RZ6	(fast)				(CYCCO2) = 0.3 "HO. + C2CO-O2. + R2O2. + RCO3. + RO2." + 0.3 RCHO + 4.2 -C
RZ8	(fast)				(BZCHO2) = 0.5 "BZ-O. + R2O2. + CO + HO."
ISZ1	(fast)				(C:CC(C)O2) = HO. + R2O2. + HCHO + C2CO-O2. + RO2. + RCO3.
ISZ2	(fast)				(C:C(C)CHO2) = 0.75 RCHO + 0.25 ISOPROD + 0.5 -C
MAZ1	(fast)				(C2(O2)CHO) = HO. + R2O2. + HCHO + HCOCO-O2. + RO2. + RCO3.
M1Z1	(fast)				(HOCCHO2) = 0.6 HO. + 0.3 "CCO-O2. + RCO3." + 0.3 "RO2-R. + HCHO + CO + RO2." + 0.8 -C
M2Z1	(fast)				(HCOCHO2) = 0.12 "HO2. + 2 CO + HO." + 0.74 -C + 0.51 "CO2 + HCHO"
M2Z2	(fast)				(C2(O2)COH) = HO. + MGLY + HO2. + R2O2. + RO2.
	(fast)				(C:CC(C)O2) = HO. + R2O2. + HCHO + C2CO-O2. + RO2. + RCO3.
	(fast)				(C:C(C)CHO2) = 0.75 RCHO + 0.25 ISOPROD + 0.5 -C
	(fast)				(C2(O2)CHO) = HO. + R2O2. + HCHO + HCOCO-O2. + RO2. + RCO3.
	(fast)				(HOCCHO2) = 0.6 HO. + 0.3 {CCO-O2. + RCO3.} + 0.3 {RO2-R. + HCHO + CO + RO2.} + 0.8 -C
	(fast)				(HCOCHO2) = 0.12 {HO2. + 2 CO + HO.} + 0.74 -C + 0.51 {CO2 + HCHO}
	(fast)				(C2(O2)COH) = HO. + MGLY + HO2. + R2O2. + RO2.
Organic Product Species					
B7	(Phot. Set = CO2H)				-OOH + HV = HO2. + HO.
B7A	1.81E-12	1.18E-12	-0.25	0.00	HO. + -OOH = HO.
B7B	3.71E-12	1.79E-12	-0.44	0.00	HO. + -OOH = RO2-R. + RO2.
C1	(Phot. Set = HCHONEWR)				HCHO + HV = 2 HO2. + CO
C2	(Phot. Set = HCHONEWM)				HCHO + HV = H2 + CO
C3	9.76E-12	1.13E-12	-1.29	2.00	HCHO + HO. = HO2. + CO + H2O
C4	7.79E-14	9.70E-15	-1.24	0.00	HCHO + HO2. = HOCOO.
C4A	1.77E+02	2.40E+12	13.91	0.00	HOCOO. = HO2. + HCHO
C4B	(Same k as for RO2.)				HOCOO. + NO = -C + NO2 + HO2.
C9	6.38E-16	2.80E-12	5.00	0.00	HCHO + NO3 = HNO3 + HO2. + CO
C10	1.57E-11	5.55E-12	-0.62	0.00	CCHO + HO. = CCO-O2. + H2O + RCO3.
C11A	(Phot. Set = CCHOR)				CCHO + HV = CO + HO2. + HCHO + RO2-R. + RO2.
C12	2.84E-15	1.40E-12	3.70	0.00	CCHO + NO3 = HNO3 + CCO-O2. + RCO3.
C25	1.97E-11	8.50E-12	-0.50	0.00	RCHO + HO. = C2CO-O2. + RCO3.
C26	(Phot. Set = RCHO)				RCHO + HV = CCHO + RO2-R. + RO2. + CO + HO2.

Table A-2 (continued)

Rxn.	Kinetic Parameters [a]				Reactions [b]
Label	k(300)	A	Ea	B	
C27	2.84E-15	1.40E-12	3.70	0.00	NO3 + RCHO = HNO3 + C2CO-O2. + RCO3.
C38	2.23E-13	4.81E-13	0.46	2.00	ACET + HO. = R2O2. + HCHO + CCO-O2. + RCO3. + RO2.
C39	(Phot. Set = ACET-93C)				ACET + HV = CCO-O2. + HCHO + RO2-R. + RCO3. + RO2.
C44	1.16E-12	2.92E-13	-0.82	2.00	MEK + HO. = H2O + 0.5 "CCHO + HCHO + CCO-O2. + C2CO-O2." + RCO3. + 1.5 "R2O2. + RO2."
C57	(Phot. Set = KETONE)				MEK + HV + #0.1 = CCO-O2. + CCHO + RO2-R. + RCO3. + RO2.
C95	2.07E-12	2.19E-11	1.41	0.00	RNO3 + HO. = NO2 + 0.155 MEK + 1.05 RCHO + 0.48 CCHO + 0.16 HCHO + 0.11 -C + 1.39 "R2O2. + RO2."
C58A	(Phot. Set = GLYOXAL1)				GLY + HV = 0.8 HO2. + 0.45 HCHO + 1.55 CO
C58B	(Phot. Set = GLYOXAL2)				GLY + HV + #0.029 = 0.13 HCHO + 1.87 CO
C59	1.14E-11	(No T Dependence)			GLY + HO. = 0.6 HO2. + 1.2 CO + 0.4 "HCOCO-O2. + RCO3."
C60	(Same k as for CCHO)				GLY + NO3 = HNO3 + 0.6 HO2. + 1.2 CO + 0.4 "HCOCO-O2. + RCO3."
C68A	(Phot. Set = MEGLYOX1)				MGLY + HV = HO2. + CO + CCO-O2. + RCO3.
C68B	(Phot. Set = MEGLYOX2)				MGLY + HV + 0.107 = HO2. + CO + CCO-O2. + RCO3.
C69	1.72E-11	(No T Dependence)			MGLY + HO. = CO + CCO-O2. + RCO3.
C70	(Same k as for CCHO)				MGLY + NO3 = HNO3 + CO + CCO-O2. + RCO3.
G7	1.14E-11	(No T Dependence)			HO. + AFG1 = HCOCO-O2. + RCO3.
G8	(Phot. Set = ACROLEIN)				AFG1 + HV + #0.029 = HO2. + HCOCO-O2. + RCO3.
U2OH	1.72E-11	(No T Dependence)			HO. + AFG2 = C2CO-O2. + RCO3.
U2HV	(Phot. Set = ACROLEIN)				AFG2 + HV = HO2. + CO + CCO-O2. + RCO3.
G46	2.63E-11	(No T Dependence)			HO. + PHEN = 0.15 RO2-NP. + 0.85 RO2-R. + 0.2 GLY + 4.7 -C + RO2.
G51	3.60E-12	(No T Dependence)			NO3 + PHEN = HNO3 + BZ-O.
G52	4.20E-11	(No T Dependence)			HO. + CRES = 0.15 RO2-NP. + 0.85 RO2-R. + 0.2 MGLY + 5.5 -C + RO2.
G57	2.10E-11	(No T Dependence)			NO3 + CRES = HNO3 + BZ-O. + -C
G30	1.29E-11	(No T Dependence)			BALD + HO. = BZ-CO-O2. + RCO3.
G31	(Phot. Set = BZCHO)				BALD + HV + #0.05 = 7 -C
G32	2.61E-15	1.40E-12	3.75	0.00	BALD + NO3 = HNO3 + BZ-CO-O2.
G58	3.60E-12	(No T Dependence)			NPHE + NO3 = HNO3 + BZ(NO2)-O.
G59	(Same k as for BZ-O.)				BZ(NO2)-O. + NO2 = 2 -N + 6 -C
G60	(Same k as for RO2.)				BZ(NO2)-O. + HO2. = NPHE
G61	(Same k as for BZ-O.)				BZ(NO2)-O. = NPHE
C13	(Same k as for RCO3.)				CCO-O2. + NO = CO2 + NO2 + HCHO + RO2-R. + RO2.
C14	(Same k as for RCO3.)				CCO-O2. + NO2 = PAN
C15	(Same k as for RCO3.)				CCO-O2. + HO2. = -OOH + CO2 + HCHO
C16	(Same k as for RCO3.)				CCO-O2. + RO2. = RO2. + 0.5 HO2. + CO2 + HCHO
C17	(Same k as for RCO3.)				CCO-O2. + RCO3. = RCO3. + HO2. + CO2 + HCHO
C18	6.50E-04	(Falloff Kinetics)			PAN = CCO-O2. + NO2 + RCO3.
	k0 =	4.90E-03	23.97	0.00	
	kINF =	4.00E+16	27.08	0.00	
		F= 0.30	n= 1.00		
C28	(Same k as for RCO3.)				C2CO-O2. + NO = CCHO + RO2-R. + CO2 + NO2 + RO2.
C29	8.40E-12	(No T Dependence)			C2CO-O2. + NO2 = PPN
C30	(Same k as for RCO3.)				C2CO-O2. + HO2. = -OOH + CCHO + CO2
C31	(Same k as for RCO3.)				C2CO-O2. + RO2. = RO2. + 0.5 HO2. + CCHO + CO2
C32	(Same k as for RCO3.)				C2CO-O2. + RCO3. = RCO3. + HO2. + CCHO + CO2
C33	6.78E-04	1.60E+17	27.97	0.00	PPN = C2CO-O2. + NO2 + RCO3.
C62	(Same k as for RCO3.)				HCOCO-O2. + NO = NO2 + CO2 + CO + HO2.
C63	(Same k as for RCO3.)				HCOCO-O2. + NO2 = GPAN
C65	(Same k as for RCO3.)				HCOCO-O2. + HO2. = -OOH + CO2 + CO
C66	(Same k as for RCO3.)				HCOCO-O2. + RO2. = RO2. + 0.5 HO2. + CO2 + CO
C67	(Same k as for RCO3.)				HCOCO-O2. + RCO3. = RCO3. + HO2. + CO2 + CO
C64	(Same k as for PAN)				GPAN = HCOCO-O2. + NO2 + RCO3.
G33	(Same k as for RCO3.)				BZ-CO-O2. + NO = BZ-O. + CO2 + NO2 + R2O2. + RO2.
G43	3.53E-11	1.30E-11	-0.60	0.00	BZ-O. + NO2 = NPHE
G44	(Same k as for RO2.)				BZ-O. + HO2. = PHEN
G45	1.00E-03	(No T Dependence)			BZ-O. = PHEN
G34	8.40E-12	(No T Dependence)			BZ-CO-O2. + NO2 = PBZN
G36	(Same k as for RCO3.)				BZ-CO-O2. + HO2. = -OOH + CO2 + PHEN
G37	(Same k as for RCO3.)				BZ-CO-O2. + RO2. = RO2. + 0.5 HO2. + CO2 + PHEN

Table A-2 (continued)

Rxn. Label	Kinetic Parameters [a] k(300)	A	Ea	B	Reactions [b]
G38	(Same k as for RCO3.)				BZ-CO-O2. + RCO3. = RCO3. + HO2. + CO2 + PHEN
G35	2.17E-04	1.60E+15	25.90	0.00	PBZN = BZ-CO-O2. + NO2 + RCO3.
	3.36E-11	(No T Dependence)			ISOPROD + HO. = 0.293 CO + 0.252 CCHO + 0.126 HCHO + 0.041 GLY + 0.021 RCHO + 0.168 MGLY + 0.314 MEK + 0.503 RO2-R. + 0.21 CCO-O2. + 0.288 C2CO-O2. + 0.21 R2O2. + 0.713 RO2. + 0.498 RCO3. + -.112 -C
	7.11E-18	(No T Dependence)			ISOPROD + O3 = 0.02 CCHO + 0.04 HCHO + 0.01 GLY + 0.84 MGLY + 0.09 MEK + 0.66 (HCHO2) + 0.09 (HCOCHO2) + 0.18 (HOCCHO2) + 0.06 (C2(O2)CHO) + 0.01 (C2(O2)COH) + -.39 -C
	(Phot. Set = ACROLEIN)				ISOPROD + HV + 0.0036 = 0.333 CO + 0.067 CCHO + 0.9 HCHO + 0.033 MEK + 0.333 HO2. + 0.7 RO2-R. + 0.267 CCO-O2. + 0.7 C2CO-O2. + 0.7 RO2. + 0.967 RCO3. + -.133 -C
	1.00E-15	(No T Dependence)			ISOPROD + NO3 = 0.643 CO + 0.282 HCHO + 0.85 RNO3 + 0.357 RCHO + 0.925 HO2. + 0.075 C2CO-O2. + 0.075 R2O2. + 0.925 RO2. + 0.075 RCO3. + 0.075 HNO3 + -2.471 -C
Hydrocarbon Species Represented Explicitly [c]					
	8.71E-15	6.25E-13	2.55	2.00	CH4 + HO. = HCHO + RO2-R. + RO2.
	2.74E-13	1.28E-12	0.92	2.00	ETHANE + HO. = RO2-R. + CCHO + RO2.
	2.56E-12	1.36E-12	-0.38	2.00	N-C4 + HO. = 0.076 RO2-N. + 0.924 RO2-R. + 0.397 R2O2. + 0.001 HCHO + 0.571 CCHO + 0.14 RCHO + 0.533 MEK + -0.076 -C + 1.397 RO2.
	5.63E-12	1.35E-11	0.52	0.00	N-C6 + HO. = 0.185 RO2-N. + 0.815 RO2-R. + 0.738 R2O2. + 0.02 CCHO + 0.105 RCHO + 1.134 MEK + 0.186 -C + 1.738 RO2.
	8.76E-12	3.15E-11	0.76	0.00	N-C8 + HO. = 0.333 RO2-N. + 0.667 RO2-R. + 0.706 R2O2. + 0.002 RCHO + 1.333 MEK + 0.998 -C + 1.706 RO2.
	5.91E-12	1.81E-12	-0.70	0.00	TOLUENE + HO. = 0.085 BALD + 0.26 CRES + 0.118 GLY + 0.9638 MGLY + 0.259 AFG2 + 0.74 RO2-R. + 0.26 HO2. + 2.486 -C + 0.74 RO2.
	2.36E-11	(No T Dependence)			M-XYLENE + HO. = 0.04 BALD + 0.18 CRES + 0.108 GLY + 1.599 MGLY + 0.4612 AFG2 + 0.82 RO2-R. + 0.18 HO2. + 2.884 -C + 0.82 RO2.
	8.43E-12	1.96E-12	-0.87	0.00	ETHENE + HO. = RO2-R. + RO2. + 1.56 HCHO + 0.22 CCHO
	1.68E-18	9.14E-15	5.13	0.00	ETHENE + O3 = HCHO + (HCHO2)
	2.18E-16	4.39E-13	4.53	2.00	ETHENE + NO3 = R2O2. + RO2. + 2 HCHO + NO2
	7.42E-13	1.04E-11	1.57	0.00	ETHENE + O = RO2-R. + HO2. + RO2. + HCHO + CO
	2.60E-11	4.85E-12	-1.00	0.00	PROPENE + HO. = RO2-R. + RO2. + HCHO + CCHO
	1.05E-17	5.51E-15	3.73	0.00	PROPENE + O3 = 0.6 HCHO + 0.4 CCHO + 0.4 (HCHO2) + 0.6 (CCHO2)
	9.74E-15	4.59E-13	2.30	0.00	PROPENE + NO3 = R2O2. + RO2. + HCHO + CCHO + NO2
	4.01E-12	1.18E-11	0.64	0.00	PROPENE + O = 0.4 HO2. + 0.5 RCHO + 0.5 MEK + -0.5 -C
	6.30E-11	1.01E-11	-1.09	0.00	T-2-BUTE + HO. = RO2-R. + RO2. + 2 CCHO
	1.95E-16	6.64E-15	2.10	0.00	T-2-BUTE + O3 = CCHO + (CCHO2)
	3.92E-13	1.10E-13	-0.76	2.00	T-2-BUTE + NO3 = R2O2. + RO2. + 2 CCHO + NO2
	2.34E-11	2.26E-11	-0.02	0.00	T-2-BUTE + O = 0.4 HO2. + 0.5 RCHO + 0.5 MEK + 0.5 -C
	9.88E-11	2.54E-11	-0.81	0.00	ISOP + HO. = 0.088 RO2-N. + 0.912 RO2-R. + 0.629 HCHO + 0.912 ISOPROD + 0.079 R2O2. + 1.079 RO2. + 0.283 -C
	1.34E-17	7.86E-15	3.80	0.00	ISOP + O3 = 0.4 HCHO + 0.6 ISOPROD + 0.55 (HCHO2) + 0.2 (C:CC(C)O2) + 0.2 (C:C(C)CHO2) + 0.05 -C
	3.60E-11	(No T Dependence)			ISOP + O = 0.75 {ISOPROD + -C }+ 0.25 {C2CO-O2. + RCO3. + 2 HCHO + RO2-R. + RO2.}
	6.81E-13	3.03E-12	0.89	0.00	ISOP + NO3 = 0.8 {RCHO + RNO3 + RO2-R.} + 0.2 {ISOPROD + R2O2. + NO2} + RO2. + -2.2 -C
	1.50E-19	(No T Dependence)			ISOP + NO2 = 0.8 {RCHO + RNO3 + RO2-R.} + 0.2 {ISOPROD + R2O2. + NO} + RO2. + -2.2 -C
	5.31E-11	1.21E-11	-0.88	0.00	APIN + HO. = RO2-R. + RCHO + RO2. + 7 -C
	1.00E-16	9.90E-16	1.37	0.00	APIN + O3 = 0.05 HCHO + 0.2 CCHO + 0.5 RCHO + 0.61 MEK + 0.075 CO + 0.05 CCO-O2. + 0.05 C2CO-O2. + 0.1 RCO3. + 0.105 HO2. + 0.16 HO. + 0.135 RO2-R. + 0.15 R2O2. + 0.285 RO2. + 5.285 -C

Table A-2 (continued)

Rxn. Label	Kinetic Parameters [a] k(300)	A	Ea	B	Reactions [b]
	6.10E-12	1.19E-12	-0.97	0.00	APIN + NO3 = NO2 + R2O2. + RCHO + RO2. + 7 -C
	3.00E-11	(No T Dependence)			APIN + O = 0.4 HO2. + 0.5 MEK + 0.5 RCHO + 6.5 -C
	6.57E-11	(No T Dependence)			UNKN + HO. = RO2-R. + RO2. + 0.5 HCHO + RCHO + 6.5 -C
	5.85E-17	(No T Dependence)			UNKN + O3 = 0.135 RO2-R. + 0.135 HO2. + 0.075 R2O2. + 0.21 RO2. + 0.025 CCO-O2. + 0.025 C2CO-O2. + 0.05 RCO3. + 0.275 HCHO + 0.175 CCHO + 0.5 RCHO + 0.41 MEK + 0.185 CO + 5.925 -C + 0.11 HO.
	4.30E-12	(No T Dependence)			UNKN + NO3 = R2O2. + RO2. + 0.5 HCHO + RCHO + 6.5 -C + NO2
	2.90E-11	(No T Dependence)			UNKN + O = 0.4 HO2. + 0.5 RCHO + 0.5 MEK + 6.5 -C
Lumped Species used for Base ROG in EKMA Simulations [c]					
	3.46E-12	2.58E-12	-0.17	1.00	ALK1 + HO. = 0.828 RO2-R. + 0.073 RO2-N. + 0.005 RO2-XN. + 0.011 HO2. + 0.574 R2O2. + 1.48 RO2. + 0.021 HO. + 0.022 HCHO + 0.339 CCHO + 0.176 RCHO + 0.26 ACET + 0.447 MEK + 0.024 CO + 0.026 GLY2 + 0.062 C2(C)-O. + 0.142 -C
	9.14E-12	5.12E-12	-0.35	1.00	ALK2 + HO. = 0.749 RO2-R. + 0.249 RO2-N. + 0.002 RO2-XN. + 0.891 R2O2. + 1.891 RO2. + 0.029 HCHO + 0.048 CCHO + 0.288 RCHO + 0.028 ACET + 1.105 MEK + 0.043 CO + 0.018 CO2 + 1.268 -C
	5.87E-12	(No T Dependence)			ARO1 + HO. = 0.742 RO2-R. + 0.258 HO2. + 0.742 RO2. + 0.015 PHEN + 0.244 CRES + 0.08 BALD + 0.124 GLY + 0.773 MGLY + 0.091 AFG1 + 0.229 AFG2 + 1.665 -C
	3.22E-11	1.20E-11	-0.59	1.00	ARO2 + HO. = 0.82 RO2-R. + 0.18 HO2. + 0.82 RO2. + 0.18 CRES + 0.036 BALD + 0.068 GLY + 1.159 MGLY + 0.49 AFG2 + 2.297 -C
	3.17E-11	2.22E-12	-1.59	1.00	OLE1 + HO. = 0.858 RO2-R. + 0.142 RO2-N. + RO2. + 0.858 HCHO + 0.252 CCHO + 0.606 RCHO + 1.267 -C
	1.08E-17	1.42E-15	2.91	1.00	OLE1 + O3 = 0.6 HCHO + 0.635 RCHO + 0.981 -C + 0.4 (HCHO2) + 0.529 (CCHO2) + 0.071 (RCHO2)
	1.16E-14	1.99E-13	1.69	1.00	OLE1 + NO3 = R2O2. + RO2. + HCHO + 0.294 CCHO + 0.706 RCHO + 1.451 -C + NO2
	4.11E-12	4.51E-12	0.06	1.00	OLE1 + O = 0.4 HO2. + 0.5 RCHO + 0.5 MEK + 1.657 -C
	6.23E-11	4.54E-12	-1.56	1.00	OLE2 + HO. = 0.861 RO2-R. + 0.139 RO2-N. + RO2. + 0.24 HCHO + 0.661 CCHO + 0.506 RCHO + 0.113 ACET + 0.086 MEK + 0.057 BALD + 0.848 -C
	1.70E-16	1.77E-15	1.40	1.00	OLE2 + O3 = 0.203 HCHO + 0.358 CCHO + 0.309 RCHO + 0.061 MEK + 0.027 BALD + 0.976 -C + 0.076 (HCHO2) + 0.409 (CCHO2) + 0.279 (RCHO2) + 0.158 (C(C)CO2 + 0.039 (C(R)CO2 + 0.04 (BZCHO2)
	1.07E-12	3.19E-13	-0.72	1.00	OLE2 + NO3 = R2O2. + RO2. + 0.278 HCHO + 0.767 CCHO + 0.588 RCHO + 0.131 ACET + 0.1 MEK + 0.066 BALD + 0.871 -C + NO2
	2.52E-11	8.66E-12	-0.64	1.00	OLE2 + O = 0.4 HO2. + 0.5 RCHO + 0.5 MEK + 2.205 -C
Reactions used to Represent Chamber-Dependent Processes [d]					
O3W	k(O3W)	(No T Dependence)			O3 = (loss of O_3)
N25I	k(N25I)	(No T Dependence)			N2O5 = 2 NOX-WALL
N25S	k(N25S)	(No T Dependence)			N2O5 + H2O = 2 NOX-WALL
NO2W	k(NO2W)	(No T Dependence)			NO2 = (yHONO) HONO + (1-yHONO) NOX-WALL
XSHC	k(XSHC)	(No T Dependence)			HO. = HO2.
RSI	(Phot. Set = NO2)				HV + (RS/K1) = HO.
ONO2	(Phot. Set = NO2)				HV + (E-NO2/K1) = NO2 + #-1 NOX-WALL

[a] Except as noted, expression for rate constant is k = A $e^{Ea/RT}$ $(T/300)^B$. Rate constants and A factor are in ppm, min units. Units of Ea is kcal $mole^{-1}$. "Phot Set" means this is a photolysis reaction, with the absorption coefficients and quantum yields given in Table A-3. In addition, if "#number" or "(parameter)" is given as a reactant, then the value of that number or parameter is multiplied by the result in the "rate constant expression" columns to obtain the rate constant used. Furthermore, "#RCONnn" as a reactant means that the rate constant for the reaction is obtained by multiplying the rate constant given by that for reaction "nn". Thus, the rate constant given is actually an equilibrium constant.

[b] Format of reaction listing same as used in documentation of the SAPRC-90 mechanism (Carter 1990).

[c] Rate constants and product yield parameters based on the mixture of species in the base ROG mixture which are being represented.

[d] See Table A-4 for the values of the parameters used for the chamber modeled in this study.

Table A-3. Absorption cross sections and quantum yields for photolysis reactions.

WL (nm)	Abs (cm^2)	QY	WL (nm)	Abs (cm^2)	QY	WL (nm)	Abs (cm^2)	QY	WL (nm)	Abs (cm^2)	QY	WL (nm)	Abs (cm^2)	QY
Photolysis File = NO2														
250.0	2.83E-20	1.000	255.0	1.45E-20	1.000	260.0	1.90E-20	1.000	265.0	2.05E-20	1.000	270.0	3.13E-20	1.000
275.0	4.02E-20	1.000	280.0	5.54E-20	1.000	285.0	6.99E-20	1.000	290.0	8.18E-20	0.999	295.0	9.67E-20	0.998
300.0	1.17E-19	0.997	305.0	1.66E-19	0.996	310.0	1.76E-19	0.995	315.0	2.25E-19	0.994	320.0	2.54E-19	0.993
325.0	2.79E-19	0.992	330.0	2.99E-19	0.991	335.0	3.45E-19	0.990	340.0	3.88E-19	0.989	345.0	4.07E-19	0.988
350.0	4.10E-19	0.987	355.0	5.13E-19	0.986	360.0	4.51E-19	0.984	365.0	5.78E-19	0.983	370.0	5.42E-19	0.981
375.0	5.35E-19	0.979	380.0	5.99E-19	0.975	381.0	5.98E-19	0.974	382.0	5.97E-19	0.973	383.0	5.96E-19	0.972
384.0	5.95E-19	0.971	385.0	5.94E-19	0.969	386.0	5.95E-19	0.967	387.0	5.96E-19	0.966	388.0	5.98E-19	0.964
389.0	5.99E-19	0.962	390.0	6.00E-19	0.960	391.0	5.98E-19	0.959	392.0	5.96E-19	0.957	393.0	5.93E-19	0.953
394.0	5.91E-19	0.950	395.0	5.89E-19	0.942	396.0	6.06E-19	0.922	397.0	6.24E-19	0.870	398.0	6.41E-19	0.820
399.0	6.59E-19	0.760	400.0	6.76E-19	0.695	401.0	6.67E-19	0.635	402.0	6.58E-19	0.560	403.0	6.50E-19	0.485
404.0	6.41E-19	0.425	405.0	6.32E-19	0.350	406.0	6.21E-19	0.290	407.0	6.10E-19	0.225	408.0	5.99E-19	0.185
409.0	5.88E-19	0.153	410.0	5.77E-19	0.130	411.0	5.88E-19	0.110	412.0	5.98E-19	0.094	413.0	6.09E-19	0.083
414.0	6.19E-19	0.070	415.0	6.30E-19	0.059	416.0	6.29E-19	0.048	417.0	6.27E-19	0.039	418.0	6.26E-19	0.030
419.0	6.24E-19	0.023	420.0	6.23E-19	0.018	421.0	6.18E-19	0.012	422.0	6.14E-19	0.008	423.0	6.09E-19	0.004
424.0	6.05E-19	0.000	425.0	6.00E-19	0.000									
Photolysis File = NO3NO														
585.0	2.77E-18	0.000	590.0	5.14E-18	0.250	595.0	4.08E-18	0.400	600.0	2.83E-18	0.250	605.0	3.45E-18	0.200
610.0	1.48E-18	0.200	615.0	1.96E-18	0.100	620.0	3.58E-18	0.100	625.0	9.25E-18	0.050	630.0	5.66E-18	0.050
635.0	1.45E-18	0.030	640.0	1.11E-18	0.000									
Photolysis File = NO3NO2														
400.0	0.00E+00	1.000	405.0	3.00E-20	1.000	410.0	4.00E-20	1.000	415.0	5.00E-20	1.000	420.0	8.00E-20	1.000
425.0	1.00E-19	1.000	430.0	1.30E-19	1.000	435.0	1.80E-19	1.000	440.0	1.90E-19	1.000	445.0	2.20E-19	1.000
450.0	2.80E-19	1.000	455.0	3.30E-19	1.000	460.0	3.70E-19	1.000	465.0	4.30E-19	1.000	470.0	5.10E-19	1.000
475.0	6.00E-19	1.000	480.0	6.40E-19	1.000	485.0	6.90E-19	1.000	490.0	8.80E-19	1.000	495.0	9.50E-19	1.000
500.0	1.01E-18	1.000	505.0	1.10E-18	1.000	510.0	1.32E-18	1.000	515.0	1.40E-18	1.000	520.0	1.45E-18	1.000
525.0	1.48E-18	1.000	530.0	1.94E-18	1.000	535.0	2.04E-18	1.000	540.0	1.81E-18	1.000	545.0	1.81E-18	1.000
550.0	2.36E-18	1.000	555.0	2.68E-18	1.000	560.0	3.07E-18	1.000	565.0	2.53E-18	1.000	570.0	2.54E-18	1.000
575.0	2.74E-18	1.000	580.0	3.05E-18	1.000	585.0	2.77E-18	1.000	590.0	5.14E-18	0.750	595.0	4.08E-18	0.600
600.0	2.83E-18	0.550	605.0	3.45E-18	0.400	610.0	1.45E-18	0.300	615.0	1.96E-18	0.250	620.0	3.58E-18	0.200
625.0	9.25E-18	0.150	630.0	5.66E-18	0.050	635.0	1.45E-18	0.000						
Photolysis File = O3O3P														
280.0	3.97E-18	0.100	281.0	3.60E-18	0.100	282.0	3.24E-18	0.100	283.0	3.01E-18	0.100	284.0	2.73E-18	0.100
285.0	2.44E-18	0.100	286.0	2.21E-18	0.100	287.0	2.01E-18	0.100	288.0	1.76E-18	0.100	289.0	1.58E-18	0.100
290.0	1.41E-18	0.100	291.0	1.26E-18	0.100	292.0	1.10E-18	0.100	293.0	9.89E-19	0.100	294.0	8.59E-19	0.100
295.0	7.70E-19	0.100	296.0	6.67E-19	0.100	297.0	5.84E-19	0.100	298.0	5.07E-19	0.100	299.0	4.52E-19	0.100
300.0	3.92E-19	0.100	301.0	3.42E-19	0.100	302.0	3.06E-19	0.100	303.0	2.60E-19	0.100	304.0	2.37E-19	0.100
305.0	2.01E-19	0.112	306.0	1.79E-19	0.149	307.0	1.56E-19	0.197	308.0	1.38E-19	0.259	309.0	1.25E-19	0.339
310.0	1.02E-19	0.437	311.0	9.17E-20	0.546	312.0	7.88E-20	0.652	313.0	6.77E-20	0.743	314.0	6.35E-20	0.816
315.0	5.10E-20	0.872	316.0	4.61E-20	0.916	317.0	4.17E-20	0.949	318.0	3.72E-20	0.976	319.0	2.69E-20	0.997
320.0	3.23E-20	1.000	330.0	6.70E-21	1.000	340.0	1.70E-21	1.000	350.0	4.00E-22	1.000	355.0	0.00E+00	1.000
400.0	0.00E+00	1.000	450.0	1.60E-22	1.000	500.0	1.34E-21	1.000	550.0	3.32E-21	1.000	600.0	5.06E-21	1.000
650.0	2.45E-21	1.000	700.0	8.70E-22	1.000	750.0	3.20E-22	1.000	800.0	1.60E-22	1.000	900.0	0.00E+00	1.000
Photolysis File = O3O1D														
280.0	3.97E-18	0.900	281.0	3.60E-18	0.900	282.0	3.24E-18	0.900	283.0	3.01E-18	0.900	284.0	2.73E-18	0.900
285.0	2.44E-18	0.900	286.0	2.21E-18	0.900	287.0	2.01E-18	0.900	288.0	1.76E-18	0.900	289.0	1.58E-18	0.900
290.0	1.41E-18	0.900	291.0	1.26E-18	0.900	292.0	1.10E-18	0.900	293.0	9.89E-19	0.900	294.0	8.59E-19	0.900
295.0	7.70E-19	0.900	296.0	6.67E-19	0.900	297.0	5.84E-19	0.900	298.0	5.07E-19	0.900	299.0	4.52E-19	0.900
300.0	3.92E-19	0.900	301.0	3.42E-19	0.900	302.0	3.06E-19	0.900	303.0	2.60E-19	0.900	304.0	2.37E-19	0.900
305.0	2.01E-19	0.888	306.0	1.79E-19	0.851	307.0	1.56E-19	0.803	308.0	1.38E-19	0.741	309.0	1.25E-19	0.661
310.0	1.02E-19	0.563	311.0	9.17E-20	0.454	312.0	7.88E-20	0.348	313.0	6.77E-20	0.257	314.0	6.35E-20	0.184
315.0	5.10E-20	0.128	316.0	4.61E-20	0.084	317.0	4.17E-20	0.051	318.0	3.72E-20	0.024	319.0	2.69E-20	0.003
320.0	3.23E-20	0.000												
Photolysis File = HONO														
311.0	0.00E+00	1.000	312.0	2.00E-21	1.000	313.0	4.20E-21	1.000	314.0	4.60E-21	1.000	315.0	4.20E-21	1.000
316.0	3.00E-21	1.000	317.0	4.60E-21	1.000	318.0	3.60E-20	1.000	319.0	6.10E-20	1.000	320.0	2.10E-20	1.000
321.0	4.27E-20	1.000	322.0	4.01E-20	1.000	323.0	3.93E-20	1.000	324.0	4.01E-20	1.000	325.0	4.04E-20	1.000
326.0	3.13E-20	1.000	327.0	4.12E-20	1.000	328.0	7.55E-20	1.000	329.0	6.64E-20	1.000	330.0	7.29E-20	1.000
331.0	8.70E-20	1.000	332.0	1.38E-19	1.000	333.0	5.91E-20	1.000	334.0	5.91E-20	1.000	335.0	6.45E-20	1.000
336.0	5.91E-20	1.000	337.0	4.58E-20	1.000	338.0	1.91E-19	1.000	339.0	1.63E-19	1.000	340.0	1.05E-19	1.000
341.0	8.70E-20	1.000	342.0	3.35E-19	1.000	343.0	2.01E-19	1.000	344.0	1.02E-19	1.000	345.0	8.54E-20	1.000
346.0	8.32E-20	1.000	347.0	8.20E-20	1.000	348.0	7.49E-20	1.000	349.0	7.13E-20	1.000	350.0	6.83E-20	1.000
351.0	1.74E-19	1.000	352.0	1.14E-19	1.000	353.0	3.71E-19	1.000	354.0	4.96E-19	1.000	355.0	2.46E-19	1.000
356.0	1.19E-19	1.000	357.0	9.35E-20	1.000	358.0	7.78E-20	1.000	359.0	7.29E-20	1.000	360.0	6.83E-20	1.000
361.0	6.90E-20	1.000	362.0	7.32E-20	1.000	363.0	9.00E-20	1.000	364.0	1.21E-19	1.000	365.0	1.33E-19	1.000
366.0	2.13E-19	1.000	367.0	3.52E-19	1.000	368.0	4.50E-19	1.000	369.0	2.93E-19	1.000	370.0	1.19E-19	1.000
371.0	9.46E-20	1.000	372.0	8.85E-20	1.000	373.0	7.44E-20	1.000	374.0	4.77E-20	1.000	375.0	2.70E-20	1.000
376.0	1.90E-20	1.000	377.0	1.50E-20	1.000	378.0	1.90E-20	1.000	379.0	5.80E-20	1.000	380.0	7.78E-20	1.000
381.0	1.14E-19	1.000	382.0	1.40E-19	1.000	383.0	1.72E-19	1.000	384.0	1.99E-19	1.000	385.0	1.90E-19	1.000
386.0	1.19E-19	1.000	387.0	5.65E-20	1.000	388.0	3.20E-20	1.000	389.0	1.90E-20	1.000	390.0	1.20E-20	1.000
391.0	5.00E-21	1.000	392.0	0.00E+00	1.000									
Photolysis File = H2O2														
250.0	8.30E-20	1.000	255.0	6.70E-20	1.000	260.0	5.20E-20	1.000	265.0	4.20E-20	1.000	270.0	3.20E-20	1.000
275.0	2.50E-20	1.000	280.0	2.00E-20	1.000	285.0	1.50E-20	1.000	290.0	1.13E-20	1.000	295.0	8.70E-21	1.000
300.0	6.60E-21	1.000	305.0	4.90E-21	1.000	310.0	3.70E-21	1.000	315.0	2.80E-21	1.000	320.0	2.00E-21	1.000
325.0	1.50E-21	1.000	330.0	1.20E-21	1.000	335.0	9.00E-22	1.000	340.0	7.00E-22	1.000	345.0	5.00E-22	1.000
350.0	3.00E-22	1.000	355.0	0.00E+00	1.000									

Table A-3. (continued)

WL (nm)	Abs (cm^2)	QY	WL (nm)	Abs (cm^2)	QY	WL (nm)	Abs (cm^2)	QY	WL (nm)	Abs (cm^2)	QY	WL (nm)	Abs (cm^2)	QY
Photolysis File = CO2H														
210.0	3.75E-19	1.000	220.0	2.20E-19	1.000	230.0	1.38E-19	1.000	240.0	8.80E-20	1.000	250.0	5.80E-20	1.000
260.0	3.80E-20	1.000	270.0	2.50E-20	1.000	280.0	1.50E-20	1.000	290.0	9.00E-21	1.000	300.0	5.80E-21	1.000
310.0	3.40E-21	1.000	320.0	1.90E-21	1.000	330.0	1.10E-21	1.000	340.0	6.00E-22	1.000	350.0	4.00E-22	1.000
360.0	0.00E+00	1.000												
Photolysis File = HCHONEWR														
280.0	2.49E-20	0.590	280.5	1.42E-20	0.596	281.0	1.51E-20	0.602	281.5	1.32E-20	0.608	282.0	9.73E-21	0.614
282.5	6.76E-21	0.620	283.0	5.82E-21	0.626	283.5	9.10E-21	0.632	284.0	3.71E-20	0.638	284.5	4.81E-20	0.644
285.0	3.95E-20	0.650	285.5	2.87E-20	0.656	286.0	2.24E-20	0.662	286.5	1.74E-20	0.668	287.0	1.13E-20	0.674
287.5	1.10E-20	0.680	288.0	2.62E-20	0.686	288.5	4.00E-20	0.692	289.0	3.55E-20	0.698	289.5	2.12E-20	0.704
290.0	1.07E-20	0.710	290.5	1.35E-20	0.713	291.0	1.99E-20	0.717	291.5	1.56E-20	0.721	292.0	8.65E-21	0.724
292.5	5.90E-21	0.727	293.0	1.11E-20	0.731	293.5	6.26E-20	0.735	294.0	7.40E-20	0.738	294.5	5.36E-20	0.741
295.0	4.17E-20	0.745	295.5	3.51E-20	0.749	296.0	2.70E-20	0.752	296.5	1.75E-20	0.755	297.0	1.16E-20	0.759
297.5	1.51E-20	0.763	298.0	3.69E-20	0.766	298.5	4.40E-20	0.769	299.0	3.44E-20	0.773	299.5	2.02E-20	0.776
300.0	1.06E-20	0.780	300.4	7.01E-21	0.780	300.6	8.63E-21	0.779	300.8	1.47E-20	0.779	301.0	2.01E-20	0.779
301.2	2.17E-20	0.779	301.4	1.96E-20	0.779	301.6	1.54E-20	0.778	301.8	1.26E-20	0.778	302.0	1.03E-20	0.778
302.2	8.53E-21	0.778	302.4	7.13E-21	0.778	302.6	6.61E-21	0.777	302.8	1.44E-20	0.777	303.0	3.18E-20	0.777
303.2	3.81E-20	0.777	303.4	5.57E-20	0.777	303.6	6.91E-20	0.776	303.8	6.58E-20	0.776	304.0	6.96E-20	0.776
304.2	5.79E-20	0.776	304.4	5.24E-20	0.776	304.6	4.30E-20	0.775	304.8	3.28E-20	0.775	305.0	3.60E-20	0.775
305.2	5.12E-20	0.775	305.4	4.77E-20	0.775	305.6	4.43E-20	0.774	305.8	4.60E-20	0.774	306.0	4.01E-20	0.774
306.2	3.28E-20	0.774	306.4	2.66E-20	0.774	306.6	2.42E-20	0.773	306.8	1.95E-20	0.773	307.0	1.58E-20	0.773
307.2	1.37E-20	0.773	307.4	1.19E-20	0.773	307.6	1.01E-20	0.772	307.8	9.01E-21	0.772	308.0	8.84E-21	0.772
308.2	2.08E-20	0.772	308.4	2.39E-20	0.772	308.6	3.08E-20	0.771	308.8	3.39E-20	0.771	309.0	3.18E-20	0.771
309.2	3.06E-20	0.771	309.4	2.84E-20	0.771	309.6	2.46E-20	0.770	309.8	1.95E-20	0.770	310.0	1.57E-20	0.770
310.2	1.26E-20	0.767	310.4	9.26E-21	0.764	310.6	7.71E-21	0.761	310.8	6.05E-21	0.758	311.0	5.13E-21	0.755
311.2	4.82E-21	0.752	311.4	4.54E-21	0.749	311.6	6.81E-21	0.746	311.8	1.04E-20	0.743	312.0	1.43E-20	0.740
312.2	1.47E-20	0.737	312.4	1.35E-20	0.734	312.6	1.13E-20	0.731	312.8	9.86E-21	0.728	313.0	7.82E-21	0.725
313.2	6.48E-21	0.722	313.4	1.07E-20	0.719	313.6	2.39E-20	0.716	313.8	3.80E-20	0.713	314.0	5.76E-20	0.710
314.2	6.14E-20	0.707	314.4	7.45E-20	0.704	314.6	5.78E-20	0.701	314.8	5.59E-20	0.698	315.0	4.91E-20	0.695
315.2	4.37E-20	0.692	315.4	3.92E-20	0.689	315.6	2.89E-20	0.686	315.8	2.82E-20	0.683	316.0	2.10E-20	0.680
316.2	1.66E-20	0.677	316.4	2.05E-20	0.674	316.6	4.38E-20	0.671	316.8	5.86E-20	0.668	317.0	6.28E-20	0.665
317.2	5.07E-20	0.662	317.4	4.33E-20	0.659	317.6	4.17E-20	0.656	317.8	3.11E-20	0.653	318.0	2.64E-20	0.650
318.2	2.24E-20	0.647	318.4	1.70E-20	0.644	318.6	1.24E-20	0.641	318.8	1.11E-20	0.638	319.0	7.70E-21	0.635
319.2	6.36E-21	0.632	319.4	5.36E-21	0.629	319.6	4.79E-21	0.626	319.8	6.48E-21	0.623	320.0	1.48E-20	0.620
320.2	1.47E-20	0.614	320.4	1.36E-20	0.608	320.6	1.69E-20	0.601	320.8	1.32E-20	0.595	321.0	1.49E-20	0.589
321.2	1.17E-20	0.583	321.4	1.15E-20	0.577	321.6	9.64E-21	0.570	321.8	7.26E-21	0.564	322.0	5.94E-21	0.558
322.2	4.13E-21	0.552	322.4	3.36E-21	0.546	322.6	2.39E-21	0.539	322.8	2.01E-21	0.533	323.0	1.76E-21	0.527
323.2	2.82E-21	0.521	323.4	4.65E-21	0.515	323.6	7.00E-21	0.508	323.8	7.80E-21	0.502	324.0	7.87E-21	0.496
324.2	6.59E-21	0.490	324.4	5.60E-21	0.484	324.6	4.66E-21	0.477	324.8	4.21E-21	0.471	325.0	7.77E-21	0.465
325.2	2.15E-20	0.459	325.4	3.75E-20	0.453	325.6	4.10E-20	0.446	325.8	6.47E-20	0.440	326.0	7.59E-20	0.434
326.2	6.51E-20	0.428	326.4	5.53E-20	0.422	326.6	5.76E-20	0.415	326.8	4.43E-20	0.409	327.0	3.44E-20	0.403
327.2	3.22E-20	0.397	327.4	2.13E-20	0.391	327.6	1.91E-20	0.384	327.8	1.42E-20	0.378	328.0	9.15E-21	0.372
328.2	6.79E-21	0.366	328.4	4.99E-21	0.360	328.6	4.77E-21	0.353	328.8	1.75E-20	0.347	329.0	3.27E-20	0.341
329.2	3.99E-20	0.335	329.4	5.13E-20	0.329	329.6	4.00E-20	0.322	329.8	3.61E-20	0.316	330.0	3.38E-20	0.310
330.2	3.08E-20	0.304	330.4	2.16E-20	0.298	330.6	2.09E-20	0.291	330.8	1.41E-20	0.285	331.0	9.95E-21	0.279
331.2	7.76E-21	0.273	331.4	6.16E-21	0.267	331.6	4.06E-21	0.260	331.8	3.03E-21	0.254	332.0	2.41E-21	0.248
332.2	1.74E-21	0.242	332.4	1.33E-21	0.236	332.6	2.70E-21	0.229	332.8	1.65E-21	0.223	333.0	1.17E-21	0.217
333.2	9.84E-22	0.211	333.4	8.52E-22	0.205	333.6	6.32E-22	0.198	333.8	5.21E-22	0.192	334.0	1.46E-21	0.186
334.2	1.80E-21	0.180	334.4	1.43E-21	0.174	334.6	1.03E-21	0.167	334.8	7.19E-22	0.161	335.0	4.84E-22	0.155
335.2	2.73E-22	0.149	335.4	1.34E-22	0.143	335.6	-1.62E-22	0.136	335.8	1.25E-22	0.130	336.0	4.47E-22	0.124
336.2	1.23E-21	0.118	336.4	2.02E-21	0.112	336.6	3.00E-21	0.105	336.8	2.40E-21	0.099	337.0	3.07E-21	0.093
337.2	2.29E-21	0.087	337.4	2.46E-21	0.081	337.6	2.92E-21	0.074	337.8	8.10E-21	0.068	338.0	1.82E-20	0.062
338.2	3.10E-20	0.056	338.4	3.24E-20	0.050	338.6	4.79E-20	0.043	338.8	5.25E-20	0.037	339.0	5.85E-20	0.031
339.2	4.33E-20	0.025	339.4	4.20E-20	0.019	339.6	3.99E-20	0.012	339.8	3.11E-20	0.006	340.0	2.72E-20	0.000
Photolysis File = HCHONEWM														
280.0	2.49E-20	0.350	280.5	1.42E-20	0.346	281.0	1.51E-20	0.341	281.5	1.32E-20	0.336	282.0	9.73E-21	0.332
282.5	6.76E-21	0.327	283.0	5.82E-21	0.323	283.5	9.10E-21	0.319	284.0	3.71E-20	0.314	284.5	4.81E-20	0.309
285.0	3.95E-20	0.305	285.5	2.87E-20	0.301	286.0	2.24E-20	0.296	286.5	1.74E-20	0.291	287.0	1.13E-20	0.287
287.5	1.10E-20	0.282	288.0	2.62E-20	0.278	288.5	4.00E-20	0.273	289.0	3.55E-20	0.269	289.5	2.12E-20	0.264
290.0	1.07E-20	0.260	290.5	1.35E-20	0.258	291.0	1.99E-20	0.256	291.5	1.56E-20	0.254	292.0	8.65E-21	0.252
292.5	5.90E-21	0.250	293.0	1.11E-20	0.248	293.5	6.26E-20	0.246	294.0	7.40E-20	0.244	294.5	5.36E-20	0.242
295.0	4.17E-20	0.240	295.5	3.51E-20	0.238	296.0	2.70E-20	0.236	296.5	1.75E-20	0.234	297.0	1.16E-20	0.232
297.5	1.51E-20	0.230	298.0	3.69E-20	0.228	298.5	4.40E-20	0.226	299.0	3.44E-20	0.224	299.5	2.02E-20	0.222
300.0	1.06E-20	0.220	300.4	7.01E-21	0.220	300.6	8.63E-21	0.221	300.8	1.47E-20	0.221	301.0	2.01E-20	0.221
301.2	2.17E-20	0.221	301.4	1.96E-20	0.221	301.6	1.54E-20	0.222	301.8	1.26E-20	0.222	302.0	1.03E-20	0.222
302.2	8.53E-21	0.222	302.4	7.13E-21	0.222	302.6	6.61E-21	0.223	302.8	1.44E-20	0.223	303.0	3.18E-20	0.223
303.2	3.81E-20	0.223	303.4	5.57E-20	0.223	303.6	6.91E-20	0.224	303.8	6.58E-20	0.224	304.0	6.96E-20	0.224
304.2	5.79E-20	0.224	304.4	5.24E-20	0.224	304.6	4.30E-20	0.225	304.8	3.28E-20	0.225	305.0	3.60E-20	0.225
305.2	5.12E-20	0.225	305.4	4.77E-20	0.225	305.6	4.43E-20	0.226	305.8	4.60E-20	0.226	306.0	4.01E-20	0.226
306.2	3.28E-20	0.226	306.4	2.66E-20	0.226	306.6	2.42E-20	0.227	306.8	1.95E-20	0.227	307.0	1.58E-20	0.227
307.2	1.37E-20	0.227	307.4	1.19E-20	0.227	307.6	1.01E-20	0.228	307.8	9.01E-21	0.228	308.0	8.84E-21	0.228
308.2	2.08E-20	0.228	308.4	2.39E-20	0.228	308.6	3.08E-20	0.229	308.8	3.39E-20	0.229	309.0	3.18E-20	0.229
309.2	3.06E-20	0.229	309.4	2.84E-20	0.229	309.6	2.46E-20	0.230	309.8	1.95E-20	0.230	310.0	1.57E-20	0.230
310.2	1.26E-20	0.233	310.4	9.26E-21	0.236	310.6	7.71E-21	0.239	310.8	6.05E-21	0.242	311.0	5.13E-21	0.245
311.2	4.82E-21	0.248	311.4	4.54E-21	0.251	311.6	6.81E-21	0.254	311.8	1.04E-20	0.257	312.0	1.43E-20	0.260
312.2	1.47E-20	0.263	312.4	1.35E-20	0.266	312.6	1.13E-20	0.269	312.8	9.86E-21	0.272	313.0	7.82E-21	0.275
313.2	6.48E-21	0.278	313.4	1.07E-20	0.281	313.6	2.39E-20	0.284	313.8	3.80E-20	0.287	314.0	5.76E-20	0.290
314.2	6.14E-20	0.293	314.4	7.45E-20	0.296	314.6	5.78E-20	0.299	314.8	5.59E-20	0.302	315.0	4.91E-20	0.305
315.2	4.37E-20	0.308	315.4	3.92E-20	0.311	315.6	2.89E-20	0.314	315.8	2.82E-20	0.317	316.0	2.10E-20	0.320
316.2	1.66E-20	0.323	316.4	2.05E-20	0.326	316.6	4.38E-20	0.329	316.8	5.86E-20	0.332	317.0	6.28E-20	0.335
317.2	5.07E-20	0.338	317.4	4.33E-20	0.341	317.6	4.17E-20	0.344	317.8	3.11E-20	0.347	318.0	2.64E-20	0.350
318.2	2.24E-20	0.353	318.4	1.70E-20	0.356	318.6	1.24E-20	0.359	318.8	1.11E-20	0.362	319.0	7.70E-21	0.365
319.2	6.36E-21	0.368	319.4	5.36E-21	0.371	319.6	4.79E-21	0.374	319.8	6.48E-21	0.377	320.0	1.48E-20	0.380
320.2	1.47E-20	0.386	320.4	1.36E-20	0.392	320.6	1.69E-20	0.399	320.8	1.32E-20	0.405	321.0	1.49E-20	0.411
321.2	1.17E-20	0.417	321.4	1.15E-20	0.423	321.6	9.64E-21	0.430	321.8	7.26E-21	0.436	322.0	5.94E-21	0.442

Table A-3. (continued)

WL (nm)	Abs (cm^2)	QY	WL (nm)	Abs (cm^2)	QY	WL (nm)	Abs (cm^2)	QY	WL (nm)	Abs (cm^2)	QY	WL (nm)	Abs (cm^2)	QY
322.2	4.13E-21	0.448	322.4	3.36E-21	0.454	322.6	2.39E-21	0.461	322.8	2.01E-21	0.467	323.0	1.76E-21	0.473
323.2	2.82E-21	0.479	323.4	4.65E-21	0.485	323.6	7.00E-21	0.492	323.8	7.80E-21	0.498	324.0	7.87E-21	0.504
324.2	6.59E-21	0.510	324.4	5.60E-21	0.516	324.6	4.66E-21	0.523	324.8	4.21E-21	0.529	325.0	7.77E-21	0.535
325.2	2.15E-20	0.541	325.4	3.75E-20	0.547	325.6	4.10E-20	0.554	325.8	6.47E-20	0.560	326.0	7.59E-20	0.566
326.2	6.51E-20	0.572	326.4	5.53E-20	0.578	326.6	5.76E-20	0.585	326.8	4.43E-20	0.591	327.0	3.44E-20	0.597
327.2	3.22E-20	0.603	327.4	2.13E-20	0.609	327.6	1.91E-20	0.616	327.8	1.42E-20	0.622	328.0	9.15E-21	0.628
328.2	6.79E-21	0.634	328.4	4.99E-21	0.640	328.6	4.77E-21	0.647	328.8	1.75E-20	0.653	329.0	3.27E-20	0.659
329.2	3.99E-20	0.665	329.4	5.13E-20	0.671	329.6	4.00E-20	0.678	329.8	3.61E-20	0.684	330.0	3.38E-20	0.690
330.2	3.08E-20	0.694	330.4	2.16E-20	0.699	330.6	2.09E-20	0.703	330.8	1.41E-20	0.708	331.0	9.95E-21	0.712
331.2	7.76E-21	0.717	331.4	6.16E-21	0.721	331.6	4.06E-21	0.726	331.8	3.03E-21	0.730	332.0	2.41E-21	0.735
332.2	1.74E-21	0.739	332.4	1.33E-21	0.744	332.6	2.70E-21	0.748	332.8	1.65E-21	0.753	333.0	1.17E-21	0.757
333.2	9.84E-22	0.762	333.4	8.52E-22	0.766	333.6	6.32E-22	0.771	333.8	5.21E-22	0.775	334.0	1.46E-21	0.780
334.2	1.80E-21	0.784	334.4	1.43E-21	0.789	334.6	1.03E-21	0.793	334.8	7.19E-22	0.798	335.0	4.84E-22	0.802
335.2	2.73E-22	0.798	335.4	1.34E-22	0.794	335.6	0.00E+00	0.790	335.8	1.25E-22	0.786	336.0	4.47E-22	0.782
336.2	1.23E-21	0.778	336.4	2.02E-21	0.773	336.6	3.00E-21	0.769	336.8	2.40E-21	0.764	337.0	3.07E-21	0.759
337.2	2.29E-21	0.754	337.4	2.46E-21	0.749	337.6	2.92E-21	0.745	337.8	8.10E-21	0.740	338.0	1.82E-20	0.734
338.2	3.10E-20	0.729	338.4	3.24E-20	0.724	338.6	4.79E-20	0.719	338.8	5.25E-20	0.714	339.0	5.85E-20	0.709
339.2	4.33E-20	0.703	339.4	4.20E-20	0.698	339.6	3.99E-20	0.693	339.8	3.11E-20	0.687	340.0	2.72E-20	0.682
340.2	1.99E-20	0.676	340.4	1.76E-20	0.671	340.6	1.39E-20	0.666	340.8	1.01E-20	0.660	341.0	6.57E-21	0.655
341.2	4.83E-21	0.649	341.4	3.47E-21	0.643	341.6	2.23E-21	0.638	341.8	1.55E-21	0.632	342.0	3.70E-21	0.627
342.2	4.64E-21	0.621	342.4	1.08E-20	0.616	342.6	1.14E-20	0.610	342.8	1.79E-20	0.604	343.0	2.33E-20	0.599
343.2	1.72E-20	0.593	343.4	1.55E-20	0.588	343.6	1.46E-20	0.582	343.8	1.38E-20	0.576	344.0	1.00E-20	0.571
344.2	8.26E-21	0.565	344.4	6.32E-21	0.559	344.6	4.28E-21	0.554	344.8	3.22E-21	0.548	345.0	2.54E-21	0.542
345.2	1.60E-21	0.537	345.4	1.15E-21	0.531	345.6	8.90E-22	0.525	345.8	6.50E-22	0.520	346.0	5.09E-22	0.514
346.2	5.15E-22	0.508	346.4	3.45E-22	0.503	346.6	3.18E-22	0.497	346.8	3.56E-22	0.491	347.0	3.24E-22	0.485
347.2	3.34E-22	0.480	347.4	2.88E-22	0.474	347.6	2.84E-22	0.468	347.8	9.37E-22	0.463	348.0	9.70E-22	0.457
348.2	7.60E-22	0.451	348.4	6.24E-22	0.446	348.6	4.99E-22	0.440	348.8	4.08E-22	0.434	349.0	3.39E-22	0.428
349.2	1.64E-22	0.423	349.4	1.49E-22	0.417	349.6	8.30E-23	0.411	349.8	2.52E-23	0.406	350.0	2.57E-23	0.400
350.2	0.00E+00	0.394	350.4	5.16E-23	0.389	350.6	0.00E+00	0.383	350.8	2.16E-23	0.377	351.0	7.07E-23	0.371
351.2	3.45E-23	0.366	351.4	1.97E-22	0.360	351.6	4.80E-22	0.354	351.8	3.13E-21	0.349	352.0	6.41E-21	0.343
352.2	8.38E-21	0.337	352.4	1.55E-20	0.331	352.6	1.86E-20	0.326	352.8	1.94E-20	0.320	353.0	2.78E-20	0.314
353.2	1.96E-20	0.309	353.4	1.67E-20	0.303	353.6	1.75E-20	0.297	353.8	1.63E-20	0.291	354.0	1.36E-20	0.286
354.2	1.07E-20	0.280	354.4	9.82E-21	0.274	354.6	8.66E-21	0.269	354.8	6.44E-21	0.263	355.0	4.84E-21	0.257
355.2	3.49E-21	0.251	355.4	2.41E-21	0.246	355.6	1.74E-21	0.240	355.8	1.11E-21	0.234	356.0	7.37E-22	0.229
356.2	4.17E-22	0.223	356.4	1.95E-22	0.217	356.6	1.50E-22	0.211	356.8	8.14E-23	0.206	357.0	0.00E+00	0.200
Photolysis File = CCHOR														
260.0	2.00E-20	0.310	270.0	3.40E-20	0.390	280.0	4.50E-20	0.580	290.0	4.90E-20	0.530	295.0	4.50E-20	0.480
300.0	4.30E-20	0.430	305.0	3.40E-20	0.370	315.0	2.10E-20	0.170	320.0	1.80E-20	0.100	325.0	1.10E-20	0.040
330.0	6.90E-21	0.000												
Photolysis File = RCHO														
280.0	5.26E-20	0.960	290.0	5.77E-20	0.910	300.0	5.05E-20	0.860	310.0	3.68E-20	0.600	320.0	1.66E-20	0.360
330.0	6.49E-21	0.200	340.0	1.44E-21	0.080	345.0	0.00E+00	0.020						
Photolysis File = ACET-93C														
250.0	2.37E-20	0.760	260.0	3.66E-20	0.800	270.0	4.63E-20	0.640	280.0	5.05E-20	0.550	290.0	4.21E-20	0.300
300.0	2.78E-20	0.150	310.0	1.44E-20	0.050	320.0	4.80E-21	0.026	330.0	8.00E-22	0.017	340.0	1.00E-22	0.000
350.0	3.00E-23	0.000	360.0	0.00E+00	0.000									
Photolysis File = KETONE														
210.0	1.10E-21	1.000	220.0	1.20E-21	1.000	230.0	4.60E-21	1.000	240.0	1.30E-20	1.000	250.0	2.68E-20	1.000
260.0	4.21E-20	1.000	270.0	5.54E-20	1.000	280.0	5.92E-20	1.000	290.0	5.16E-20	1.000	300.0	3.44E-20	1.000
310.0	1.53E-20	1.000	320.0	4.60E-21	1.000	330.0	1.10E-21	1.000	340.0	0.00E+00	1.000			
Photolysis File = GLYOXAL1 (used for aromatics and SAPRC-90 acetylene mechanisms)														
230.0	2.87E-21	1.000	235.0	2.87E-21	1.000	240.0	4.30E-21	1.000	245.0	5.73E-21	1.000	250.0	8.60E-21	1.000
255.0	1.15E-20	1.000	260.0	1.43E-20	1.000	265.0	1.86E-20	1.000	270.0	2.29E-20	1.000	275.0	2.58E-20	1.000
280.0	2.87E-20	1.000	285.0	3.30E-20	1.000	290.0	3.15E-20	1.000	295.0	3.30E-20	1.000	300.0	3.58E-20	1.000
305.0	2.72E-20	1.000	310.0	2.72E-20	1.000	312.5	2.87E-20	1.000	315.0	2.29E-20	1.000	320.0	1.43E-20	1.000
325.0	1.15E-20	1.000	327.5	1.43E-20	1.000	330.0	1.15E-20	1.000	335.0	2.87E-21	1.000	340.0	0.00E+00	1.000
Photolysis File = GLYOXAL2 (used for aromatics and SAPRC-90 acetylene mechanisms)														
355.0	0.00E+00	1.000	360.0	2.29E-21	1.000	365.0	2.87E-21	1.000	370.0	8.03E-21	1.000	375.0	1.00E-20	1.000
380.0	1.72E-20	1.000	382.0	1.58E-20	1.000	384.0	1.49E-20	1.000	386.0	1.49E-20	1.000	388.0	2.87E-20	1.000
390.0	3.15E-20	1.000	391.0	3.24E-20	1.000	392.0	3.04E-20	1.000	393.0	2.23E-20	1.000	394.0	2.63E-20	1.000
395.0	3.04E-20	1.000	396.0	2.63E-20	1.000	397.0	2.43E-20	1.000	398.0	3.24E-20	1.000	399.0	3.04E-20	1.000
400.0	2.84E-20	1.000	401.0	3.24E-20	1.000	402.0	4.46E-20	1.000	403.0	5.27E-20	1.000	404.0	4.26E-20	1.000
405.0	3.04E-20	1.000	406.0	3.04E-20	1.000	407.0	2.84E-20	1.000	408.0	2.43E-20	1.000	409.0	2.84E-20	1.000
410.0	6.08E-20	1.000	411.0	5.07E-20	1.000	411.5	6.08E-20	1.000	412.0	4.86E-20	1.000	413.0	8.31E-20	1.000
413.5	6.48E-20	1.000	414.0	7.50E-20	1.000	414.5	8.11E-20	1.000	415.0	8.11E-20	1.000	415.5	6.89E-20	1.000
416.0	4.26E-20	1.000	417.0	4.86E-20	1.000	418.0	5.88E-20	1.000	419.0	6.69E-20	1.000	420.0	3.85E-20	1.000
421.0	5.67E-20	1.000	421.5	4.46E-20	1.000	422.0	5.27E-20	1.000	422.5	1.05E-19	1.000	423.0	8.51E-20	1.000
424.0	6.08E-20	1.000	425.0	7.29E-20	1.000	426.0	1.18E-19	1.000	426.5	1.30E-19	1.000	427.0	1.07E-19	1.000
428.0	1.66E-19	1.000	429.0	4.05E-20	1.000	430.0	5.07E-20	1.000	431.0	4.86E-20	1.000	432.0	4.05E-20	1.000
433.0	3.65E-20	1.000	434.0	4.05E-20	1.000	434.5	6.08E-20	1.000	435.0	5.07E-20	1.000	436.0	8.11E-20	1.000
436.5	1.13E-19	1.000	437.0	5.27E-20	1.000	438.0	1.01E-19	1.000	438.5	1.38E-19	1.000	439.0	7.70E-20	1.000
440.0	2.47E-19	1.000	441.0	8.11E-20	1.000	442.0	6.08E-20	1.000	443.0	7.50E-20	1.000	444.0	9.32E-20	1.000
445.0	1.13E-19	1.000	446.0	5.27E-20	1.000	447.0	2.43E-20	1.000	448.0	2.84E-20	1.000	449.0	3.85E-20	1.000
450.0	6.08E-20	1.000	451.0	1.09E-19	1.000	451.5	9.32E-20	1.000	452.0	1.22E-19	1.000	453.0	2.39E-19	1.000
454.0	1.70E-19	1.000	455.0	3.40E-19	1.000	455.5	4.05E-19	1.000	456.0	1.01E-19	1.000	457.0	1.62E-20	1.000
458.0	1.22E-20	1.000	458.5	1.42E-20	1.000	459.0	4.05E-21	1.000	460.0	4.05E-21	1.000	460.5	6.08E-21	1.000
461.0	2.03E-21	1.000	462.0	0.00E+00	1.000									
Photolysis File = MEGLYOX1														
220.0	2.10E-21	1.000	225.0	2.10E-21	1.000	230.0	4.21E-21	1.000	235.0	7.57E-21	1.000	240.0	9.25E-21	1.000
245.0	8.41E-21	1.000	250.0	9.25E-21	1.000	255.0	9.25E-21	1.000	260.0	9.67E-21	1.000	265.0	1.05E-20	1.000

Table A-3. (continued)

WL (nm)	Abs (cm^2)	QY	WL (nm)	Abs (cm^2)	QY	WL (nm)	Abs (cm^2)	QY	WL (nm)	Abs (cm^2)	QY	WL (nm)	Abs (cm^2)	QY
270.0	1.26E-20	1.000	275.0	1.43E-20	1.000	280.0	1.51E-20	1.000	285.0	1.43E-20	1.000	290.0	1.47E-20	1.000
295.0	1.18E-20	1.000	300.0	1.14E-20	1.000	305.0	9.25E-21	1.000	310.0	6.31E-21	1.000	315.0	5.47E-21	1.000
320.0	3.36E-21	1.000	325.0	1.68E-21	1.000	330.0	8.41E-22	1.000	335.0	0.00E+00	1.000			
Photolysis File = MEGLYOX2														
350.0	0.00E+00	1.000	354.0	4.21E-22	1.000	358.0	1.26E-21	1.000	360.0	2.10E-21	1.000	362.0	2.10E-21	1.000
364.0	2.94E-21	1.000	366.0	3.36E-21	1.000	368.0	4.21E-21	1.000	370.0	5.47E-21	1.000	372.0	5.89E-21	1.000
374.0	7.57E-21	1.000	376.0	7.99E-21	1.000	378.0	8.83E-21	1.000	380.0	1.01E-20	1.000	382.0	1.09E-20	1.000
384.0	1.35E-20	1.000	386.0	1.51E-20	1.000	388.0	1.72E-20	1.000	390.0	2.06E-20	1.000	392.0	2.10E-20	1.000
394.0	2.31E-20	1.000	396.0	2.48E-20	1.000	398.0	2.61E-20	1.000	400.0	2.78E-20	1.000	402.0	2.99E-20	1.000
404.0	3.20E-20	1.000	406.0	3.79E-20	1.000	408.0	3.95E-20	1.000	410.0	4.33E-20	1.000	412.0	4.71E-20	1.000
414.0	4.79E-20	1.000	416.0	4.88E-20	1.000	418.0	5.05E-20	1.000	420.0	5.21E-20	1.000	422.0	5.30E-20	1.000
424.0	5.17E-20	1.000	426.0	5.30E-20	1.000	428.0	5.21E-20	1.000	430.0	5.55E-20	1.000	432.0	5.13E-20	1.000
434.0	5.68E-20	1.000	436.0	6.22E-20	1.000	438.0	6.06E-20	1.000	440.0	5.47E-20	1.000	441.0	6.14E-20	1.000
442.0	5.47E-20	1.000	443.0	5.55E-20	1.000	443.5	6.81E-20	1.000	444.0	5.97E-20	1.000	445.0	5.13E-20	1.000
446.0	4.88E-20	1.000	447.0	5.72E-20	1.000	448.0	5.47E-20	1.000	449.0	6.56E-20	1.000	450.0	5.05E-20	1.000
451.0	3.03E-20	1.000	452.0	4.29E-20	1.000	453.0	2.78E-20	1.000	454.0	2.27E-20	1.000	456.0	1.77E-20	1.000
458.0	8.41E-21	1.000	460.0	4.21E-21	1.000	464.0	1.68E-21	1.000	468.0	0.00E+00	1.000			
Photolysis File = BZCHO														
299.0	1.78E-19	1.000	304.0	7.40E-20	1.000	306.0	6.91E-20	1.000	309.0	6.41E-20	1.000	313.0	6.91E-20	1.000
314.0	6.91E-20	1.000	318.0	6.41E-20	1.000	325.0	8.39E-20	1.000	332.0	7.65E-20	1.000	338.0	8.88E-20	1.000
342.0	8.88E-20	1.000	346.0	7.89E-20	1.000	349.0	7.89E-20	1.000	354.0	9.13E-20	1.000	355.0	8.14E-20	1.000
364.0	5.67E-20	1.000	368.0	6.66E-20	1.000	369.0	8.39E-20	1.000	370.0	8.39E-20	1.000	372.0	3.45E-20	1.000
374.0	3.21E-20	1.000	376.0	2.47E-20	1.000	377.0	2.47E-20	1.000	380.0	3.58E-20	1.000	382.0	9.90E-21	1.000
386.0	0.00E+00	1.000												
Photolysis File = ACROLEIN														
250.0	1.80E-21	1.000	252.0	2.05E-21	1.000	253.0	2.20E-21	1.000	254.0	2.32E-21	1.000	255.0	2.45E-21	1.000
256.0	2.56E-21	1.000	257.0	2.65E-21	1.000	258.0	2.74E-21	1.000	259.0	2.83E-21	1.000	260.0	2.98E-21	1.000
261.0	3.24E-21	1.000	262.0	3.47E-21	1.000	263.0	3.58E-21	1.000	264.0	3.93E-21	1.000	265.0	4.67E-21	1.000
266.0	5.10E-21	1.000	267.0	5.38E-21	1.000	268.0	5.73E-21	1.000	269.0	6.13E-21	1.000	270.0	6.64E-21	1.000
271.0	7.20E-21	1.000	272.0	7.77E-21	1.000	273.0	8.37E-21	1.000	274.0	8.94E-21	1.000	275.0	9.55E-21	1.000
276.0	1.04E-20	1.000	277.0	1.12E-20	1.000	278.0	1.19E-20	1.000	279.0	1.27E-20	1.000	280.0	1.27E-20	1.000
281.0	1.26E-20	1.000	282.0	1.26E-20	1.000	283.0	1.28E-20	1.000	284.0	1.33E-20	1.000	285.0	1.38E-20	1.000
286.0	1.44E-20	1.000	287.0	1.50E-20	1.000	288.0	1.57E-20	1.000	289.0	1.63E-20	1.000	290.0	1.71E-20	1.000
291.0	1.78E-20	1.000	292.0	1.86E-20	1.000	293.0	1.95E-20	1.000	294.0	2.05E-20	1.000	295.0	2.15E-20	1.000
296.0	2.26E-20	1.000	297.0	2.37E-20	1.000	298.0	2.48E-20	1.000	299.0	2.60E-20	1.000	300.0	2.73E-20	1.000
301.0	2.85E-20	1.000	302.0	2.99E-20	1.000	303.0	3.13E-20	1.000	304.0	3.27E-20	1.000	305.0	3.39E-20	1.000
306.0	3.51E-20	1.000	307.0	3.63E-20	1.000	308.0	3.77E-20	1.000	309.0	3.91E-20	1.000	310.0	4.07E-20	1.000
311.0	4.25E-20	1.000	312.0	4.39E-20	1.000	313.0	4.44E-20	1.000	314.0	4.50E-20	1.000	315.0	4.59E-20	1.000
316.0	4.75E-20	1.000	317.0	4.90E-20	1.000	318.0	5.05E-20	1.000	319.0	5.19E-20	1.000	320.0	5.31E-20	1.000
321.0	5.43E-20	1.000	322.0	5.52E-20	1.000	323.0	5.60E-20	1.000	324.0	5.67E-20	1.000	325.0	5.67E-20	1.000
326.0	5.62E-20	1.000	327.0	5.63E-20	1.000	328.0	5.71E-20	1.000	329.0	5.76E-20	1.000	330.0	5.80E-20	1.000
331.0	5.95E-20	1.000	332.0	6.23E-20	1.000	333.0	6.39E-20	1.000	334.0	6.38E-20	1.000	335.0	6.24E-20	1.000
336.0	6.01E-20	1.000	337.0	5.79E-20	1.000	338.0	5.63E-20	1.000	339.0	5.56E-20	1.000	340.0	5.52E-20	1.000
341.0	5.54E-20	1.000	342.0	5.53E-20	1.000	343.0	5.47E-20	1.000	344.0	5.41E-20	1.000	345.0	5.40E-20	1.000
346.0	5.48E-20	1.000	347.0	5.90E-20	1.000	348.0	6.08E-20	1.000	349.0	6.00E-20	1.000	350.0	5.53E-20	1.000
351.0	5.03E-20	1.000	352.0	4.50E-20	1.000	353.0	4.03E-20	1.000	354.0	3.75E-20	1.000	355.0	3.55E-20	1.000
356.0	3.45E-20	1.000	357.0	3.46E-20	1.000	358.0	3.49E-20	1.000	359.0	3.41E-20	1.000	360.0	3.23E-20	1.000
361.0	2.95E-20	1.000	362.0	2.81E-20	1.000	363.0	2.91E-20	1.000	364.0	3.25E-20	1.000	365.0	3.54E-20	1.000
366.0	3.30E-20	1.000	367.0	2.78E-20	1.000	368.0	2.15E-20	1.000	369.0	1.59E-20	1.000	370.0	1.19E-20	1.000
371.0	8.99E-21	1.000	372.0	7.22E-21	1.000	373.0	5.86E-21	1.000	374.0	4.69E-21	1.000	375.0	3.72E-21	1.000
376.0	3.57E-21	1.000	377.0	3.55E-21	1.000	378.0	2.83E-21	1.000	379.0	1.69E-21	1.000	380.0	8.29E-24	1.000
381.0	0.00E+00	1.000												
Photolysis File = HOBR [a]														
240.0	4.30E-21	1.000	245.0	1.90E-20	1.000	250.0	4.50E-20	1.000	255.0	8.20E-20	1.000	260.0	1.29E-19	1.000
265.0	1.85E-19	1.000	270.0	2.40E-19	1.000	275.0	2.85E-19	1.000	280.0	3.08E-19	1.000	285.0	3.04E-19	1.000
290.0	2.73E-19	1.000	295.0	2.23E-19	1.000	300.0	1.64E-19	1.000	305.0	1.10E-19	1.000	310.0	7.00E-20	1.000
315.0	4.80E-20	1.000	320.0	3.90E-20	1.000	325.0	4.20E-20	1.000	330.0	4.90E-20	1.000	335.0	5.30E-20	1.000
340.0	5.70E-20	1.000	345.0	6.00E-20	1.000	350.0	6.00E-20	1.000	355.0	5.90E-20	1.000	360.0	5.70E-20	1.000
365.0	5.20E-20	1.000	370.0	4.50E-20	1.000	375.0	3.80E-20	1.000	380.0	3.00E-20	1.000	385.0	2.20E-20	1.000
390.0	1.70E-20	1.000	395.0	1.10E-20	1.000	400.0	1.80E-21	1.000	405.0	0.00E+00	1.000			
Photolysis File = BRO [a]														
300.0	2.00E-18	1.000	304.9	2.00E-18	1.000	305.1	2.59E-18	1.000	309.9	2.59E-18	1.000	310.1	4.54E-18	1.000
314.9	4.54E-18	1.000	315.1	3.91E-18	1.000	319.9	3.91E-18	1.000	320.1	6.00E-18	1.000	324.9	6.00E-18	1.000
325.1	7.53E-18	1.000	329.9	7.53E-18	1.000	330.1	6.28E-18	1.000	334.9	6.28E-18	1.000	335.1	5.89E-18	1.000
339.9	5.89E-18	1.000	340.1	5.15E-18	1.000	344.9	5.15E-18	1.000	345.1	3.99E-18	1.000	349.9	3.99E-18	1.000
350.1	2.28E-18	1.000	354.9	2.28E-18	1.000	355.1	1.72E-18	1.000	359.9	1.72E-18	1.000	360.1	1.61E-18	1.000
364.9	1.61E-18	1.000	365.1	9.20E-19	1.000	369.9	9.20E-19	1.000	370.1	5.10E-19	1.000	374.9	5.10E-19	1.000
375.0	0.00E+00	1.000												
Photolysis File = BRONO2 [a]														
186.0	1.50E-17	1.000	190.0	1.30E-17	1.000	195.0	1.00E-17	1.000	200.0	7.20E-18	1.000	205.0	4.30E-18	1.000
210.0	3.20E-18	1.000	215.0	2.70E-18	1.000	220.0	2.40E-18	1.000	225.0	2.10E-18	1.000	230.0	1.90E-18	1.000
235.0	1.70E-18	1.000	240.0	1.30E-18	1.000	245.0	1.00E-18	1.000	250.0	7.80E-19	1.000	255.0	6.10E-19	1.000
260.0	4.80E-19	1.000	265.0	3.90E-19	1.000	270.0	3.40E-19	1.000	275.0	3.10E-19	1.000	280.0	2.90E-19	1.000
285.0	2.70E-19	1.000	290.0	2.40E-19	1.000	295.0	2.20E-19	1.000	300.0	1.90E-19	1.000	305.0	1.80E-19	1.000
310.0	1.50E-19	1.000	315.0	1.40E-19	1.000	320.0	1.20E-19	1.000	325.0	1.10E-19	1.000	330.0	1.00E-19	1.000
335.0	9.50E-20	1.000	340.0	8.70E-20	1.000	345.0	8.50E-20	1.000	350.0	7.70E-20	1.000	360.0	6.20E-20	1.000
370.0	4.90E-20	1.000	380.0	4.00E-20	1.000	390.0	2.80E-20	1.000	400.0	0.00E+00	1.000			

[a] This is a BrO_x species which was added to the mechanism to represent reactions of bromine-containing compounds. See Table 1 for a listing of the BrO_x reactions.

Table A-4. Values of chamber-dependent parameters used in the model simulations of the experiments for this study. [a]

Parm.	Value(s)	Discussion
k(1)	0.193 - 0.202 min^{-1}	Derived by fitting results of quartz tube NO_2 actinometry measurements to curve similar to that derived for other blacklight chambers by Carter et al (1995b). The results of the actinometry experiments carried out during this study were within the uncertainty range of this extrapolation.
k(O3W)	$1.5x10^{-4}$ min^{-1}	The results of the O_3 dark decay experiments in this chamber are consistent with the recommended default of Carter et al (1995b) for Teflon bag chambers in general.
k(N25I) k(N25S)	$2.8\ x10^{-3}$ min^{-1}, $1.5x10^{-6}$ - k_g ppm^{-1} min^{-1}	Based on the N_2O_5 decay rate measurements in a similar chamber reported by Tuazon et al. (1983). Although we previously estimated there rate constants were lower in the larger Teflon bag chambers (Carter and Lurmann, 1990, 1991), we now consider it more reasonable to use the same rate constants for all such chambers (Carter et al., 1995b).
k(NO2W) yHONO	$1.6x10^{-4}$ min^{-1} 0.2	Based on dark NO_2 decay and HONO formation measured in a similar chamber by Pitts et al. (1984). Assumed to be the same in all Teflon bag chambers (Carter et al, 1995b).
k(XSHC)	250 min^{-1}	Estimated by modeling pure air irradiations. Not an important parameter affecting model predictions except for pure air or NO_x-air runs.
RS/K1	$3.27x10^{6}$ $e^{-7297/T}$ ppm	Based on model simulations of n-butane - NO_x experiments. The temperature dependence is derived from simulating outdoor experiments as discussed by Carter et al. (1995b).
E-NO2/K1	0.03 ppb	Based on model simulations of pure air experiments.

[a] See Table A-2 for definitions of the parameters.